2002

Finite element modeling of LENS deposition using SYSWELD

Aaron Mengel
Lehigh University

Mengel, Aaron

Finite Element Modeling of LENS Deposition Using SYSWELD

January 2003

Finite Element Modeling of LENS Deposition Using SYSWELD

By

Aaron Mengel

A Thesis

Presented to the Graduate and Research Committee

of Lehigh University

in Candidacy for the Degree of

Master of Science

In

Mechanical Engineering and Mechanics

Lehigh University

2002

This thesis is accepted and approved in partial fulfillment of the requirements of the Master of Science.

12/4/2002

Date

Thesis Advisor

Chairperson of Department

Table Of Contents

Table of Figures

Abstract

The purpose of the research discussed in this thesis is to develop a preliminary finite element model for the LENS (Laser Engineered Net Shaping) process using SYSWELD. Once a model has been developed and improved, it will be studied to determine the effects of various parameters on residual stresses, distortion, and ultimately part quality. In addition, a series of finite element models were developed to illustrate the effects of including various thermal and mechanical phenomena into a welding model. Results from these models allow for the creation of highly accurate and resource-efficient simulations.

Chapter 1 – Introduction

1.1 History of LENS

Rapid prototyping processes as they are known today have developed mainly in the last fifteen years, however many ideas which serve as a foundation to these processes are far from new.

In 1860, Francois Willeme developed a method for creating exact three-dimensional replicas of objects. The process was known as photosculpture, and used twenty-four cameras placed about a room to record silhouettes from each angle, allowing the operator to create a series of three-dimensional wedges that would later be assembled to create a solid model. Several years later, C. Baese refined the process, using photosensitive gelatin to reduce the labor intensive carving of the earlier method. (Ref 1)

In another field, J. E. Blanther was working in 1890 to develop a process for creating topographical relief maps. The process used layers of wax plates to make a mold to generate raised paper maps. (Ref. 1) This process was refined significantly over the next century to increase efficiency and accuracy.

By the mid twentieth century, I. Morioka created a hybrid process between photosculpture and topography by using structured light to effectively create a contour map of an object. These lines became sheets that were cut and stacked together to create a solid model. In 1951, O.J. Munz developed a system that uses a photo emulsion to create layers that become a solid model. This system has become the foundation for current stereolithography techniques. (Ref. 1)

In 1968, W. K. Swainson proposed the first process intended for direct fabrication. The process used selective, three-dimensional polymerization of a photosensitive polymer at the intersection of two laser beams. (Ref. 1)

The first process introduced that was intended to create functional metal parts was proposed by P.A. Ciraud in 1971. The process used powdered materials that were organized in a basic shape, then sintered together with a laser, electron beam, or plasma beam. (Ref. 1)

In 1992, work began at Fraunhofer IPT on a project called Controlled Metal Buildup (CMB), which employs a laser to create a weld pool, into which metal powder is injected while a shrouding gas protects the part from corrosion. The Controlled Metal Buildup process is subtractive as well as additive, as a high-speed milling cutter follows the laser and flattens layers, cleans edges, and improves tolerances and surface finishes. (Ref. 2) In 1993, research began at Sandia National Laboratories regarding a process called Laser Engineered Net Shaping (LENS). (Ref. 1) Like CMB, this process also employs a laser to create a weld pool. Powder suspended in argon is injected into the weld pool by four copper nozzles. (See Figure 1)

As the entire process occurs in an inert environment, no shrouding gas is required. (Ref. 1) Since CMB and LENS have been developed, several other groups have begun research into Direct metal deposition, including Direct Light Fabrication at Los Alamos National Laboratories, Direct metal deposition at Precision Optical Manufacturing (POM) and the University of Michigan, Direct Light Fabrication at the University of Birmingham's School of Metallurgy and Materials, Laser Aided Direct Rapid

Prototyping (LADRP) at the University of Central Florida, and Laser-aided Powder Solidification / Powder Jet (LAPS-J) at the Institute für Strahlwerkzeuge. (Ref 3)

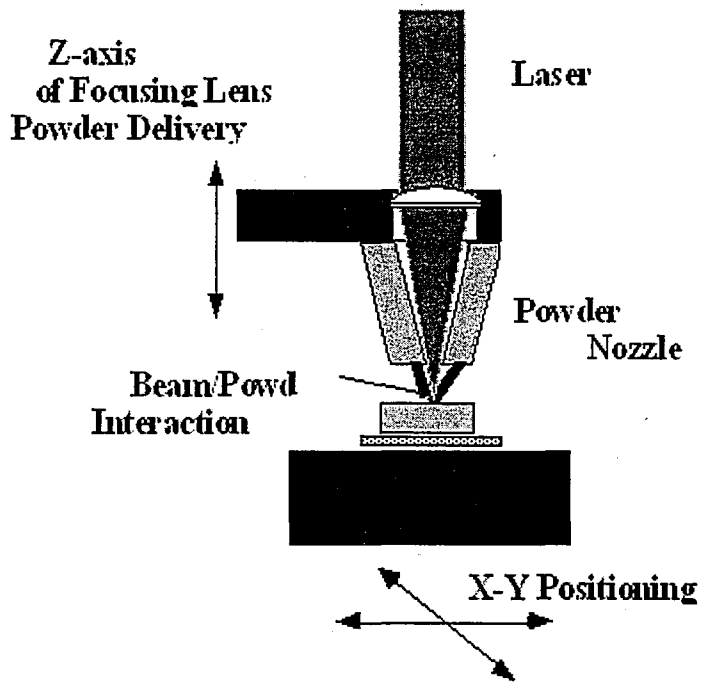

Figure 1 - LENS Process Illustration (Ref. 5)

Also, a group called Aeromet was founded in 1997 as a subsidiary of MTS Systems Corporation and in cooperation with the Applied Physics Laboratory of Johns Hopkins University and the Applied Physics Laboratory of Penn State University, specializing in Lasform, which involves the laser deposition of titanium for structural enhancements. (Ref 4).

Of all the direct metal deposition processes currently under development, only LENS (See Figure 2), POM, Aeromet's Lasform, and recently CMB have actually achieved commercial exposure to date. While only the LENS process is considered in this paper, the similarities of these processes indicate that much of the knowledge gained from LENS research should be applicable to any direct metal deposition processes.

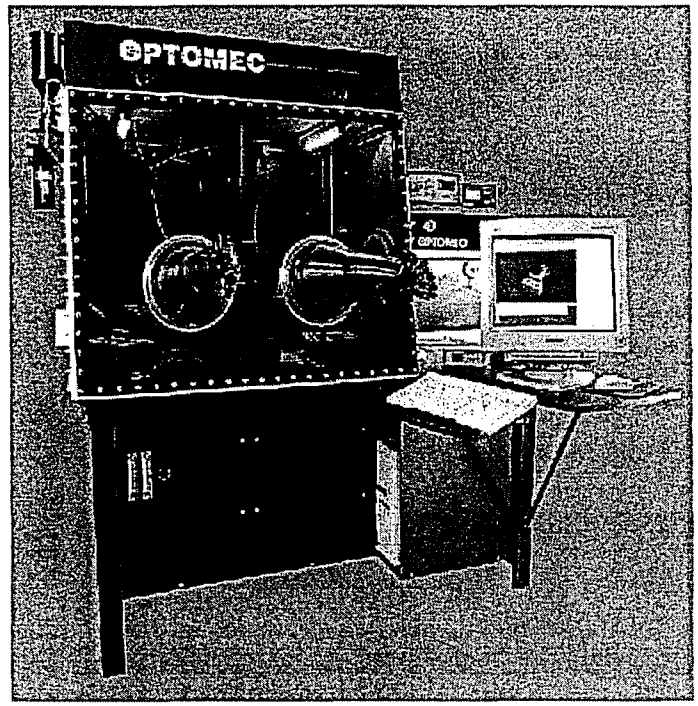

Figure 2 - Optomec's LENS Machine

Since 1997, Optomec Design Company of Albuquerque, New Mexico has commercialized the LENS process and has created CRADA, otherwise known as a Cooperative Research and Development Agreement. In this agreement, companies including Allied Signal Inc., Lockheed Martin Corp., Eastman Kodak Co., 3M Co., MTS Systems Corp., Ford Motor Company, Los Alamos National Laboratories, and several others have volunteered to offer assistance in financing research and development of the LENS process. (Ref. 5) The research supported by this agreement has made possible tremendous advances in the understanding of the science behind Direct metal deposition.

1.2 Market Demand/Utilization

While the most obvious and most publicized application for direct metal deposition involves functional prototyping, several process attributes make direct metal deposition desirable for other applications.

One example of a desirable process attribute involves the need to heat a remarkably small area in order to add material in direct metal deposition. For this reason, Optomec and POM have found considerable corporate and military interest for applications such as the repair of turbine blades and engine components or surface modification. (Refs. 5, 6) In these applications, direct metal deposition is a superior solution, as it makes a fully dense and strong addition without tampering with heat-treating. (Ref. 5) This ability to repair expensive machinery has tremendous market potential.

Another desirable feature of direct metal deposition is that it requires no fixed tooling such as molds or dies. For this reason, parts can be created that are impossible to mold, extrude, or machine. Parts with overhangs and indentations, parts with sharp inside corners, parts that are extremely complex and intricate, and parts deep enough to make machining extremely difficult are easily accommodated by the Direct metal deposition process. (Ref. 5) Therefore, this process is extremely useful for limited run production of parts that are otherwise extremely difficult to manufacture. Also due to the lack of expensive fixed tooling, direct metal deposition is an affordable option for short run manufacturing. (Ref. 6)

Direct metal deposition is also an affordable and advantageous method for fabricating injection-molding tooling. This process allows for the creation of molds with reduced warpage out of tough materials previously too difficult to machine economically. This leads to better tool wear and therefore reduced long-term cost. (Ref. 6) Furthermore, cooling passages can be built directly into molds that are far more complex than has ever been possible with conventional machining, enabling mold makers to produce molds with

more efficient cooling, resulting in faster molding, reduced costs, and higher profits. (Ref. 5)

Direct metal deposition also has the capacity to create parts with embedded sensors in otherwise homogeneous parts. This allows for more accurate and more real time measurements. For this reason, embedded sensors are of particular interest to high precision applications such as ballistic missiles and other defense related projects. (Ref. 5)

Finally, a particularly unique ability of direct metal deposition involves Functionally Graded Materials (FGM). Since direct metal deposition parts are created from powdered metals, it is quite possible to simply add a second powder feeder to a LENS machine and vary the powder composition over time. (Ref. 5) This capacity for creating parts with material gradients is truly a novel manufacturing capability, and is of tremendous commercial interest. With FGM capabilities, injection mold tooling can be created that is composed of a strong and hard material on the surface and a highly conductive material on the inside with integrated cooling passages. This process is also of interest to manufacturers of heat exchangers. While little is currently know about processing conditions for Functionally Graded Materials, test parts have been generated with copper/tool steel gradients. (Ref. 5)

With a surprisingly diverse list of applications and an endless list of possibilities, it appears that direct metal deposition will be a considerable asset to the world of manufacturing in the future.

1.3 Research

1.3.1 Introduction to Welding Research

As direct metal deposition is essentially an application of laser welding, much of the vast knowledge base that exists for welding can be applied to this process. After Fourier developed a basic theory of heat flow, the first useful analysis of welding with moving heat sources occurred in the late 1930's, when Rosenthal developed a solution for conduction from a moving heat source on a semi-infinite solid. (Ref. 7) This model was based on assumptions that heat transfer is via conduction only, the heat source can be modeled as a point source, latent heat of fusion is negligible, material properties are constant and homogeneous, and the initial temperature distribution is uniform. (Ref. 8) Rosenthal also developed a model for a thin plate based on the same assumptions. These models provide an excellent model for heat transfer in areas where temperature is less than 20% of the melting temperature (Ref. 7). However, as these models assume a point source and therefore infinite temperature at the source, the model breaks down close to the weld pool. One additional limitation of the Rosenthal solution when applied to Direct metal deposition is that it does not include any mass addition to the weld pool. (Ref. 8)

In 1969, Pavelic *et al* suggested a heat source modeled with a Gaussian distribution of flux deposited over the surface. With this model, the concentration of the heat source can be varied by changing a parameter called the concentration coefficient. (Ref. 7) Friedmen, Krutz, and Segerlind developed a variation of Pavelic's model that is expressed in coordinates that move with the heat source. (Ref. 9) While these models are a significant improvement over Rosenthal's model, they fail to reflect the digging action of a highly concentrated heat source. (Ref. 7) To better represent high power

density sources, a hemispherical Gaussian distribution was developed. Unfortunately, this model was still ill suited to deal with deep penetration welds that are not spherically symmetric. (Ref. 7) To account for this problem, Goldak, Chakravarti, and Bibby proposed a nonaxisymmetric three-dimensional heat source model. This model accommodates shallow welds, deep welds, symmetrical welds, and asymmetrical welds, all of which lead to more accurate models of the welding process. (Ref. 9) Thermal models of welding processes have also improved to consider parameters such as weld torch width, non-linearities due to variation of thermo-mechanical properties of material with temperature, radiation heat transfer from the weld pool, temperature-dependent convective heat transfer coefficients, and more. (Ref. 10)

When the temperature is known at all points in a part as a function of time during the welding process, it is possible to determine the state of stress in the part. While residual stress calculations relating to welding date back to the 1930's, the complexity of these calculations limited early efforts to empirical relations or simplified problems. Since the advent of modern computers and finite element and finite difference techniques, there has been a renewed effort to learn more about welding induced stresses. (Ref. 11) Over time, computer models to determine these stresses have grown to include more parameters and produce more accurate and more useful results.

In a general welding problem, residual stresses are produced by plastic strains due to tremendous thermal gradients, by material dilation during solid phase transformations, and by plastic deformations caused by plastic strains and solid phase transformations. (Ref. 10)

Plastic strains due to the large thermal gradients inherent to welding are the most important and most studied cause of residual stresses. Near the weld pool, the temperature change due to welding is extremely rapid and the temperature distribution uneven. In the region of the weld, the molten metal supports no load, and the strength of the solid, but high-temperature metal around the weld is drastically reduced. As the temperature far from the weld is relatively low, the expansion of metal near the weld is constrained and forced into high compression. This high compression coupled with the reduced strength of the high temperature metal leads to significant plastic deformation. Regions far from the weld are forced into tension to balance the compressive stresses close to the weld. (See Figure 3) When the part cools, the yielded material near the weld contracts and results in tension, while the regions far from the weld balance with compression. (Ref. 11)

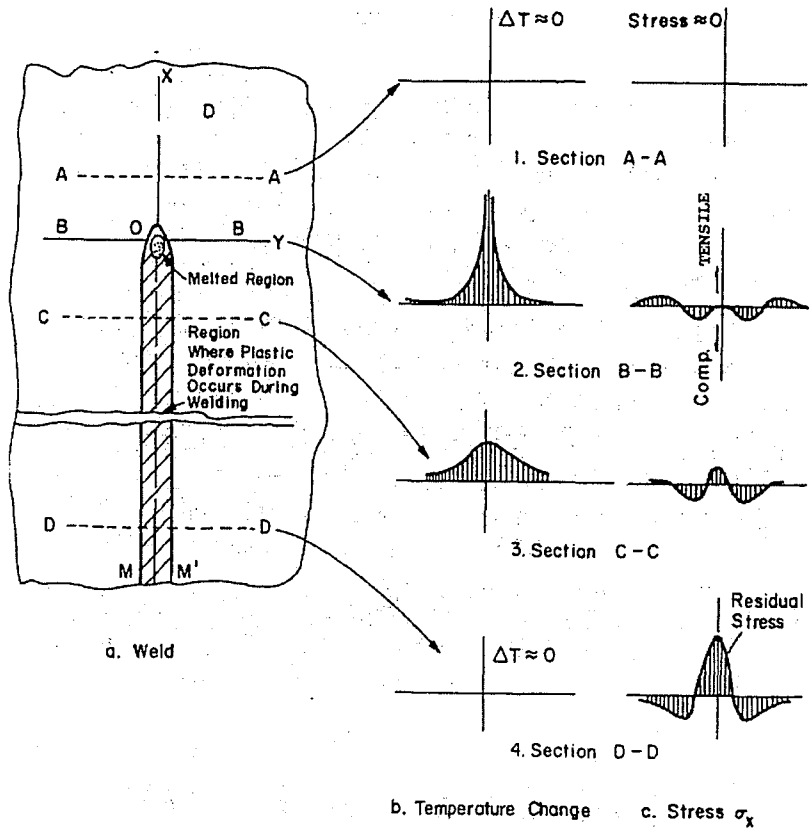

Figure 3 - Stresses in a Welded Part

Stresses resulting from solid phase transformations are clearly only relevant in materials that exhibit solid phase transformations, such as steel. Transformations from austenite to ferrite, pearlite, bainite and martensite during cooling cause material dilations locally and contribute to additional strains similar to thermal strains. These dilations induce microscopic plastic flow even though the stress state is elastic. This plastic flow is modeled in stress calculations either by locally reducing the yield stress of the material when the transformation is occurring or, preferably, by including an additional plastic strain related to the progress of transformation and also to the instantaneous deviatoric stress state. (Ref. 10) Stresses due to solid phase transformations were ignored in welding models until recently to reduce complexity of models and allow for reasonable solution times.

Once the state of stress in a welded part is known, it is possible to determine the distortion of the part. Distortion due to welding can be broken into three categories. The first is transverse shrinkage, or shrinkage perpendicular to the weld line. With this type of distortion, the part often contracts uniformly along the weld. (See Figure 4) The second is longitudinal shrinkage parallel to the weld line, and the final category is angular distortion about the weld line. (Ref. 11) With thin-walled structures, buckling is also an important problem.

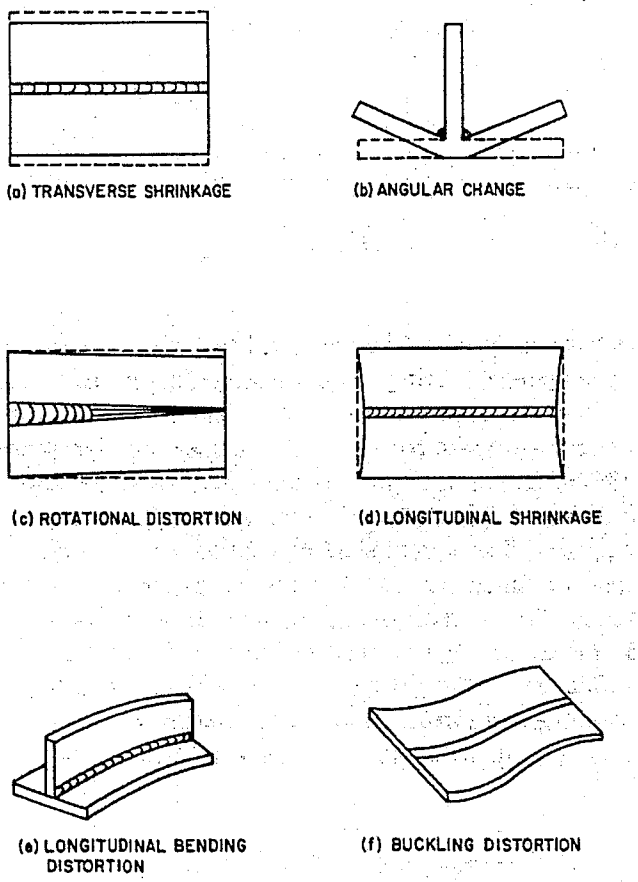

Figure 4 - Distortions in Welding

In 1994, Murthy, Rao, and Iyer sought to establish a computer model for transient thermal and thermo-elasto-plastic stress analyses considering various non-linearities due to material properties variation and heat transfer coefficients variation with temperature,

radiative boundary conditions, latent heat and solid phase transformations. While previous welding models accounted for latent heat by locally varying the specific heat of the material near the weld pool, this code uses an iterative process to include the effects of latent heat by evaluating enthalpy due to latent heat in proportion to the quantities of various material phases formed. (Ref. 10)

Until recently, the analytical solution of welding distortion was too difficult to be practical. Therefore, most early weld distortion relations were empirical. As early as 1940, Naka studied analytically and experimentally the shrinkage of a butt weld. Due to the complexity of mathematics, the study was restricted to one dimension. In the 1950's, Japanese scientists Kihara, Watanbe, Masubuchi, and Satoh carried out extensive research in welding distortion in practical joints. This research resulted in a number of empirical relations and focused entirely on welding distortion that remains after the completion of the weld and ignoring the intermediate states. Of particular utility were the Watanbe – Satoh distortion formulas. These formulas give "inherent shrinkage" and "inherent angular change" in terms of arc characteristics, joint characteristics, and electrode characteristics. These relations are valid for bead-on-plate, fillet, and butt welds. Since Watanbe and Satoh developed these formulas, the advent of the modern computer has made possible many calculations that were simply too complex and time consuming to be considered. (Ref. 11)

While empirical relations based on experiments are useful for estimating distortion in parts similar to those used for deriving the relations, they are not applicable for other geometric configurations. Closed form analytical solutions also exist for the evaluation of welding conditions susceptible to buckling, but these solutions are available

only for simple geometries. (Ref. 12) For complex geometry, the finite element method is most appropriate.

1.3.2 Advances in Finite Element Modeling of Welding

Finite element models of reasonable complexity offer unprecedented accuracy and a better understanding of what goes on inside a welded part. While many finite element solutions consider only the region immediately surrounding the weld, Brown and Song indicate that the interaction between the weld zone and the structure is critical in evaluating buckling susceptibility. Furthermore, many finite element calculations are two-dimensional on a plane perpendicular to the weld. Some modes of distortion, however, including buckling caused by longitudinal stress, cannot be represented by a two-dimensional model. As a full three-dimensional model is computationally expensive and unnecessary in the temperature and stress calculations, Daniewicz developed a hybrid experimental/numerical approach. This approach does not deliver the desired accuracy due to the difficulty in measuring weld shrinkage. (Ref. 12)

Therefore, Michaleris and DeBiccari developed a two-step, uncoupled numerical analysis that combines the computational ease of a two-dimensional welding simulation with the required accuracy of a three-dimensional structural analysis. Two-dimensional models on the plane perpendicular to the weld offer good residual stress approximations for continuous welds with a relatively high weld speed. Unfortunately, large or thin-walled structures may buckle due to residual stresses parallel to the welding direction. During welding, a section perpendicular to the weld direction experiences compression near the weld and tension elsewhere. This stress state is not susceptible to buckling; however when the part cools, the stress state reverses and the part may buckle. For this

reason, the structural analysis simply must be three-dimensional. Michaleris and DeBiccari's two-step approach is advantageous because it is computationally simple and efficient. After a two-dimensional welding simulation has been carried out, three separate analyses are carried out. The first, an elastic small deformation analysis, assumes that the displacements are infinitesimal and that loads are applied on undeformed geometry. This analysis is computationally cheap, cannot account for buckling, and is used here only to scale the weld load from the welding analysis to the structural analysis. Next, an eigenvalue analysis provides an estimate of the structure's critical buckling load and distorted shape. Finally, an incremental large deformation analysis is used to determine the critical buckling load and distortion magnitude with greater precision. This method delivers good results for all regions except those immediately around the weld pool, where temperatures are overpredicted since the two-dimensional model neglects conduction in the weld direction. (Ref. 12)

1.3.3 Simulation of Welding with Filler Metal Addition

While the research mentioned above represents tremendous progress in the welding industry, none of these models have considered the addition of filler metal. In Direct metal deposition, the addition of filler metal, in this case powder, is what eventually builds a part. Obviously, the effect of powder injection here is not negligible. In the past, a few models for laser cladding by powder injection have been developed. Kar and Mazumder considered the dissolution of the powder and the mixing of the clad in a one-dimensional study, while Weerasinghe and Steen developed a finite difference model of laser cladding by powder injection. This study also included the effect of pre-heating the powder by the laser beam and also the effect of powder in the shadowing part

of the laser energy from the surface. However, by assuming that the powder melted instantaneously on the clad surface, they did not allow for mixing within the melt pool. If mixing is not accounted for, the melted powder must be carried away from the surface by flow in the melt, requiring the solution of the Navier-Stokes equations, as considered by Picasso and Hoadley. (Ref. 13)

Hoadley and Rappaz have also developed a two-dimensional numerical model for laser cladding that assumes that mixing distributes powder instantaneously through the melt. Though fluid flow is not solved for directly, convective heat transfer is partially accounted for by the uniform redistribution of the latent heat associated with the powder. As this simplification eliminates the input requirements of the powder distribution in the gas stream or the powder's exact temperature at the clad surface, this model may be applied to many real world processing conditions. The laser power predicted by this model for a given clad thickness agreed well with experimental results. (Ref. 13)

1.3.4 Studies of Direct metal deposition

In recent years, researchers have worked to apply much of the wealth of knowledge about welding to Layered Manufacturing processes. As in welding, residual stresses are of tremendous concern. In a study by Nickel et al., an analytical model is developed to determine overall part warpage. Then a finite element model is used to determine how the pattern used to deposit material influences substrate warpage and to investigate an inter-layer surface defect known as the Christmas Tree Step. The analytical model developed here approximates the welding process with two time steps. The first time step includes the laser heating, while the second includes the part cooling after the laser energy has been removed. By calculating the expansion of the substrate

when heated and the shrinkage of the weld bead when cooled, one can develop an approximation for the forces and moments exerted on a part. Then, by simply summing forces and moments to zero, the part deformation can be determined.

The results from this calculation were quite accurate and display the dependence of deflection on material and process conditions. For materials and parts that do not yield plastically during welding, deflection depends on the expansion coefficient, remelted depth, and change in temperature that occurs during substrate cooling. For materials that exhibit elastically-perfectly plastic behavior, the deflection depends on yield strength, elastic modulus, and remelted depth. The finite element portion of this study is used to analyze the effects of deposition pattern on residual stresses and substrate warpage.

The results of this study indicate that patterns of short weld beads, called short raster patterns, cause less distortion than long raster patterns. The study also indicates that depositing thick layers distorts the part and substrate more than depositing thin layers. An effect called the Christmas Tree Step was also considered with both finite element models and experiments. The Christmas Tree Step is found at the layer interface and results in poor surface quality. (See Figure 5)

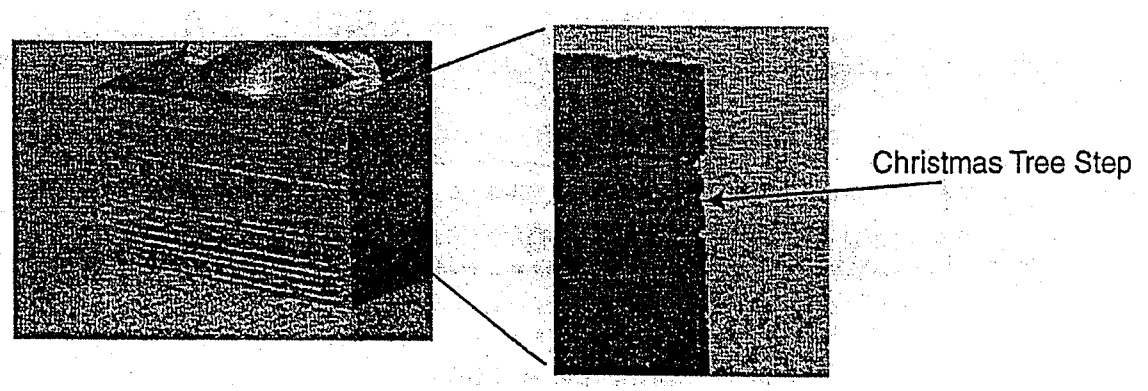

Figure 5 - Defects in DMD Fabricated Parts

when heated and the shrinkage of the weld bead when cooled, one can develop an approximation for the forces and moments exerted on a part. Then, by simply summing forces and moments to zero, the part deformation can be determined.

The results from this calculation were quite accurate and display the dependence of deflection on material and process conditions. For materials and parts that do not yield plastically during welding, deflection depends on the expansion coefficient, remelted depth, and change in temperature that occurs during substrate cooling. For materials that exhibit elastically-perfectly plastic behavior, the deflection depends on yield strength, elastic modulus, and remelted depth. The finite element portion of this study is used to analyze the effects of deposition pattern on residual stresses and substrate warpage.

The results of this study indicate that patterns of short weld beads, called short raster patterns, cause less distortion than long raster patterns. The study also indicates that depositing thick layers distorts the part and substrate more than depositing thin layers. An effect called the Christmas Tree Step was also considered with both finite element models and experiments. The Christmas Tree Step is found at the layer interface and results in poor surface quality. (See Figure 5)

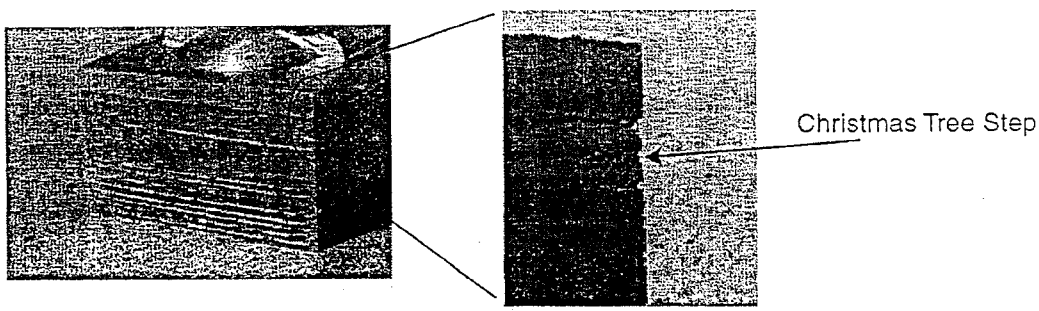

Figure 5 - Defects in DMD Fabricated Parts

It was determined that the step is an edge effect, the occurrence of the step is independent of deposition patterns, and the step size depends on the material used. (Ref. 14)

In another investigation into the thermal history experienced by a part during Direct metal deposition, Griffith et al. employ thermocouple measurements as well as digital imagining to measure temperature and predict material hardness and residual stresses. Thermocouples are the quickest, easiest, and least expensive method of determining the actual thermal history of a direct metal deposition fabricated part. When the full thermal history of a part is known, it is possible, with a phase diagram of the material, to determine the material properties of the part. This study analyzed the deposition of H13 tool steel in the construction of a thin walled box. When the laser first passes over a point, the temperature of the deposited steel is over 1200°C. In the next forty seconds, the temperature at the same point may cool to 150°C. Typically, this extremely rapid cooling rate would result in a high hardness, martensitic microstructure; however, in a direct metal deposition process, the laser passes over the same point many more times and tempers the material. For example, after seven layers are deposited on top of the aforementioned point, the peak temperature during deposition is 800°C, which is hot enough to re-austenize the material. After eleven layers, the temperature is 600°C, which is still hot enough to have an aging or tempering effect through reprecipitation or coarsening of the carbide distribution. (See Figure 6)

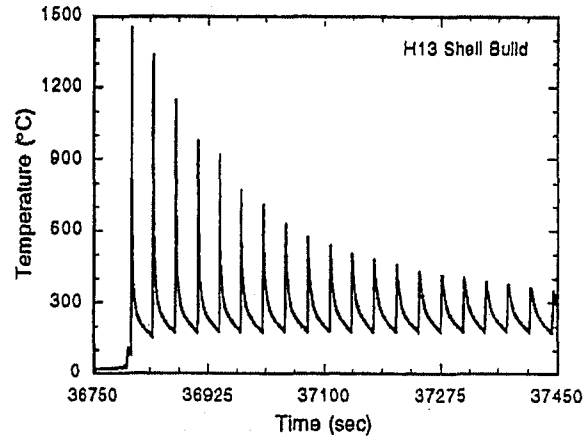

Figure 6 - Temperature History of a DMD Fabricated Part

Hence, where it might be initially assumed that the rapid cooling inherent to a Direct metal deposition process would result in extremely hard and brittle parts, it is evident after investigation that this process, if properly controlled, can yield parts with very desirable properties. Predictions of microstructure using the above information agree with the microstructures of finished parts that undergo experimental analysis. It is further noted in this investigation that processing parameters, particularly traverse velocities, have a great effect on final material hardness. (Ref. 15)

To determine the residual stresses in a part experimentally, Griffith et al. employ a technique called holographic hole drilling. With this technique, it was observed that the state of stress in a LENS deposited part is biaxial, with the fabrication plane principal stress in tension and the through-layer principal stress in compression. While this effect is not well understood in this study, further investigation is proposed. Finally, this study explores the utility of non-invasive thermal imaging techniques such as digital infrared imaging and high-speed visible imaging. While not much is currently known about emissivity values for metal objects fabricated using laser deposition, it is useful to observe the general temperature profile around the molten pool. This technique is very

promising for the future, as Optomec's goal is to use an IR camera to determine the temperature and size of the weld pool, then employ this information in a feedback loop that would allow the machine to dynamically change operating parameters to optimize part quality, material properties, or production rate. While little research has been conducted regarding temperature measurements using high-speed visible imaging, early experiments provide insight as to the size of the molten pool and thermal gradient in stainless steel samples. In addition to providing information leading to a better understanding of the welding process, a detailed thermal profile of the molten pool is also extremely useful when developing finite element models for welding heat sources. (Ref. 15)

Hofmeister et al. has conducted further investigation into thermal imaging, finding that temperature gradients below the laser are as high as 400 K mm^{-1}, tapering off to 200 K mm^{-1} in the trail of the molten pool. With the complete thermal picture of the welding process, it is possible to scale these gradients with the sample velocity to derive cooling rates for material deposited. With this information, very accurate estimates of material properties can be made. Furthermore, this study revealed that above a certain laser power, melt temperature increases without any real effect on the length of the molten zone. Meanwhile, the temperature gradients around the molten pool decrease as power increases. Hence, higher power leads to higher bulk heating of the sample away from the molten zone. This slows cooling rates throughout the part, leading to significant changes in microstructure of the finished part. (Ref.16)

Also included in Hofmeister's study is a finite element model with element activation. Here, elements near melting temperature are effectively deposited on the

surface of a substrate. Before the next element is deposited, temperatures are calculated at all nodes. Then the next node is deposited, or born, and the process repeats. While Hofmeister's model considers heat transfer by conduction only, it offers insight into the heat flow throughout the LENS part and substrate, the thermal gradients experienced at all points during fabrication and cooling, and the material properties derived from these cooling rates. (Ref. 16)

1.3.5 Application of Research

All of the research discussed to this point has sought an understanding of the happenings inside a part under construction by a direct metal deposition machine. The ultimate goal, however, is to use the information gleaned from all of this research to properly control and optimize Direct metal deposition processes to make better parts. In "Process Maps for Laser Deposition of Thin-Walled Structures," Vasinonta et al. determine the effects of changes in laser power, deposition speed, and part preheating on process parameters such as melt pool size. The numerical models used in this study do not include effects of convective heat transfer from the wall free surfaces to the surrounding air and do not model convective flows in the melt pool itself. Work by Dobranich and Dykhuizen indicates that the role of these effects in determining melt pool size is insignificant. These models also assume that the heat source is a point source. Further assumptions include insulated boundary conditions on all sides and a fixed substrate temperature. While this is a vastly simplified two-dimensional model it is still useful in determining relationships between variables. Results indicate that uniform preheating will not increase melt pool lengths significantly, and any increase in melt pool size that does occur can be easily eliminated by a small decrease in laser power or

increase in laser velocity. As preheating promises reduced residual stresses and warping, this is a significant finding. Also, a process map is developed that relates melt pool length to wall height and melting temperature. (Ref. 17)

In another study, Brooks et al. explores microstructure and property optimization of H13 Tool Steel. The purpose of this investigation is to demonstrate the ability to "process for properties" (Ref. 18) with a Direct metal deposition process. In order to accomplish this task, it is critical to select the appropriate alloy with metallurgical characteristics capable of producing the required engineering properties. Next, it is necessary to develop process models that can be used to describe the thermal history for different processing parameters at all locations. Third, it is necessary to develop a material model that describes the relevant microstructural changes and properties during processing. The final task is to combine the process and microstructural models to predict and tailor build properties. In this study, H13 tool steel is selected and a microstructural model is developed experimentally. Process models are also developed using thermocouples to gain a result similar to Griffith's. These results are used to verify a finite element model with element birthing. Finally, an aging model is developed for H13 that is useful for determining the microstructure for a given thermal history. The results indicate that hardness and percent martensite decrease with heat addition, as found in Hofmeister.

Furthermore, hardness depends strongly on the peak temperature of the single thermal cycle within the intercritical region. (See Figure 7) Predicting the actual hardness at a point is, of course, complex. Hardness is highly dependent on the height of the individual build passes and the thermal gradient throughout the tempering pass.

Therefore, it is quite possible that the hardness of a part will vary in all directions. Furthermore, to make any prediction of material hardness at a point requires the precise knowledge of the local thermal history. This investigation successfully demonstrated that the Direct metal deposition process is capable of producing parts with very specific material properties by specifying processing parameters. (Ref. 18)

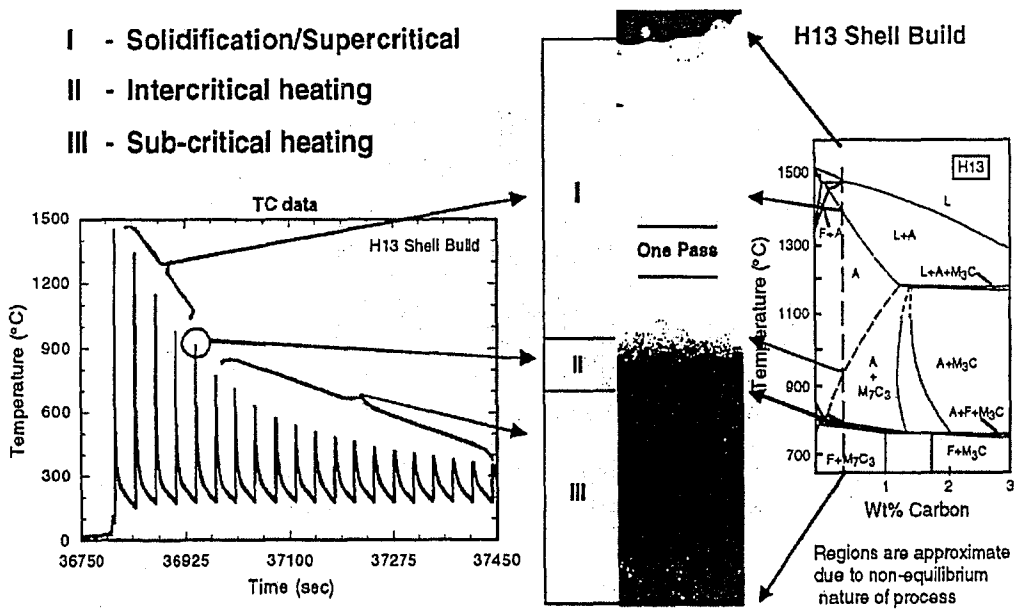

Figure 7 - Solidification Diagram for H13 Tool Steel

1.4 Current Research

Direct metal deposition is a process with many unique attributes, such as real time control of microstructure, tailored material properties at different part locations, and the production of graded structures, to name a few. (Ref. 18)

Before manufacturers can take advantage of these abilities, however, it is essential to fully understand all of the phenomena at work in a part. One indication that a process is well understood involves the accurate prediction of results for a given set of input parameters. While several finite element models for the LENS process have been

created, none are complete in accounting for all of the phenomena that affect the temperature distributions, residual stresses, and part quality. The purpose of this research is to begin the development of a comprehensive finite element model of the LENS process.

Chapter 2 – Thermal Modeling Concerns

2.1 Introduction

In order to develop a comprehensive finite element model for the LENS process, it is essential to know the effect each parameter and phenomenon has on the desired results. Many references indicate whether or not a parameter is significant to an individual study, but it is very difficult to determine the scale of that significance. This chapter describes a sensitivity study conducted to establish the aforementioned scale. A series of finite element models were generated using a multitude of input parameters and modeling techniques. Finite element modeling of welding can be carried out in many commercial modeling packages, but SYSWELD is by far the most powerful welding specific package. To establish preliminary results with minimum complexity, all models are autogenous and similar to one found in Goldak. (Ref 9)

2.2 Numerical Modeling Techniques

When modeling the welding process, one of the first and most important choices to be made is whether the part will be modeled in two or three dimensions. Both two and three-dimensional simulations have advantages and disadvantages. The most important advantage of two-dimensional modeling is reduced computation time. Many of the two-dimensional models considered here solved on an SGI Octane in a few minutes, where even the most basic three-dimensional simulations took a few hours. This indicates that time savings are one to two orders of magnitude. Two-dimensional models (See Figure 8) are also easy to create and efficient to store. Fewer time steps are usually required as the welding source only affects the modeling plane for a few seconds. This smaller number

of time steps further speeds solutions and results in smaller files containing transient information.

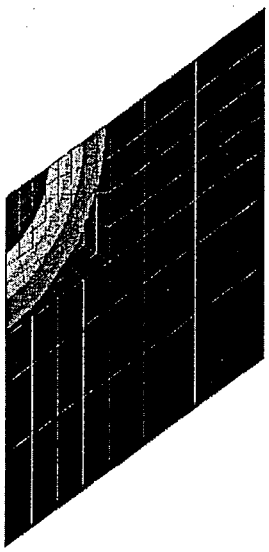

Figure 8 - 2-D Thermal Simulation

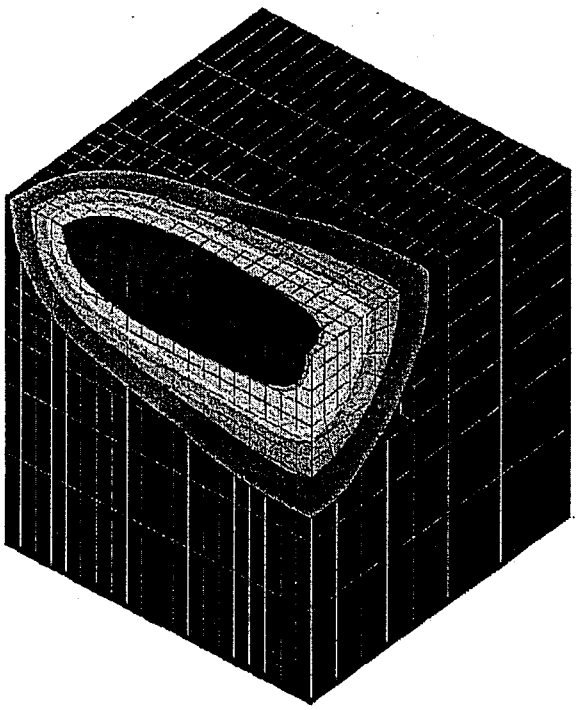

Figure 9 - 3-D Thermal Simulation

of time steps further speeds solutions and results in smaller files containing transient information.

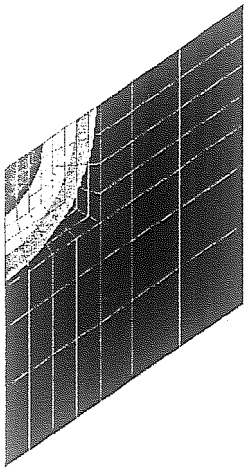

Figure 8 - 2-D Thermal Simulation

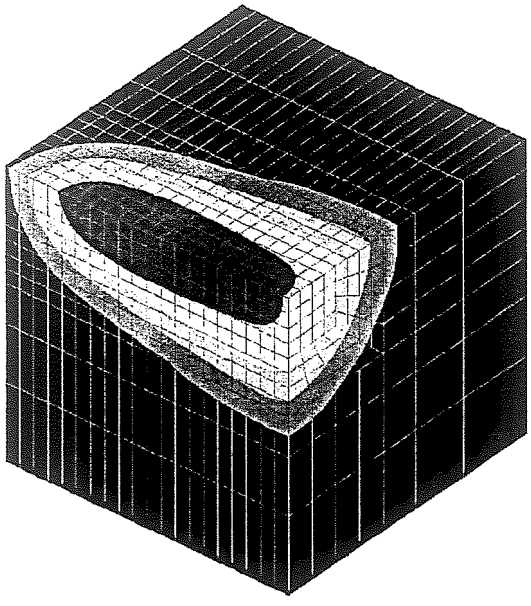

Figure 9 - 3-D Thermal Simulation

Once a simulation has finished running, results of plane simulations are quicker and easier to observe and understand.

2.2.1 Effects of Welding Speed on Accuracy

Unfortunately, two-dimensional simulations are not appropriate in all circumstances. The plane thermal approximation suffers a significant loss of accuracy if welding speed is slow, as there is assumed to be no conduction in the axial direction. It has been shown by Anderson that longitudinal heat flow is not large if welding speed is high (Ref 19). Therefore, it is claimed that the plane thermal model is a good assumption as long as welding speed is high. To test the effect of welding speed on accuracy in a two-dimensional model, several models were created and run at welding speeds ranging from 0.1 mm/s to 100 mm/s (Pèclèt Numbers from 0.2 to 200). These models were compared to three-dimensional models with identical input parameters. Two-dimensional models here consisted of 307 nodes and 330 linear elements, while three-dimensional models were constructed from 15657 nodes and 17076 linear elements. The two-dimensional mesh is shown in Figure 11, and is thirty millimeters square. The three-dimensional mesh is shown in Figure 12, and is thirty millimeters wide, thirty millimeters high, and fifty millimeters long.. The material used was AL6XN, with the properties shown in Figure 10.

Temp	Spec Heat	Temp	Thermal Conductivity
C	J/kgK	C	W/mK
20	0.00403	20	0.0137
500	0.004836	100	0.0137
1200	0.005239	500	0.025
1320	0.0053599	1320	0.04

Density	8060 kg/m^3

Figure 10 – Thermal Properties of AL6XN

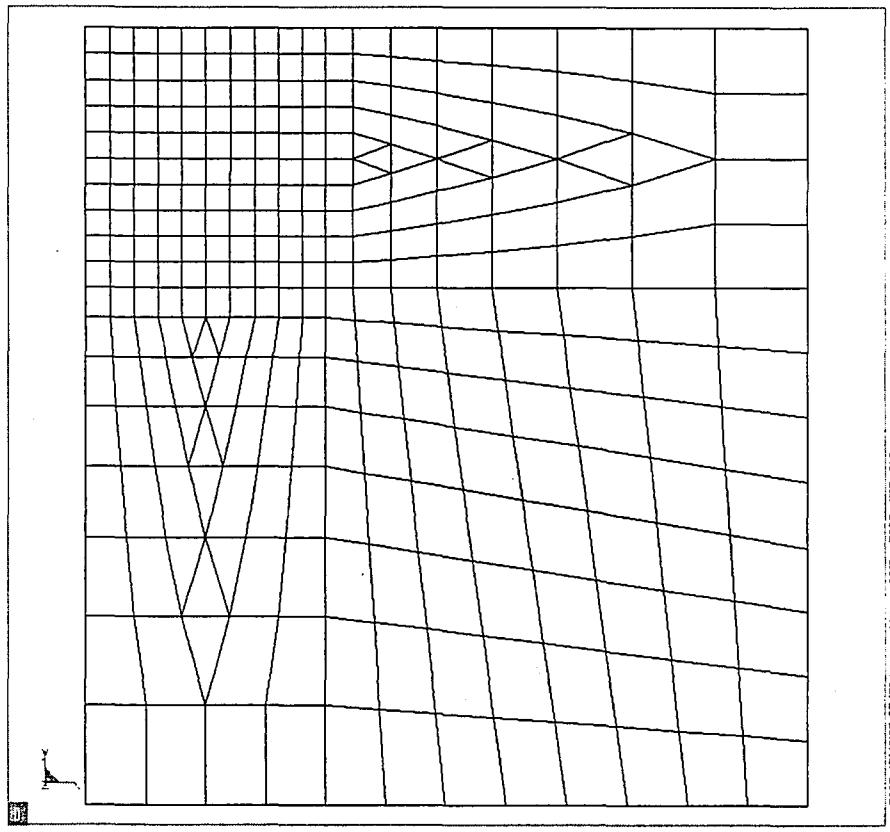

Figure 11 – Two-Dimensional Mesh for Speed Comparisons

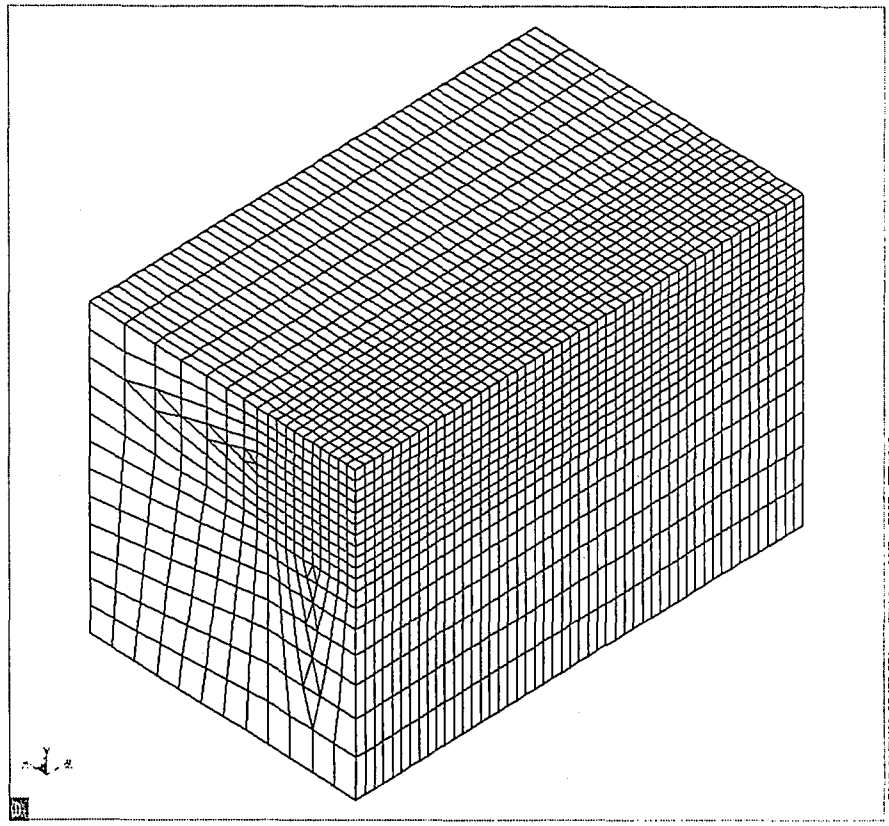

Figure 12 – Three-Dimensional Mesh for Speed Comparisons

Heat inputs for these models were not based on real welding parameters, but were generated to maintain a fusion zone of around five millimeters on the two-dimensional models for consistency. Input parameters are given in Figure 13.

Velocity	Power	a	b	Zf	Zr	Qf	Qr
mm/s	W	mm	mm	mm	mm		
0.1	500	5	5	5	5	1	1
0.5	750	5	5	5	5	1	1
1	1500	5	5	5	5	1	1
5	3000	5	5	2.5	7.5	0.6	1.4
10	5000	5	5	2.5	7.5	0.6	1.4
25	15000	6	6	5	22.5	0.35	1.65
50	15000	4	4	2	23	0.1	1.9
100	20000	4	4	2	28	0.1	1.9

Figure 13 – Inputs for Goldak Heat Source for Speed Comparison

Results are given in welding speeds (mm/s) and Pèclèt numbers so that the results can be generalized. The Pèclèt number is given by Equation 2.1, where v is velocity, l is a characteristic length (plate thickness in this case), ρ is density, C_p is specific heat, κ is thermal diffusivity, and λ is thermal conductivity.

$$Pe = \frac{v \cdot l}{\kappa} \tag{2.1}$$

where $\kappa = \frac{\lambda}{\rho C_p}$

The Pèclèt number is a dimensionless quantity that compares welding velocity to a material's ability to diffuse heat.

For the lowest welding speeds of 0.1mm/s and 0.5mm/s (Pèclèt numbers of around 0.2 and 1.0), the three-dimensional models never reached the fusion temperature, as heat rapidly diffuses away from the source in all directions. (See Figure 14) As heat

cannot escape out of plane, two-dimensional models indicate that melting does occur and provide highly inaccurate and useless results.

At speeds of around 5mm/s (Pèclèt numbers of around 10), results are much better. While two-dimensional models slightly overestimate peak temperatures in the fusion zone, heating and cooling rates in the more important cooler temperatures are well represented in the two-dimensional model. (See Figure 15) Note that peak temperatures in the two dimensional models are over estimated. This is the result of increased conduction in the molten pool, which has a greater effect in three-dimensional models as the increased conduction acts in all directions, where in two-dimensional models, the heat still cannot escape the plane.

At higher welding speeds of 25mm/s to 100mm/s (Pèclèt numbers of 50 to 200), thermal results from the two-dimensional and three-dimensional models are nearly indistinguishable. (See Figure 16).

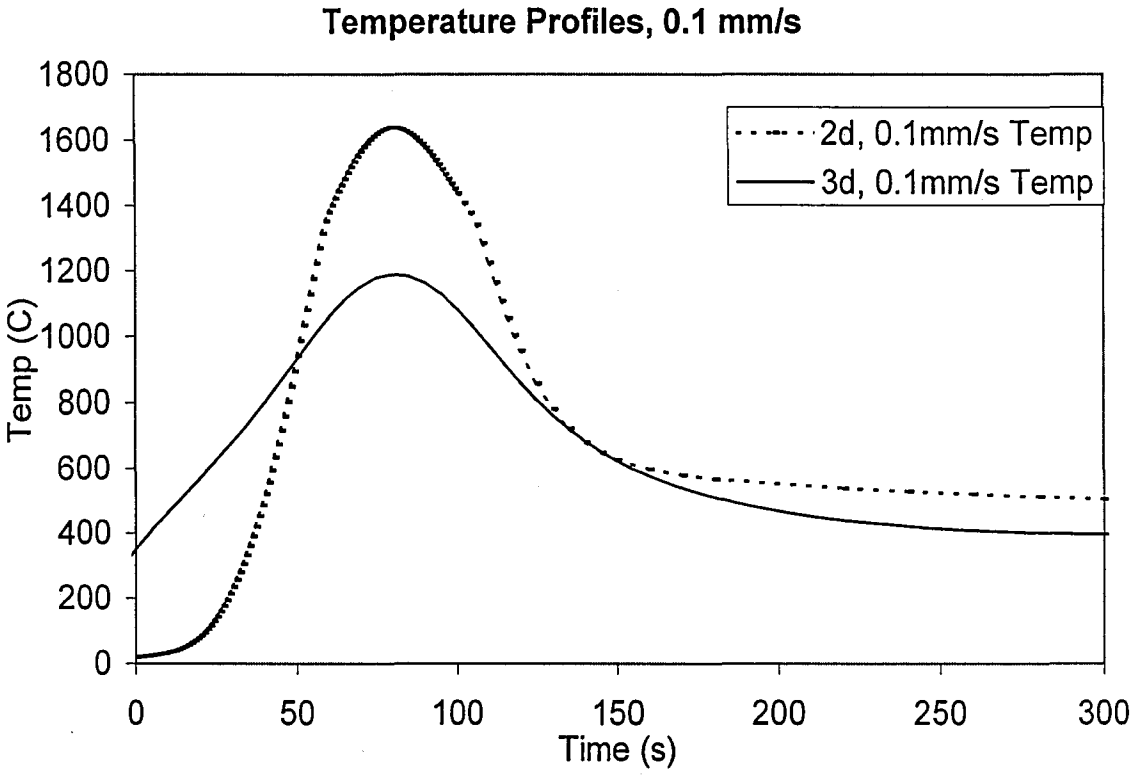

Figure 14 – 0.1mm/s Welding Comparison

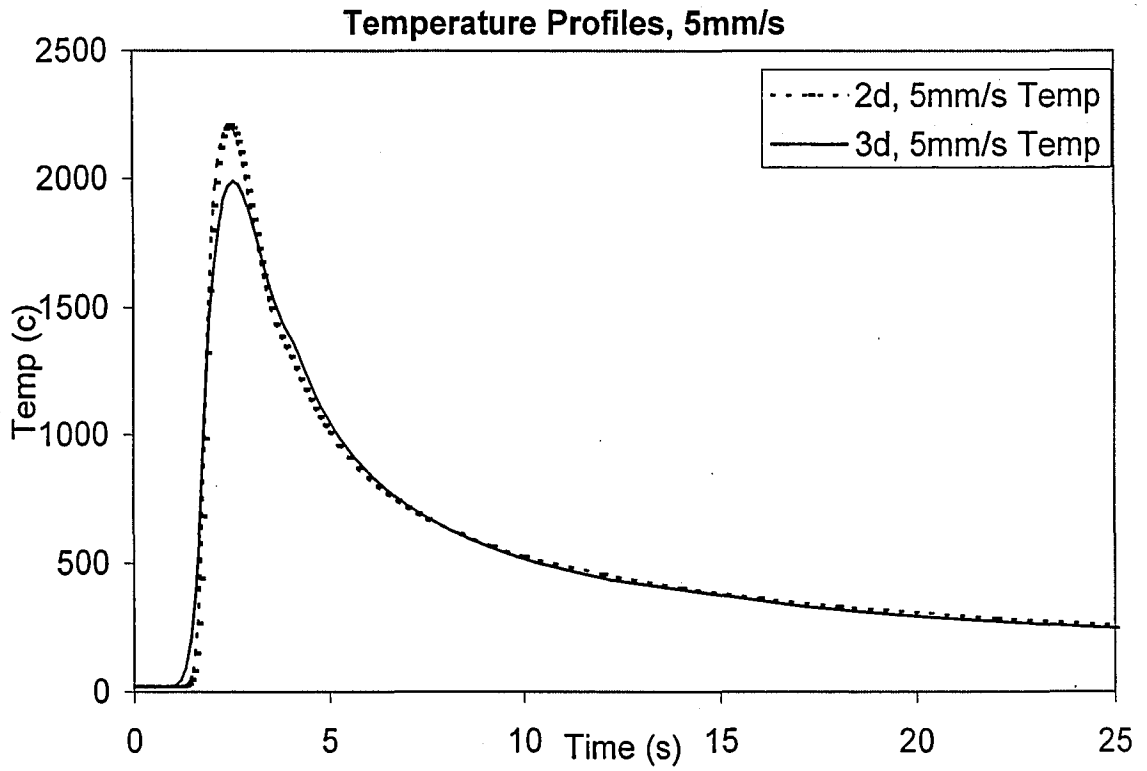

Figure 15 – 5mm/s Welding Comparison

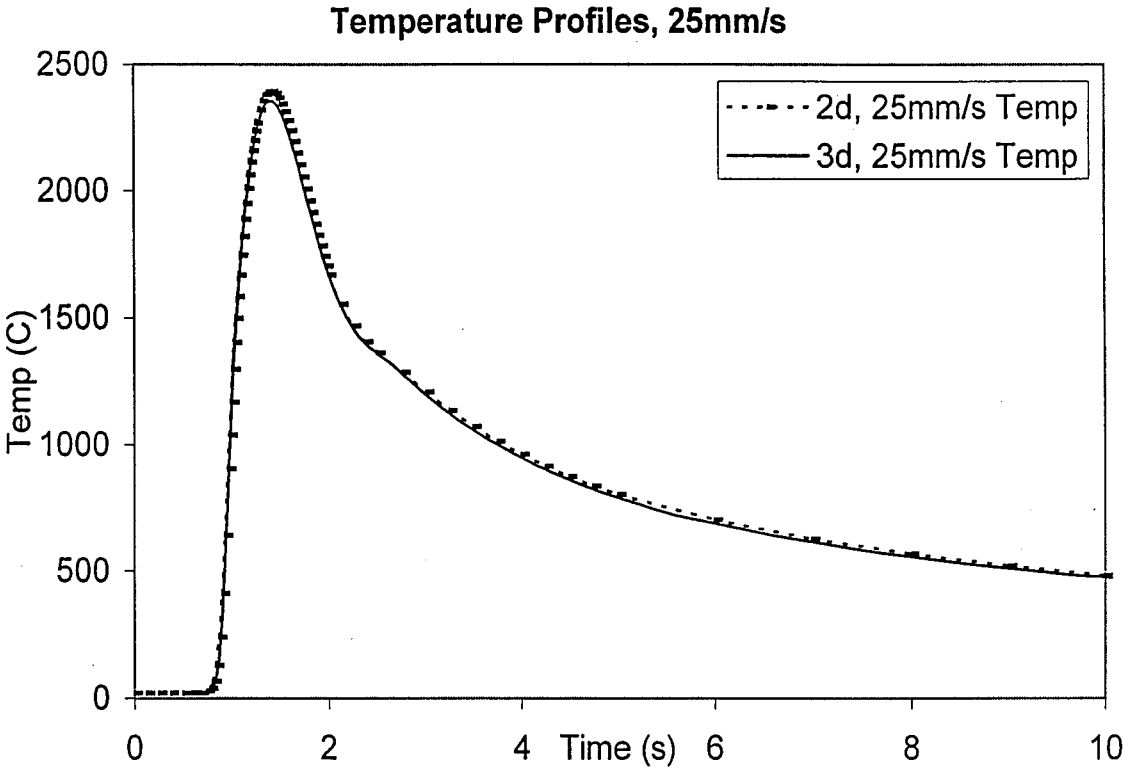

Figure 16 – 25mm/s Welding Comparison

Three-dimensional models (Figure 9) offer good accuracy for low speed welding and the best overall thermal picture. However, these benefits come with tremendous computational expense and storage requirements. Modeling is also more difficult, as is post processing. The three-dimensional models considered in this section took between ten and twelve hours on an SGI Origin 3800, while two-dimensional models took twenty to forty minutes on a much less powerful SGI O2. Clearly, these savings are substantial enough that two-dimensional modeling is preferable whenever it is applicable. It is also very important to note that the three-dimensional models considered here are extremely simple. For any realistic model, computation time becomes prohibitive.

2.3 Source Modeling

One of the most obvious and important requirements of a welding simulation involves the input of heat to a model. Rosenthal's early model approximated this input as a single, infinitesimal point, leading to an infinite peak temperature.

$$T(w,y,z) = T_0 + \frac{Q_p e^{-\frac{v(w+R)}{2K}}}{2\pi\lambda R} \tag{2.2}$$

Rosenthal's solution for a thick plate is shown in Equation 2.2. Here, T_0 is the base temperature of the plate, Q_p is the power input by the heat source, v is the welding velocity, w is the moving coordinate ($w = x - vt$), λ is the thermal conductivity, κ is the thermal diffusivity ($\kappa = \frac{\lambda}{\rho C_p}$), and R is the distance from the heat source ($R = \sqrt{w^2 + y^2 + z^2}$)

The two-dimensional disk models that followed eliminated the peak temperature problems, but still lead to convergence problems as energy is applied over a small area and no depth. The mathematical formulation of the two-dimensional Gaussian disk source is shown in Equation 2.3.

$$q(r) = q(0)e^{-Cr^2} \tag{2.3}$$

Here, *q(r)* is the surface flux at radius *r*, *q(0)* is the maximum surface flux at the center of the heat source, *C* is the concentration coefficient, and *r* is the radial distance from the center of the source. (Ref 9)

The model best suited for arc-welding applications is the Goldak, or double ellipsoid, source. (See Figure 17) Goldak's source corrects the Rosenthal model's point source assumption by distributing power through a volume of specified size and shape.

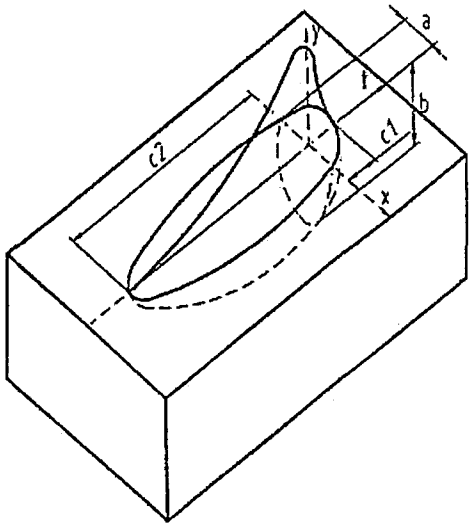

Figure 17 - Goldak Source

This size and shaped is adjusted through a number of Gaussian parameters, each independently controlling the width, forward length, rearward length, and depth of heating. By manipulating these parameters, the heat source can be changed to reflect a very wide variety of welding conditions. The formulation of the Goldak model is shown in Equations 2.4 and 2.5. By using different parameters for the front and rear ellipsoids, it is possible to specify an asymmetric distribution of power. Here, f_f and f_r are the fractions of power sent to the front and rear ellipsoids, respectively. Parameters a, b, c_f, and c_r determine the shapes of the ellipsoids as shown in Figure 17. Finally, Q is the total power that enters the part, given by $Q = \eta VI$, where η is the arc efficiency, V is the voltage, and I is the current. (Ref 9)

$$q(x,y,z,t) = \frac{6\sqrt{3}f_f Q}{abc_f \pi\sqrt{\pi}} e^{-3x^2/a^2} e^{-3y^2/b^2} e^{-3[z+v(\tau-t)]^2/c_f^2} \quad (2.4)$$

$$q(x,y,z,t) = \frac{6\sqrt{3}f_r Q}{abc_r \pi\sqrt{\pi}} e^{-3x^2/a^2} e^{-3y^2/b^2} e^{-3[z+v(\tau-t)]^2/c_r^2} \quad (2.5)$$

One feature of the Goldak source is that the heat intensity (W/mm^3) decreases in all directions according to the aforementioned Gaussian parameters from a single point, usually located on the welding surface. This leads to difficulty when modeling deep, narrow welds. At the bottom of a deep, narrow Goldak source, there is often not enough power to melt the part. For this reason, the Goldak source is not very suitable for modeling laser or electron beam welds. For these applications, a conical heat source is more appropriate.

The conical heat source model is specifically designed for laser and electron beam welding applications. (Figure 18) As in the Goldak source, power is distributed through a volume of specified shape. The parameters that determine the shape of the conical source are: the location of the welding surface, the radius at the top of the weld, the radius at the bottom of the weld, and the depth of the weld. The formulation of the conical source is shown in Equation 2.6.

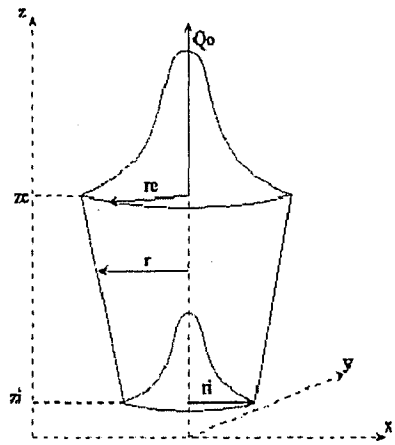

Figure 18 - Conical Source

Here, Q is the total power entering the part, r_e is the radius of the source at the surface of the part, r_i is the radius of the bottom of the source, y_e is the y location of the top of the source, and y_i is the y location of the bottom of the source. Also, $r_0(y)$ is given by $r_0(y) = re - \frac{(re - ri)(ye - y)}{(ye - yi)}$.

$$q(r, y, t) = -\frac{9Q}{\pi(r_e^2 y_i + y_i r_i^2 + r_e r_i y_i - r_e^2 y_e - y_e r_i^2 - y_e r_i r_e)} e^{-3\frac{r^2}{r_0(y)^2}} \quad (2.6)$$

To more accurately model deep welds, heat intensity decreases from the axis of the laser instead of from a point. Therefore, material at the bottom of the weld melts without overheating material at the top surface of the part. The conical welding source is also very useful in modeling deep welding applications associated with the keyhole effect. In keyhole welding, there is sufficient energy to cause evaporation in the weld pool. The hole formed by the vaporized metal allows multiple laser reflections and drastically increased absortivity. (Ref. 20) As the objective of this research involves laser

deposition of metals with the LENS process, it is important to note that the LENS process does not enter the keyhole mode.

The models generated in this section are for the purpose of determining the effects of different parameters on thermal and mechanical models. As more information is available about the Goldak source as well as more sets of parameters published, the Goldak source was used in nearly all test models while the conical source was used in the LENS models.

2.4 Thermal Effects of Material Property Inputs

In the following sections, thermal models are constructed and evaluated for various material property inputs. The purpose of this section is to develop at least a qualitative feel for the importance of each input on thermal results. Models are evaluated in two and three dimensions, where two-dimensional models consist of 222 nodes and 244 linear elements and three-dimensional models have 2100 nodes and 2262 linear elements. Two-dimensional models were also considered with 8 node quadratic elements, with similar results. The two-dimensional mesh is shown in Figure 20, while the three-dimensional mesh is shown in Figure 21. Material properties are those of AL6XN stainless steel, and are given in Figure 10. Weld source inputs are identical to those used in Goldak (Ref 9), and are listed in Figure 19.

Velocity	Power	a	b	Zf	Zr	Qf	Qr
mm/s	W	mm	mm	mm	mm		
5	33000	15	15	15	30	0.6	1.4

Figure 19 – Source Parameters for Input Comparisons

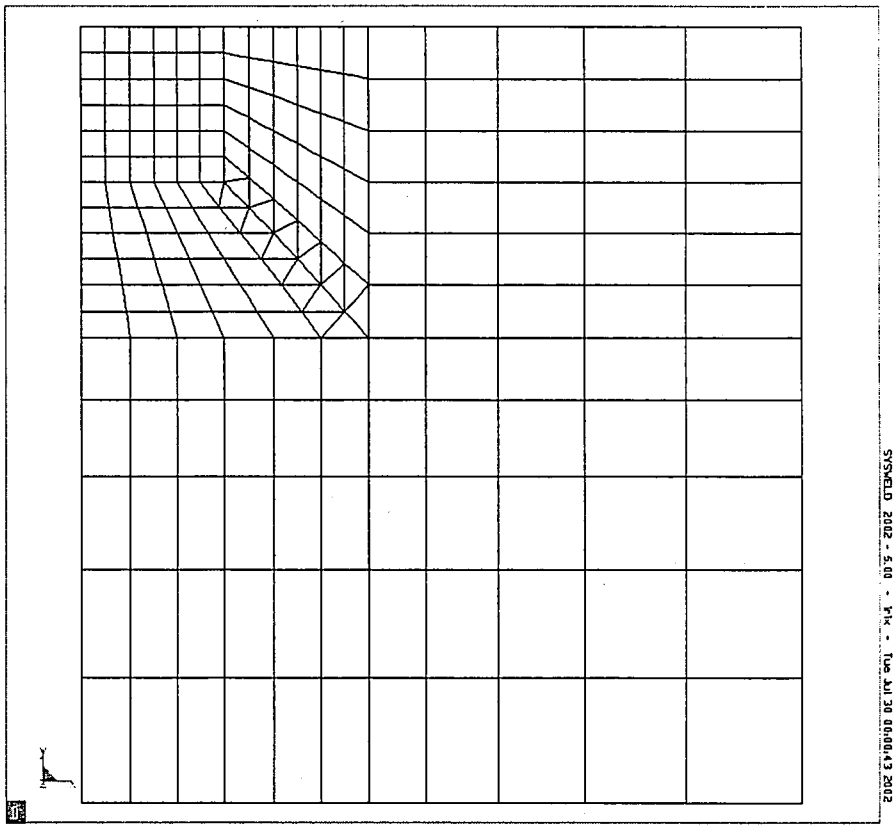

Figure 20 – Two-Dimensional Mesh for Thermal Input Comparison

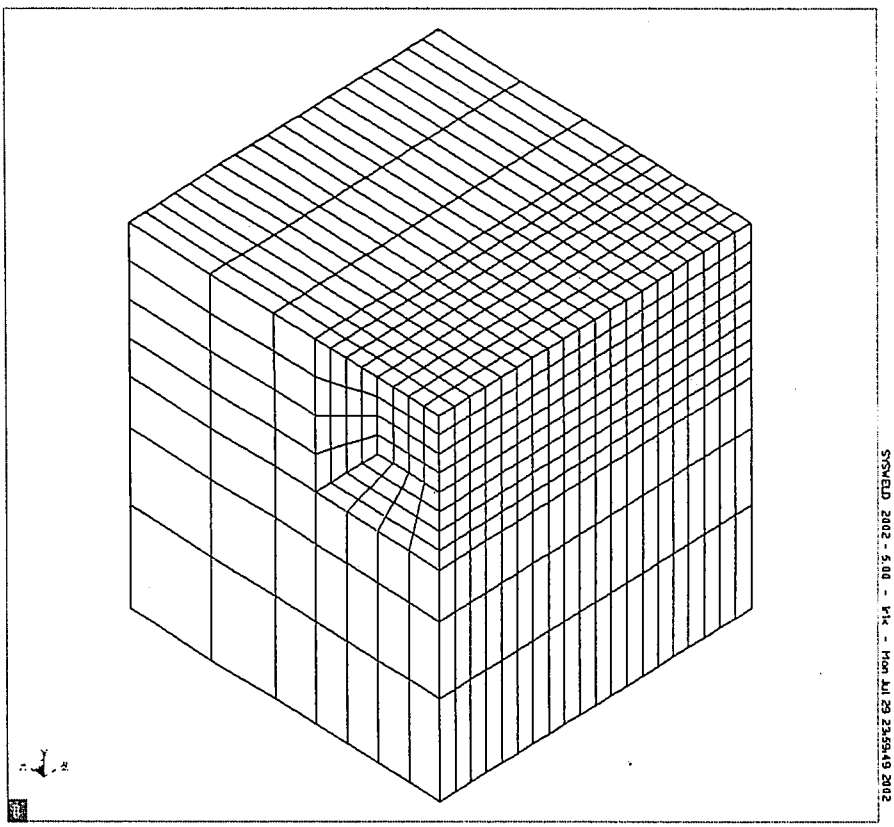

Figure 21 – Three-Dimensional Mesh for Thermal Input Comparison

2.5 Heat of Fusion

Heat of fusion is energy required to change a solid at its melting temperature to liquid at the same temperature. Clearly, the storage and release of latent heat of fusion is a phenomenon that occurs continuously in welding. In the simulation of welding, however, it is not clear what effect the latent heat of fusion has on thermal and mechanical results. Previous welding models (Refs 9,21) have accounted for the heat of fusion using a variety of techniques. One technique works directly with the enthalpy curve, which increases linearly through the melting range. (See Figure 22) This approach offers the best accuracy and more stability while converging, but is somewhat awkward to employ in most commercial finite element codes. (Ref 21) Sysweld, however, offers a thermal enthalpy option that allows the easy input of enthalpy as a function of temperature. Another technique for accounting for latent heats involves artificially increasing the value of specific heat in the melting range. (Ref. 21)

Adjusting the specific heat in many commercial finite element codes is easier than accessing enthalpies directly, and it is the approach most often used. The original specific heat curve (Figure 23) is increased in the melting range such that the area under the curve, or enthalpy, is unchanged at temperatures below the melting range and is increased such that the area beneath the curve is increased by the latent heat of fusion at temperatures above the melting range. If the specific heat curve is sharply adjusted to reflect the heat of fusion, the model will typically become unstable and will not converge. Therefore, the curve is smoothed and convergence improves, but is still considerably more difficult and requires substantially more iterations to solve than a model that does not account for heat of fusion. (Figure 24) For most steels, the latent heat of fusion is

about 2.1 MJ/m^3 (Refs 9,21). Both enthalpy models and specific heat models have been employed in the models considered in this research with very similar results.

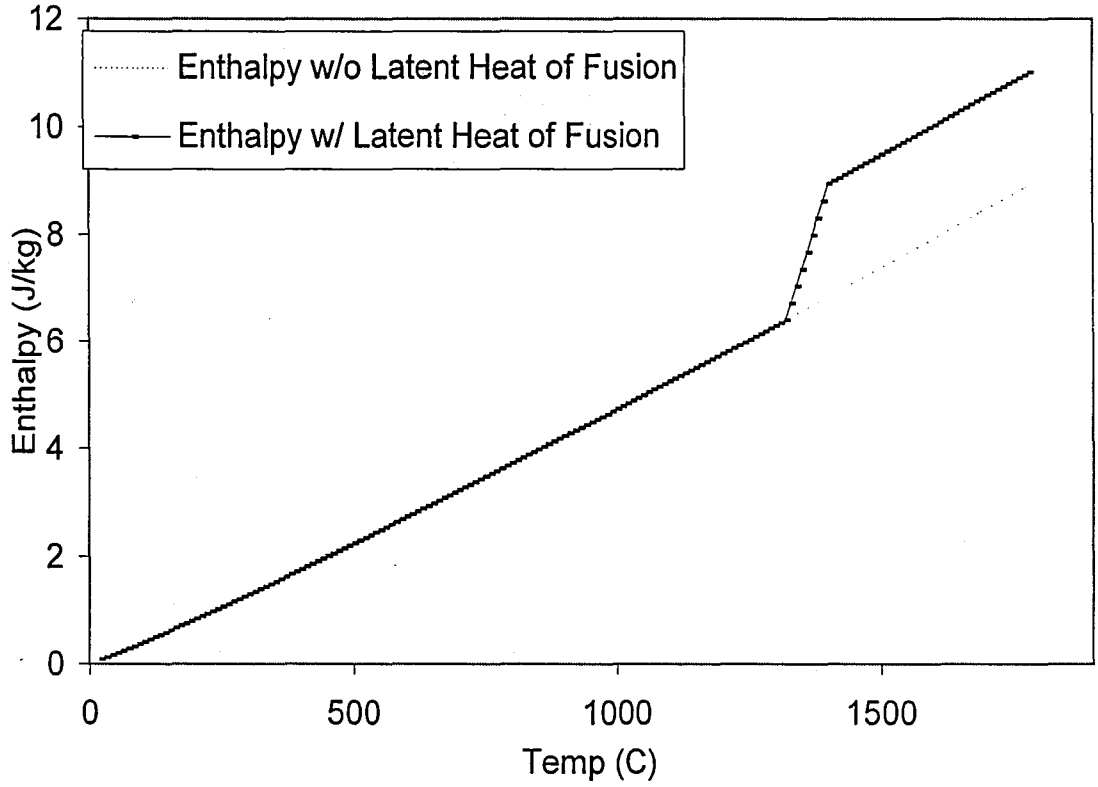

Figure 22 – Enthalpy of AL6XN

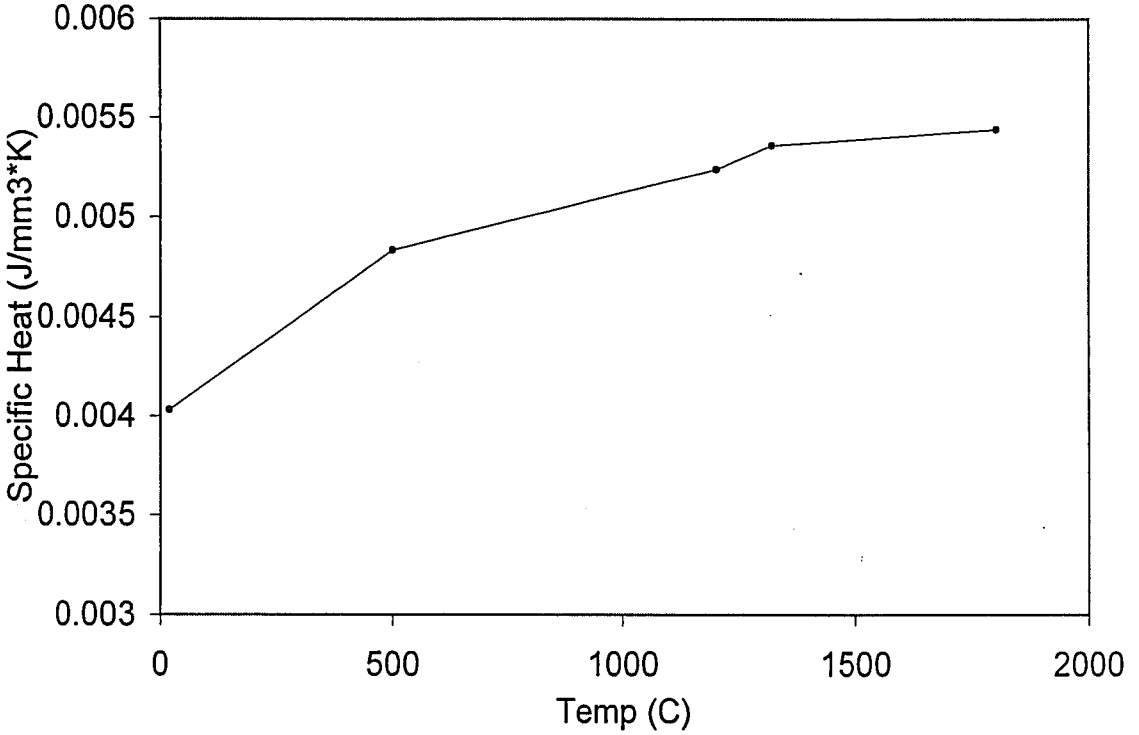

Figure 23 - Unmodified Specific Heat of AL6XN

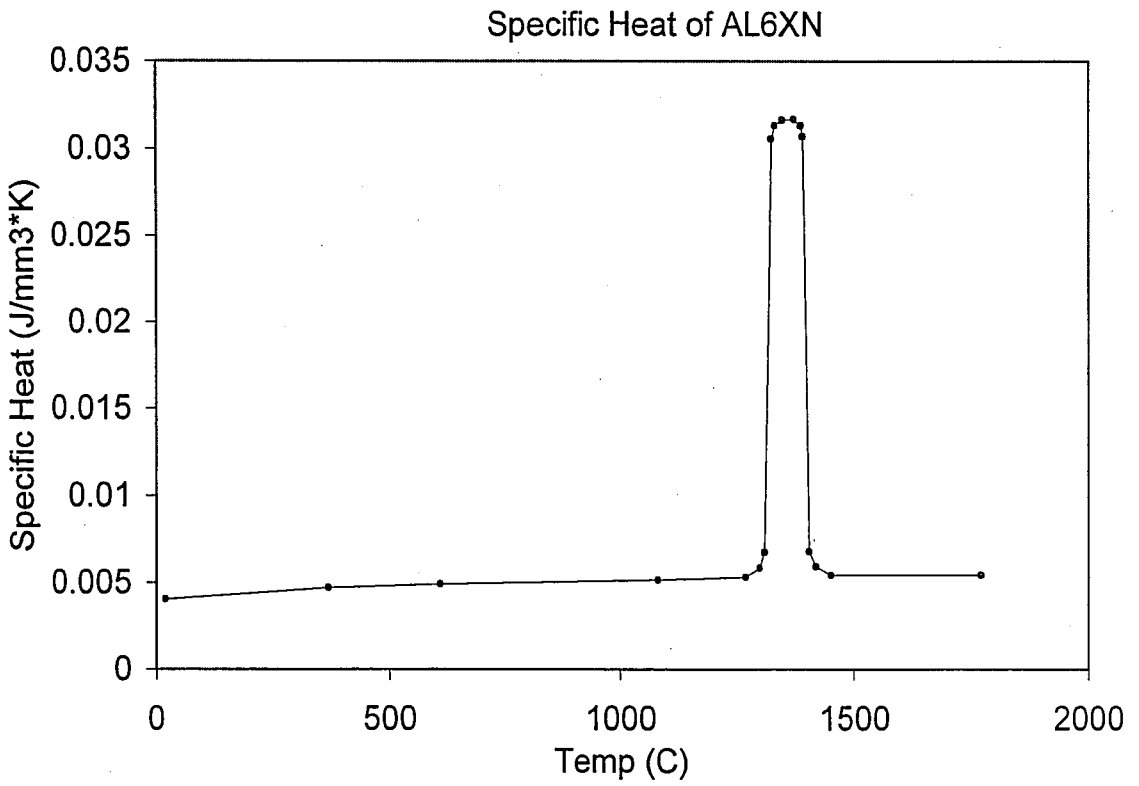

Figure 24 – Adjusted and Smoothed Specific Heat of AL6XN

Including the heat of fusion in a thermal model has several interesting effects. First, the peak temperature and, in general, the temperature of the molten pool, decreases by around a hundred degrees. In one experiment, a simple model with no heat of fusion calculation predicted a peak temperature of 3269°C, while the same model with the heat of fusion calculation predicted a peak temperature of 3143°C (Figure 25). It should be noted that while this difference is fairly typical of results from other simulations, higher peak temperatures yield larger effects from the heat of fusion calculation, while lower peak temperatures see smaller effects.

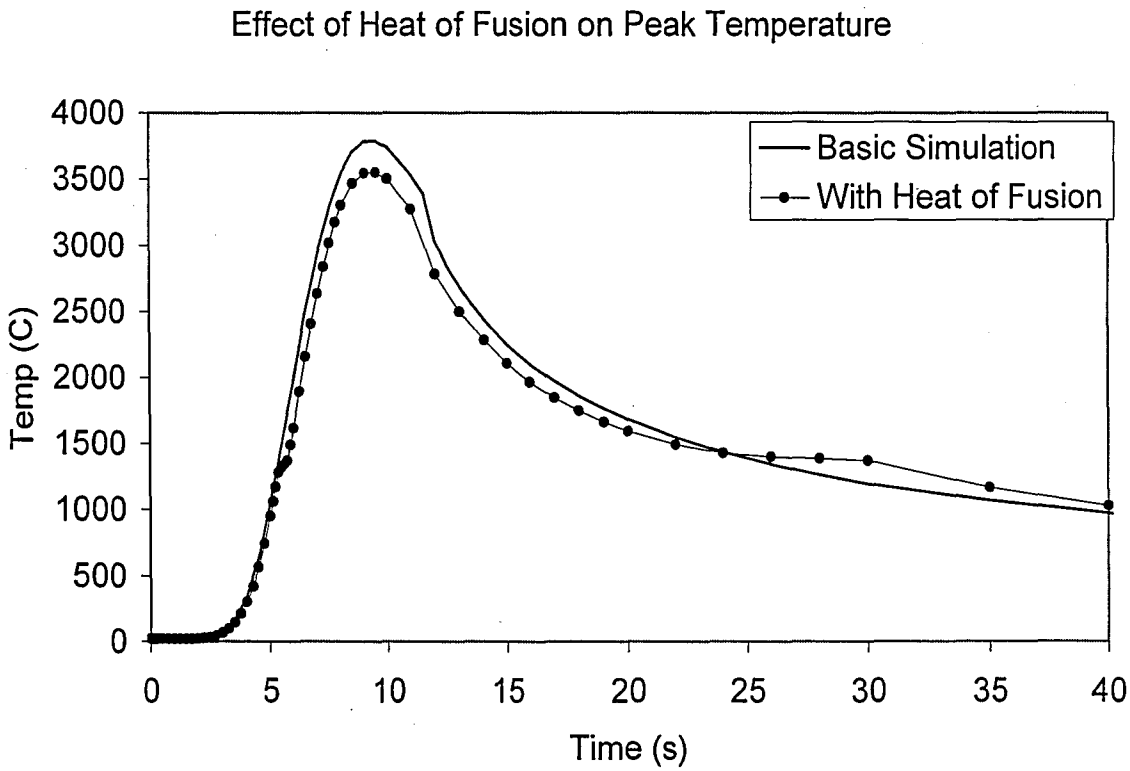

Figure 25 - Peak Temperature Profiles

Also, the predicted size of the fusion zone is smaller when accounting for latent heat of fusion. In the aforementioned simulation, the half width of the predicted fusion zone in the model without a heat of fusion adjustment was 15.25 mm, while the half

width of the fusion zone with the heat of fusion adjustment was 14.35 mm (See Figure 9). This is as one might expect, as more energy is required to change from solid to liquid.

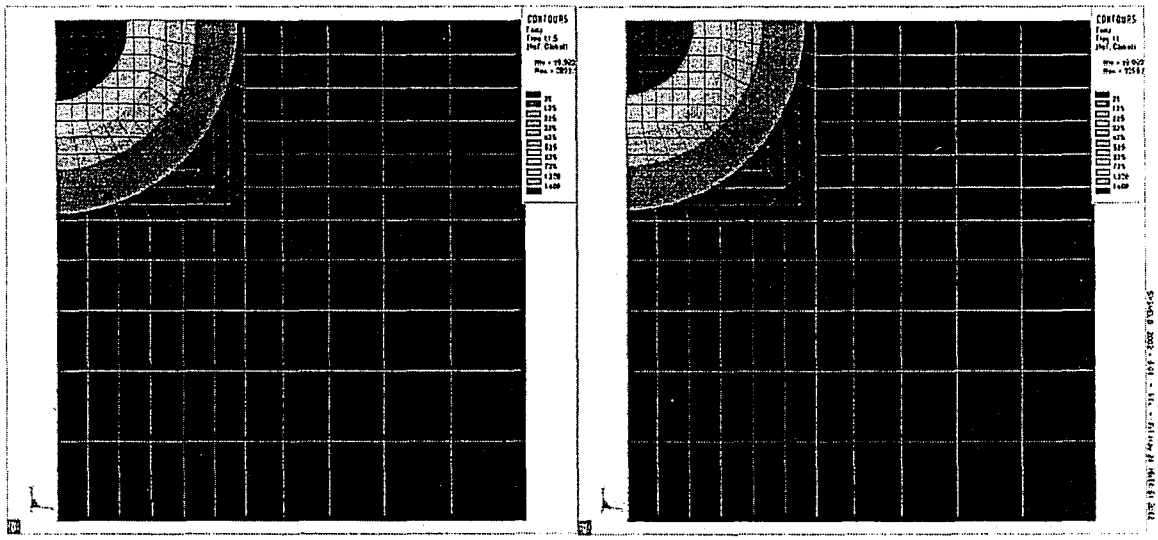

Figure 26 - Fusion Zone Comparison

2.6 Convective Mixing in Molten Pool

In recent years, much attention has been paid to the modeling of fluid flow in the molten pool. Models including magnetohydrodynamic effects, thermo-solutal buoyancy effects, and Marangoni or surface tension effects have been developed with considerable success and offer new insight into the formation of the melt pool in welding. (Refs 21, 22, 23, 24) As the research outlined in this paper represents a first attempt at modeling direct metal deposition, the remarkable complexity associated with modeling the aforementioned convective effects is not appropriate here. By artificially increasing the thermal conductivity above the melting temperature, one can achieve a reasonable approximation for the effects of convective mixing without much increase in complexity or solution times (Refs 9, 21). For stainless steels, thermal conductivity in the melting area was increased to 160 W/mK as in Leung et al. (Ref 25) (See Figure 27). The effect

width of the fusion zone with the heat of fusion adjustment was 14.35 mm (See Figure 9). This is as one might expect, as more energy is required to change from solid to liquid.

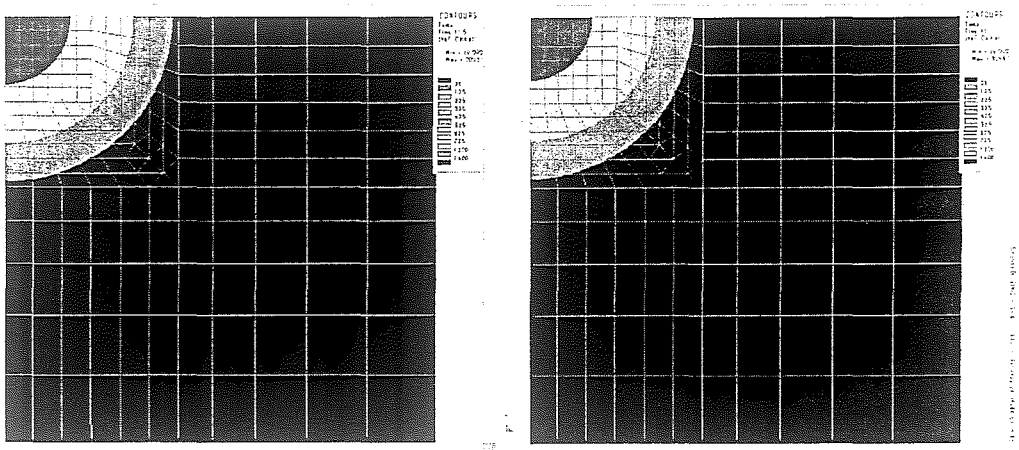

Without Heat of Fusion With Heat of Fusion

Figure 26 - Fusion Zone Comparison

2.6 Convective Mixing in Molten Pool

In recent years, much attention has been paid to the modeling of fluid flow in the molten pool. Models including magnetohydrodynamic effects, thermo-solutal buoyancy effects, and Marangoni or surface tension effects have been developed with considerable success and offer new insight into the formation of the melt pool in welding. (Refs 21, 22, 23, 24) As the research outlined in this paper represents a first attempt at modeling direct metal deposition, the remarkable complexity associated with modeling the aforementioned convective effects is not appropriate here. By artificially increasing the thermal conductivity above the melting temperature, one can achieve a reasonable approximation for the effects of convective mixing without much increase in complexity or solution times (Refs 9, 21). For stainless steels, thermal conductivity in the melting area was increased to 160 W/mK as in Leung et al. (Ref 25) (See Figure 27). The effect

of this adjustment on temperatures in the molten zone is substantial. In the basic experiment described in Section 2.4 and shown in Figure 25, the peak temperature in the center of the weld was 3269°C. The increased thermal conductivity in the molten zone lowered this peak temperature to 2347°C as shown in Figure 28. Also, the radius of the fusion zone increased from 15.25 mm to 16.85 mm.

Clearly, to achieve a truly accurate model of any welding process, future simulations will have to confront the significant complication of modeling fluid flow inside the molten zone. However, as a first approximation, adjusting the thermal conductivity in the molten zone yields a significant improvement in model realism.

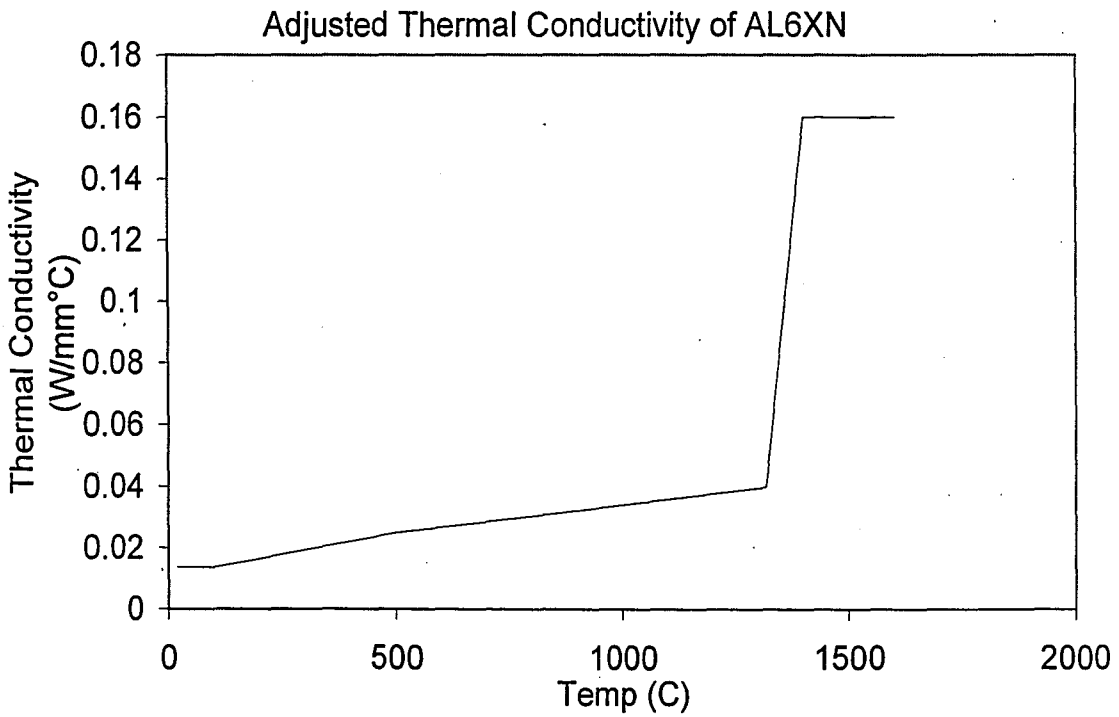

Figure 27 – Adjusted Thermal Conductivity of AL6XN

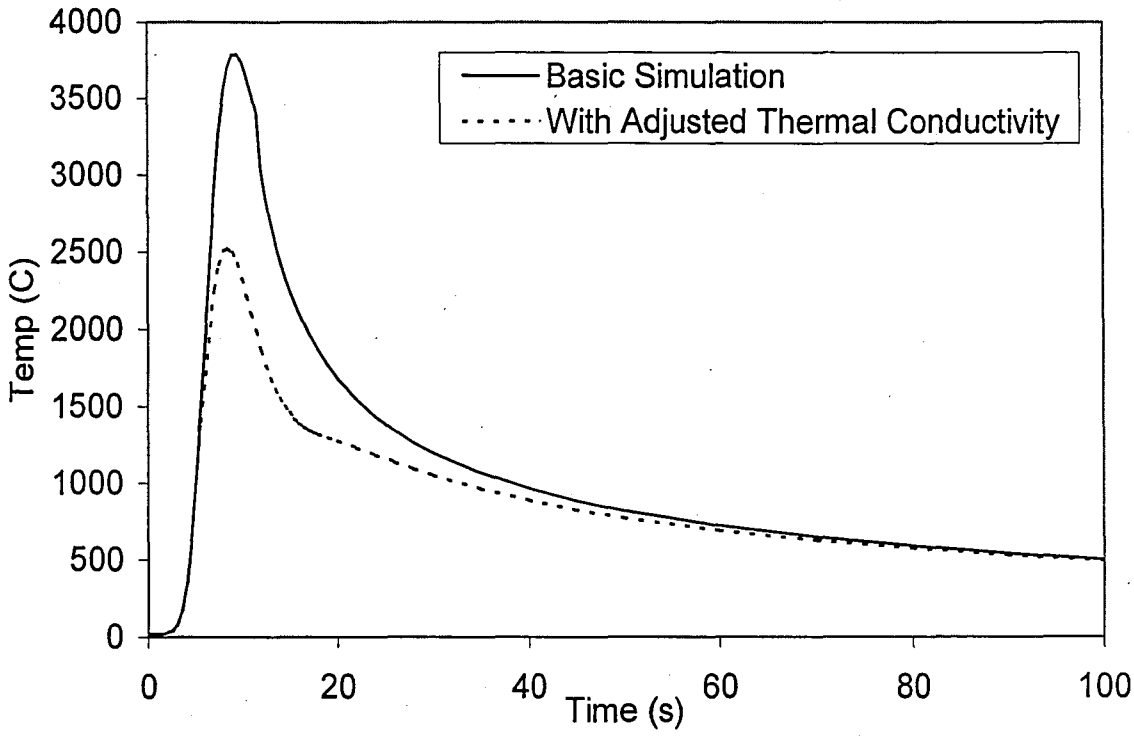

Figure 28 – Thermal Effect of Adjusted Thermal Conductivity

While the effects of the heat of fusion and convective mixing in the molten pool have both been considered individually, these phenomena are both present in all welding applications. Therefore, for maximum realism, a model was considered with both phenomena. This model exhibited a peak temperature of 2224°C. Temperature profiles are shown in Figure 29. Fusion zone predictions increased from 15.25mm to 16.3mm in radius. It should be noted that the baseline model, without corrections, indicated a peak temperature well above the vaporization temperature of commonly welded metals, while models with adjusted thermal conductivity and latent heat of fusion give peak temperatures that are reasonable for high power arc-welding applications. This suggests that to achieve a realistic thermal model, it is quite important to account for both heat of fusion and convective mixing.

Thermal model accuracy is especially important if metallurgy is of interest, but the dependence of mechanical model accuracy on thermal behavior is largely unknown, and will be explored in the following chapter.

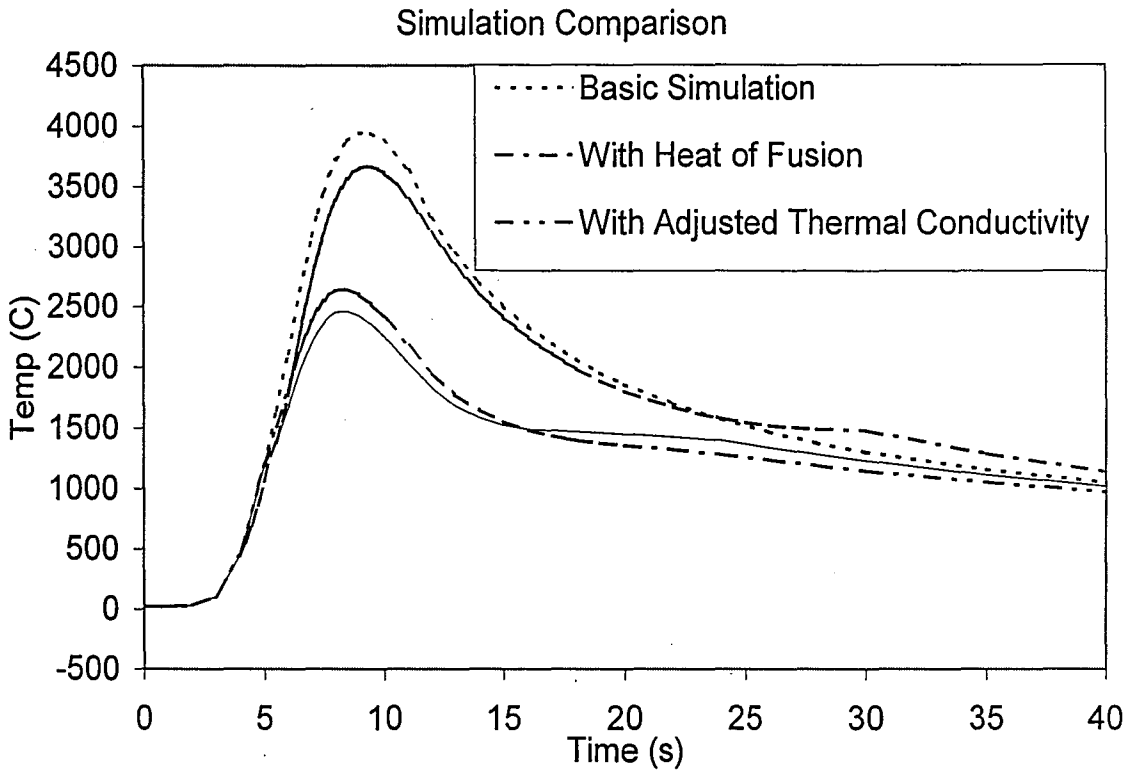

Figure 29 – Thermal Results of Various Simulation Inputs

2.7 Metallurgy and Solid Phase Changes

This study examined the process of welding stainless steel, largely because it exhibits no solid phase changes and leads to very simple metallurgical modeling. Unfortunately, most welding and LENS deposition involves materials that have multiple solid phases. Similar to the latent heat of fusion, there is a latent heat associated with each solid phase transformation. These values are comparatively small and will most likely have a negligible effect on temperature distributions, but must be tested in future models.

2.8 Requirements of Thermal Solutions

One danger of thermal solutions is that time stepping must be carefully considered. Time steps that are too large lead to the loss of important information between time steps, poor simulation convergence, and incorrect integration of material laws in the mechanical simulations that often follow. Time steps that are too fine lead to oscillations in the computed temperature. This instability leads to large errors and results, and can be avoided by adjusting time steps such that:

$$\Delta t > \frac{\rho C_p e^2}{3\lambda}$$

Here, ρ is density, C_p is specific heat, e is the element length in the direction of thermal shock, and λ is thermal conductivity. (Ref. 26)

Chapter 3 - Mechanical Modeling Concerns

While the effects of thermal inputs on the temperature distribution in the weldment are discussed in the previous chapter, thermal history is only an intermediate result in many welding simulations. Often, it is the residual stress and distortion that are of greater interest. This chapter discusses the difficulties of mechanical modeling and attempts to at least qualitatively describe the effects of various inputs on mechanical results.

Results from the thermal finite element models generated in the last chapter are treated here as inputs to mechanical simulations. Again, all simulations are carried out in SYSWELD, and all welding is autogenous. Meshes are identical to those discussed in the previous chapter, but material properties are changed to reflect mechanical instead of thermal behavior.

3.1 General Discussion of Mechanical Simulation

As with thermal simulations, the first major modeling decision is whether to model in two or three dimensions. Advantages of two-dimensional models are once again short solution times, small storage requirements, ease of model generation, and ease of post processing.

In thermal models, temperatures are stored as displacements in elements. Therefore, a linear element allows linear variation of temperature across the element. In a mechanical model with linear elements, nodal displacements are stored and interpolated linearly across elements. From elasticity, we have that stresses are related to strains by Hooke's Law. For example, for isotropic, homogeneous materials, stress and strain are related by equations 3.1.

$$\sigma_{xx} = \frac{E}{(1+\nu)(1-2\nu)}\left[(1-\nu)\varepsilon_{xx} + \nu(\varepsilon_{yy} + \varepsilon_{zz})\right]$$
$$\sigma_{yy} = \frac{E}{(1+\nu)(1-2\nu)}\left[(1-\nu)\varepsilon_{yy} + \nu(\varepsilon_{xx} + \varepsilon_{zz})\right] \quad (3.1)$$
$$\sigma_{zz} = \frac{E}{(1+\nu)(1-2\nu)}\left[(1-\nu)\varepsilon_{zz} + \nu(\varepsilon_{xx} + \varepsilon_{yy})\right]$$

Furthermore, equations 3.2 give strain-displacement relations.

$$\varepsilon_{xx} = \frac{\partial u}{\partial x} + \frac{1}{2}\left[\left(\frac{\partial u}{\partial x}\right)^2 + \left(\frac{\partial v}{\partial x}\right)^2 + \left(\frac{\partial w}{\partial x}\right)^2\right]$$
$$\varepsilon_{yy} = \frac{\partial v}{\partial y} + \frac{1}{2}\left[\left(\frac{\partial u}{\partial y}\right)^2 + \left(\frac{\partial v}{\partial y}\right)^2 + \left(\frac{\partial w}{\partial y}\right)^2\right] \quad (3.2)$$
$$\varepsilon_{zz} = \frac{\partial w}{\partial z} + \frac{1}{2}\left[\left(\frac{\partial u}{\partial z}\right)^2 + \left(\frac{\partial v}{\partial z}\right)^2 + \left(\frac{\partial w}{\partial z}\right)^2\right]$$

By substituting the strains from equation 3.2 into equation 3.1, it is clear that stresses vary linearly with the derivatives of displacements. Therefore, stresses in linear elements are constant across each element. (Ref. 27)

For quadratic elements, temperatures and displacements vary quadratically across elements, but stresses are linear. Since stresses are of great interest and are always represented by a lower order function than temperatures or displacements, a mesh used for a thermal simulation will often be too coarse to provide good results for a mechanical simulation.

Along with finer meshes, mechanical simulations also require finer time stepping, as time step lengths are related to element sizes. A general guideline is to set smaller time steps than the length of the elements along the weld divided by the welding speed. (Ref 28)

The combination of finer meshes and more time steps leads to very large storage requirements. For many of the models discussed in this chapter, none of which are complex, the file containing all of the mechanical results demanded more than fifteen gigabytes of storage. As models become larger and more complicated, file sizes become astronomical.

All of the above concerns apply mainly to three-dimensional models, as it is possible to keep two-dimensional mechanical models fairly small. Unfortunately, the plane strain assumption that is most often used in welding simulations is not without consequence. In plane strain, longitudinal displacements are assumed to be zero, which is simply not true. Experimental measurements of displacement during welding have shown small longitudinal displacements in the direction of welding before the source arrives and a larger displacement in the opposite direction after the source has passed. (Ref. 28) (See Figure 30)

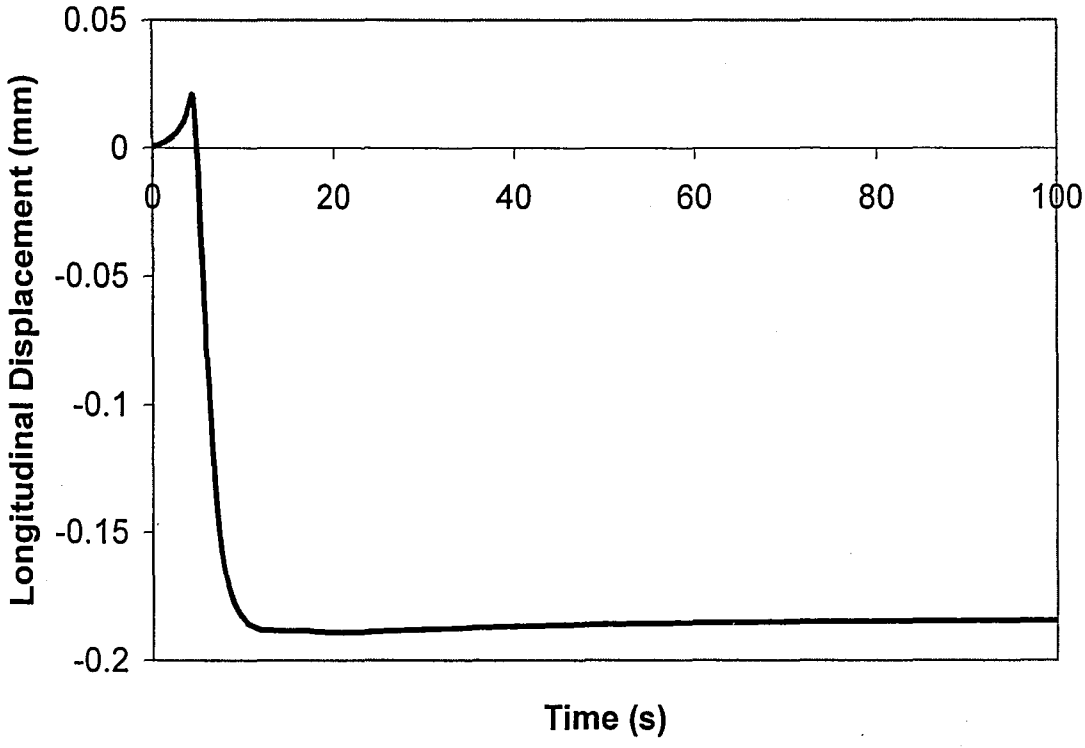

Figure 30 – Longitudinal Displacement of Material Surrounding Weld Pool

By assuming that these displacements do not exist, the compressive stress that occurs before the arrival of the source is overestimated. (See Figure 31)

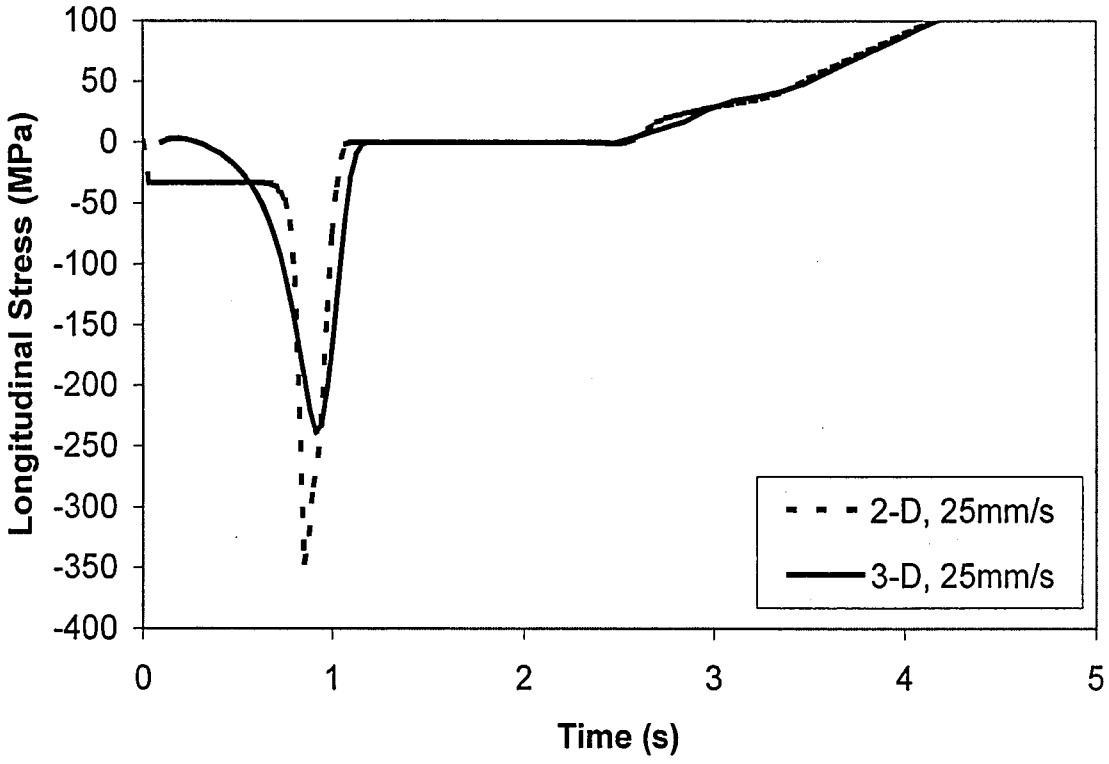

Figure 31 – Initial Compression in Two and Three-Dimensional Models

Also, the final residual stresses in parts are overestimated. More yielding and strain hardening are predicted, which leads to entirely different material properties. Overall, however, accuracy of two-dimensional models improves with welding speeds. (See Figure 32, Figure 33, and Figure 34)

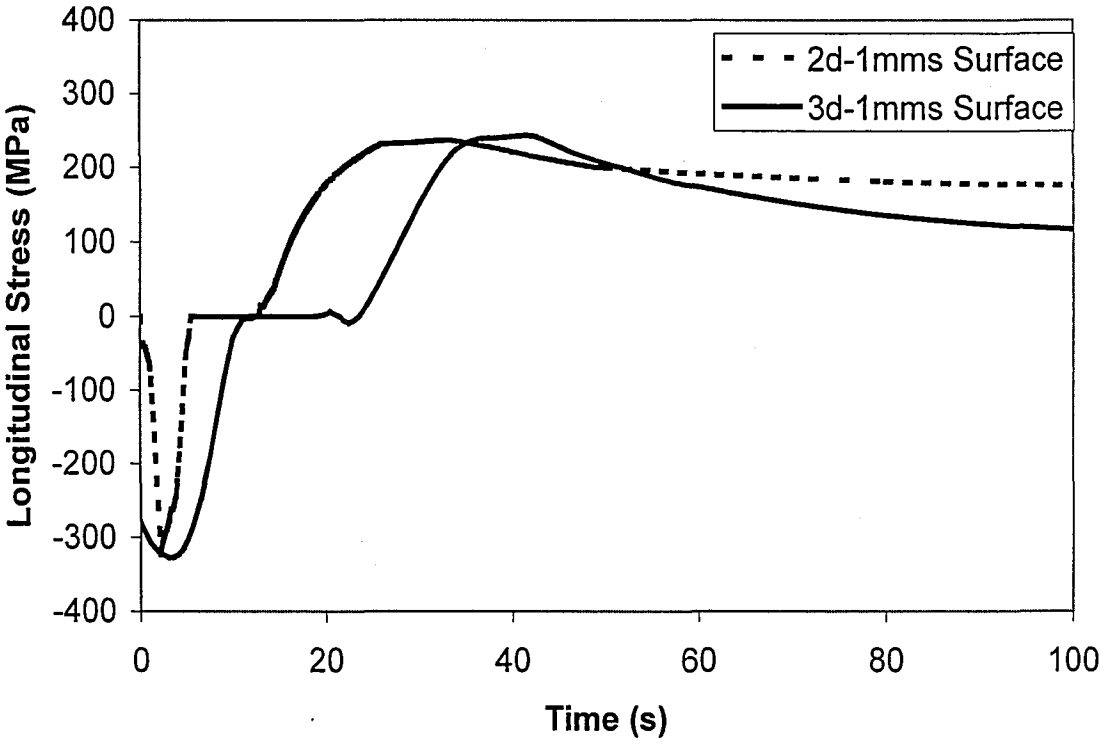

Figure 32 – 2-D vs. 3-D Mechanical Comparison, 1mm/s

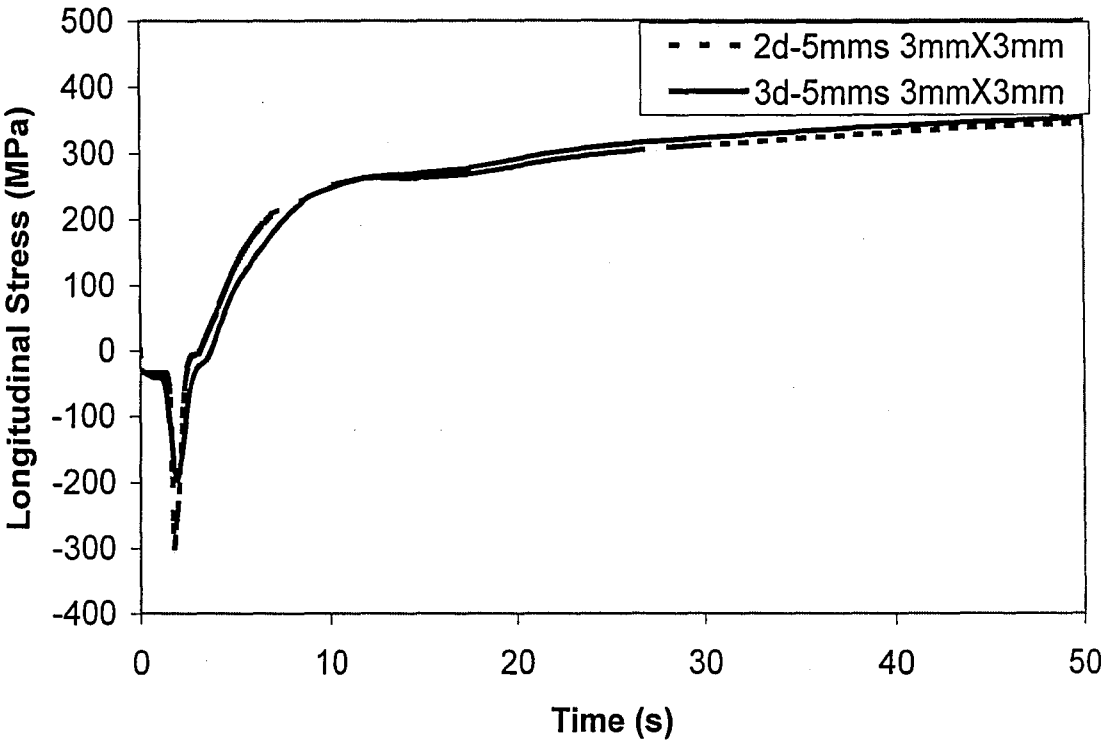

Figure 33 – 2-D vs. 3-D Mechanical Comparison, 5mm/s

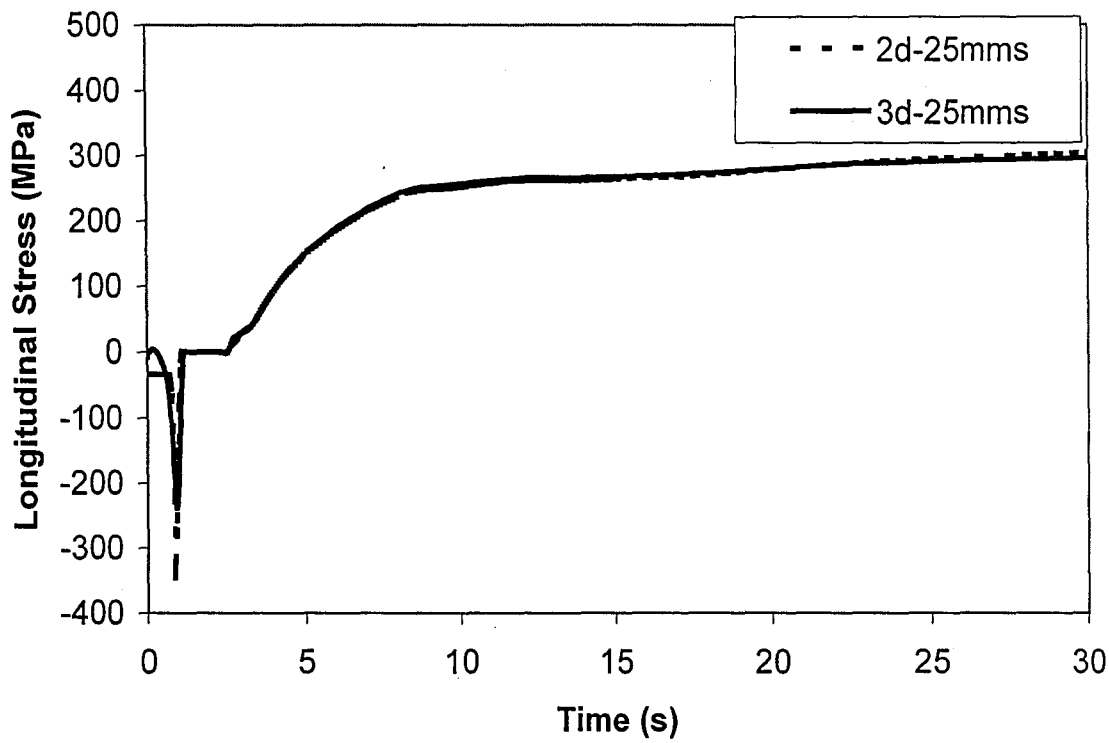

Figure 34 – 2-D vs. 3-D Mechanical Comparison, 25 mm/s

Final cross sections of two-dimensional and three-dimensional models may differ considerably at any welding speed. This is largely due to differences in boundary conditions. In three-dimensional models, both ends of the model are free to expand in the longitudinal direction. This corresponds with reasonable clamping conditions on a thick plate of finite length. These boundary conditions are not realizable with the plane strain assumption, which effectively clamps both ends of a plate in a rigid fixture such that there is no out of plane displacement. This explains the greater yielding experienced by the plane strain model. Also, the area in the block away from the bead experiences some final compression in the plane strain model, while the three dimensional model far from the bead is nearly stress free. This is due in part to the smaller compressive area in the solid model needed to balance the bead, which is yielded in tension, and also due to the more relaxed boundary conditions which allow for out of plane displacement.

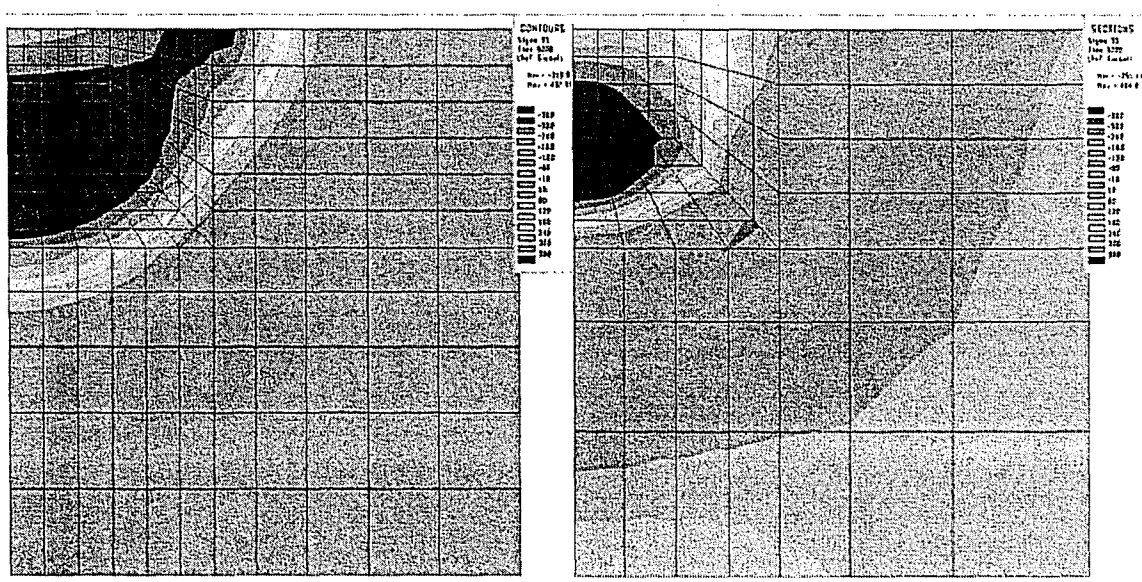

Figure 35 – Final Longitudinal Stress in 2-D (Left) and 3-D (Right) Models

A computationally inexpensive method for improving the results of plane strain models involves generalized strain. The generalized strain model allows the entire

Final cross sections of two-dimensional and three-dimensional models may differ considerably at any welding speed. This is largely due to differences in boundary conditions. In three-dimensional models, both ends of the model are free to expand in the longitudinal direction. This corresponds with reasonable clamping conditions on a thick plate of finite length. These boundary conditions are not realizable with the plane strain assumption, which effectively clamps both ends of a plate in a rigid fixture such that there is no out of plane displacement. This explains the greater yielding experienced by the plane strain model. Also, the area in the block away from the bead experiences some final compression in the plane strain model, while the three dimensional model far from the bead is nearly stress free. This is due in part to the smaller compressive area in the solid model needed to balance the bead, which is yielded in tension, and also due to the more relaxed boundary conditions which allow for out of plane displacement.

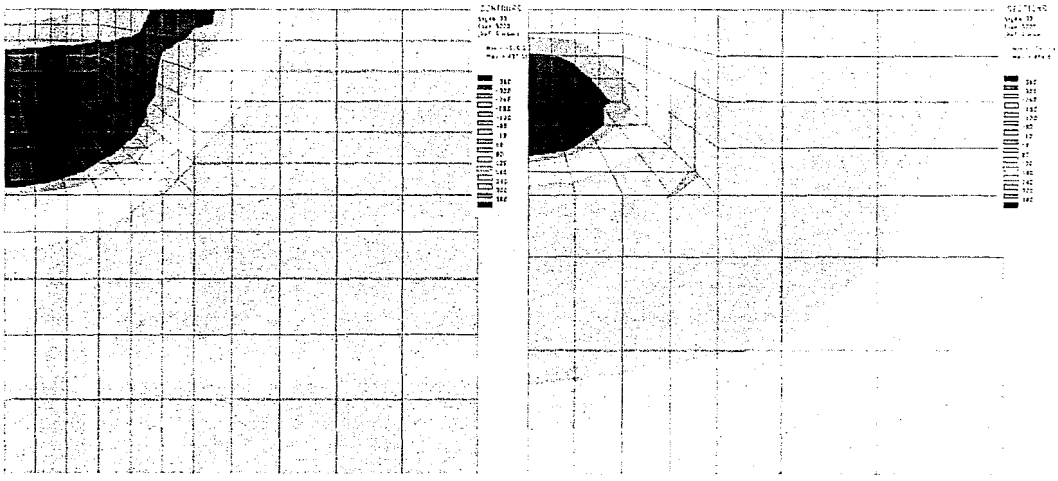

Figure 35 – Final Longitudinal Stress in 2-D (Left) and 3-D (Right) Models

A computationally inexpensive method for improving the results of plane strain models involves generalized strain. The generalized strain model allows the entire

modeling plane to translate in the out of plane direction, relieving a constraint and adding a degree of freedom. (Ref 29) Generalized strain models typically agree more closely with three-dimensional models. (Ref. 28) Result comparisons are given in Figure 36 and Figure 37. It must be noted in these figures that the effect of the generalized strain assumption does not become large until quite late. In Figure 36, the generalized strain model is nearly indistinguishable from the plane strain model. In Figure 37, however, it is quite apparent that the weld bead in the plane strain model moves into progressively higher tension, while the generalized strain and three-dimensional models become stable. Generalized strain models do seem to require slightly finer meshing and more refined time stepping than plane strain models, and must be carefully tested with finer meshes and time stepping to ensure mesh independence.

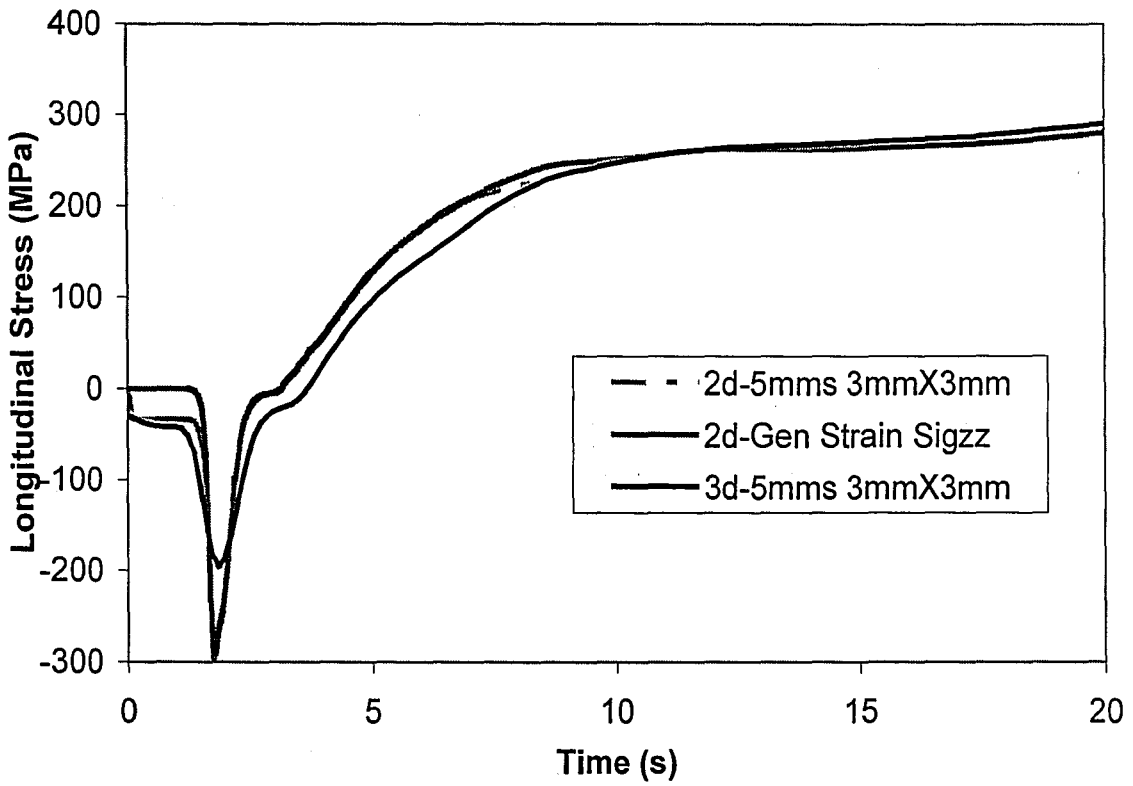

Figure 36 – Effect of Generalized Strain Assumption, t=0 to t=20 Seconds

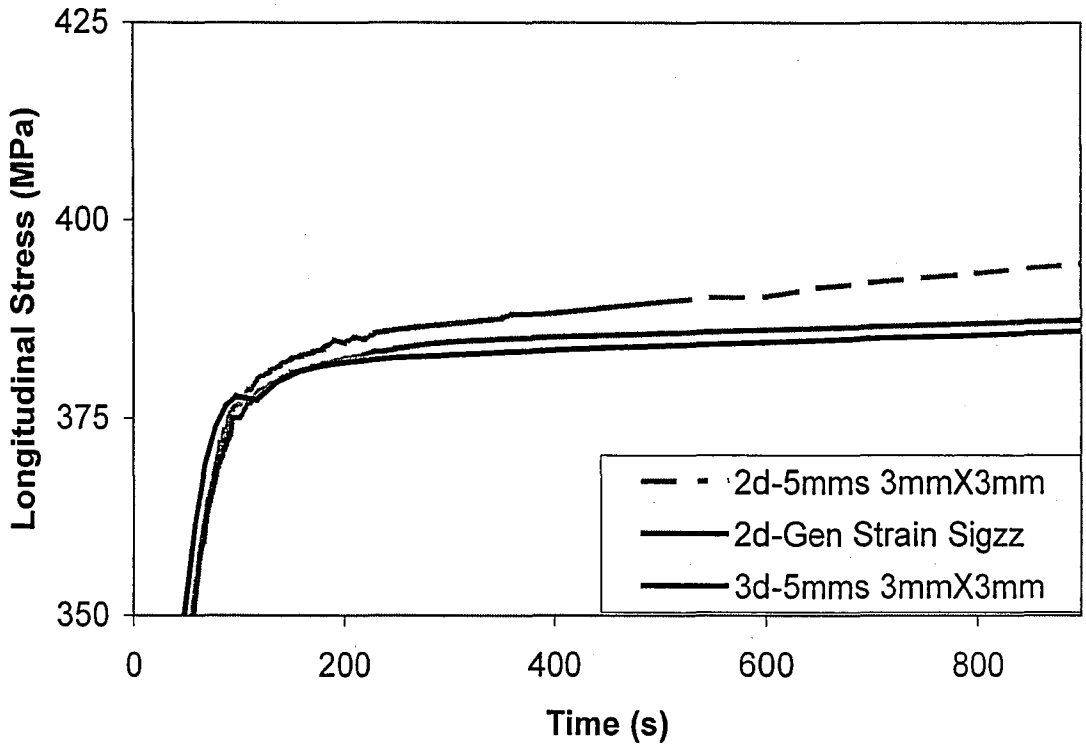

Figure 37 – Effect of Generalized Strain Assumption, t=0 to t=900 Seconds

3.2 Effects of Thermo-Metallurgical Inputs

While the thermal effects of various simulation inputs are well understood from the previous chapter, the effects of different temperature profiles on mechanical results is unclear and not well explored in literature. To determine these effects, mechanical models of all cases were developed and results compared.

The adjustment of thermal conductivity to approximate convection in the molten pool lowers the peak temperature in the center of the weld by over 900 °C. It is somewhat surprising, then, that this temperature difference has very little effect on the mechanical results. The longitudinal stress profile is shown in Figure 38, while the final cross sections are shown in Figure 39. Final stresses are around 350 MPa without adjusted thermal conductivity and 345 MPa with adjusted thermal conductivity. The change in the mechanical results is small most likely because the affected area of the thermal profiles is

almost entirely above the liquidus temperature. At temperatures above melting, the material is stress-free, and upon cooling, it has no memory of the peak temperature.

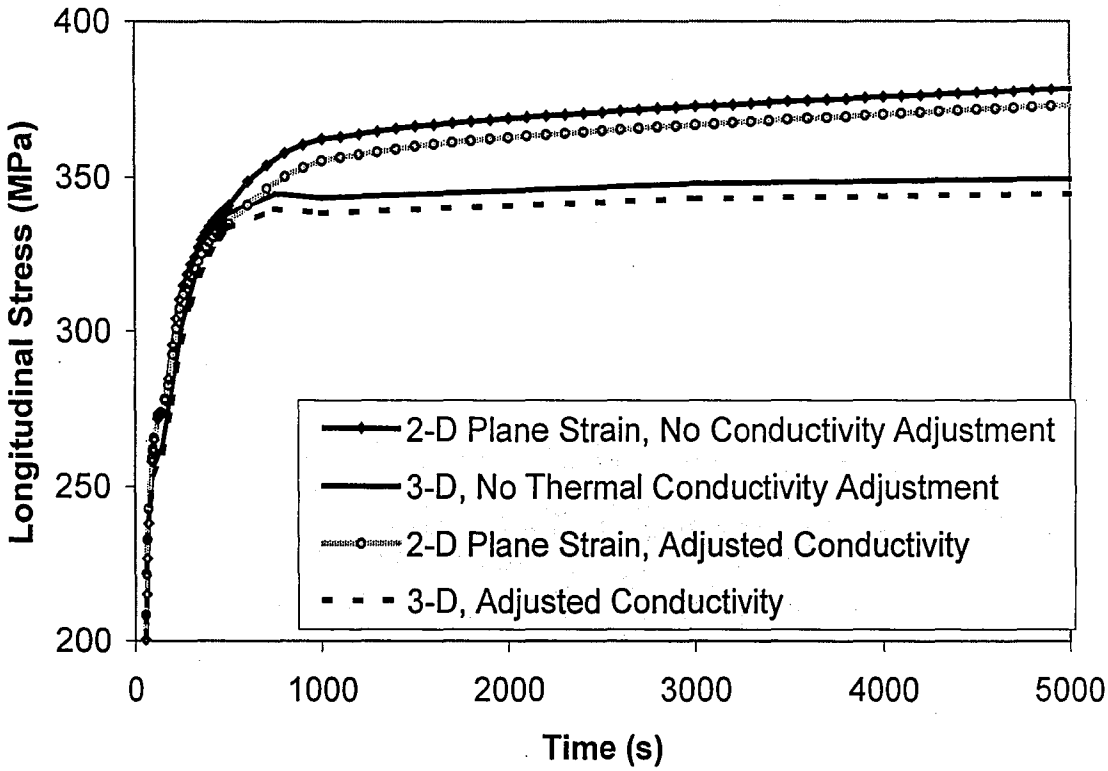

Figure 38 – Longitudinal Stress Profiles With and Without Adjusted Conductivity

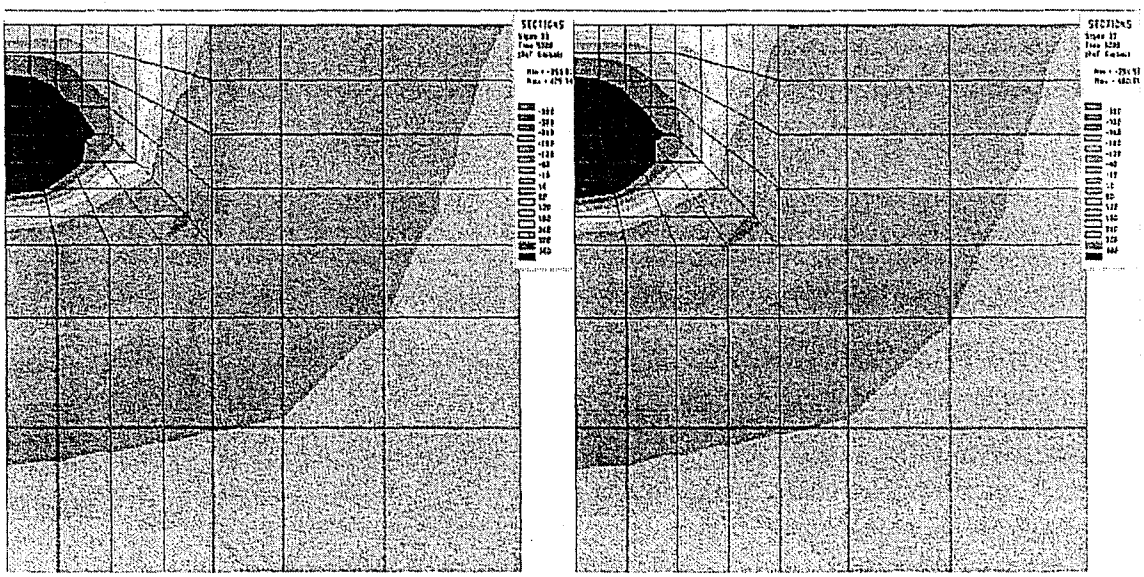

Figure 39 – Final Longitudinal Stress State Without (Left) and With (Right) Adjusted Conductivity

almost entirely above the liquidus temperature. At temperatures above melting, the material is stress-free, and upon cooling, it has no memory of the peak temperature.

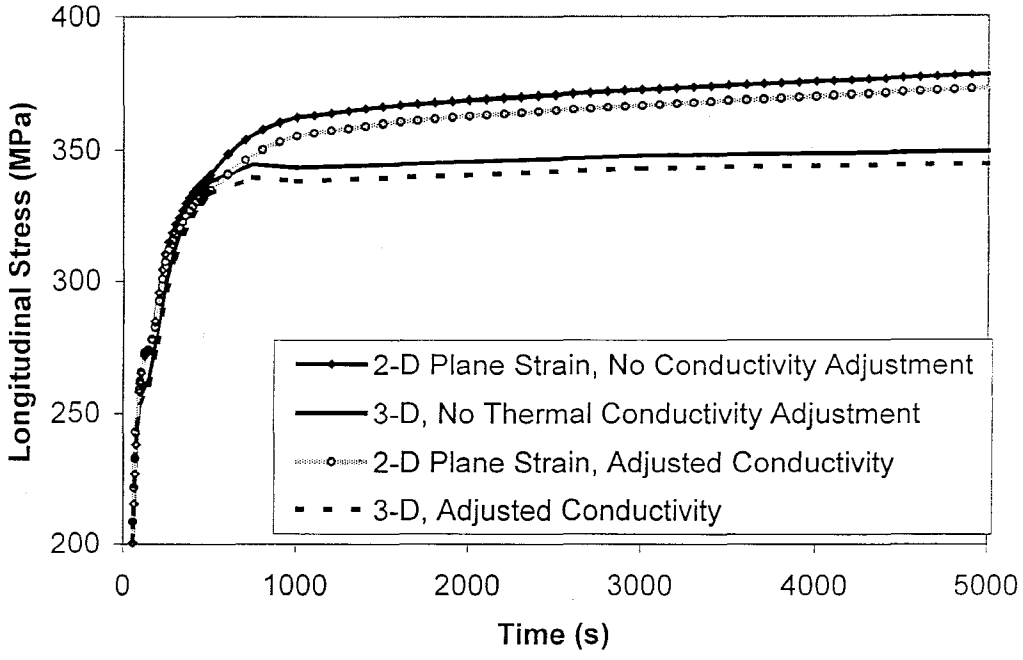

Figure 38 – Longitudinal Stress Profiles With and Without Adjusted Conductivity

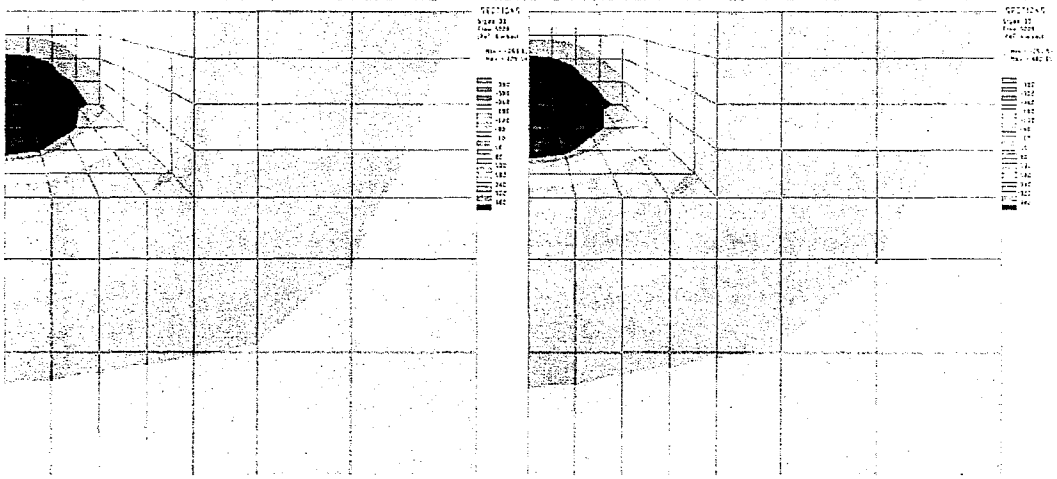

Figure 39 – Final Longitudinal Stress State Without (Left) and With (Right) Adjusted Conductivity

The adjustment for heat of fusion has only a similarly insignificant result on mechanical results. The longitudinal stress profile is shown in Figure 40, and the final cross sections are shown in Figure 41. Here, final stresses with and without the heat of fusion are about 350 MPa. It is interesting to note that while the inclusion of the heat of fusion largely affects temperatures above the solidus, it also changes the cooling rates just after solidification. (See Figure 42) In a simulation accounting for metallurgy, this would likely lead to different solid phase transformations, which would in turn lead to significantly different material properties and a different final state of stress.

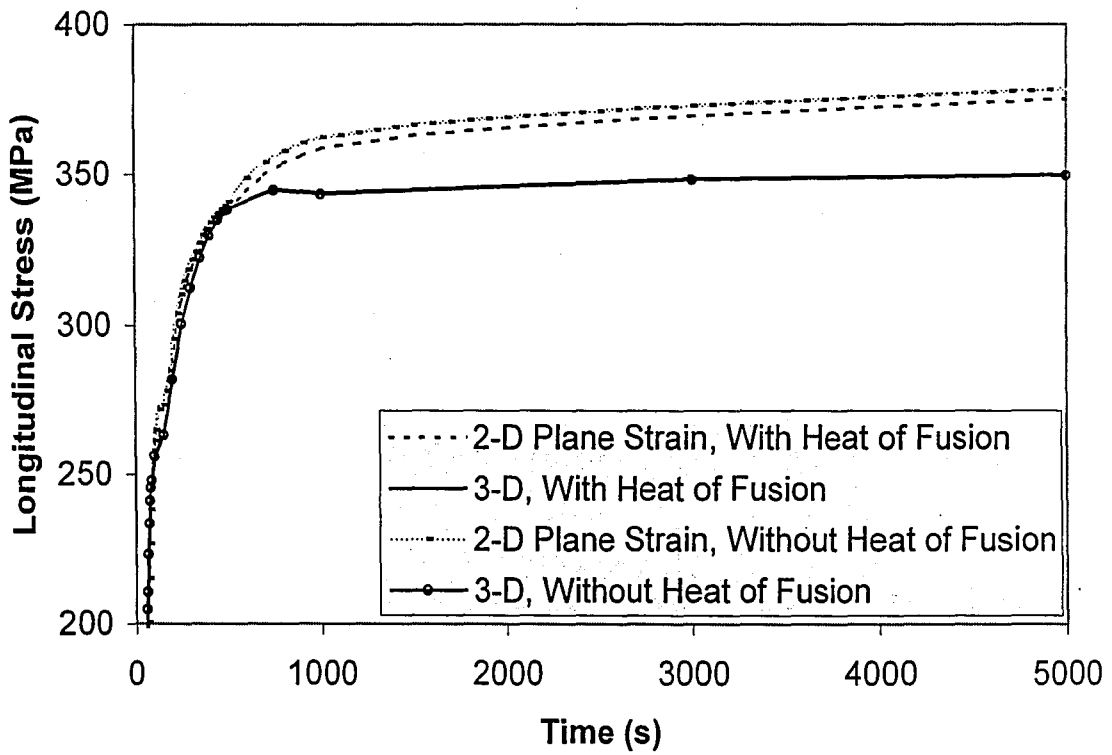

Figure 40 - Longitudinal Stress Profiles With and Without Heat of Fusion

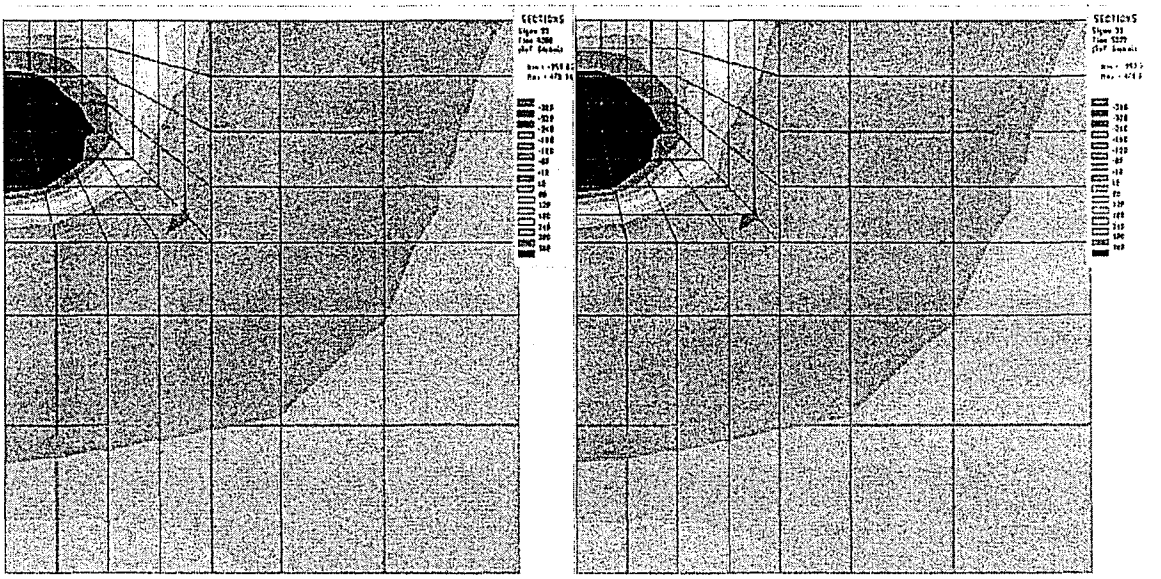

Figure 41 – Final Longitudinal Stress Without (Left) and With (Right) Heat of Fusion

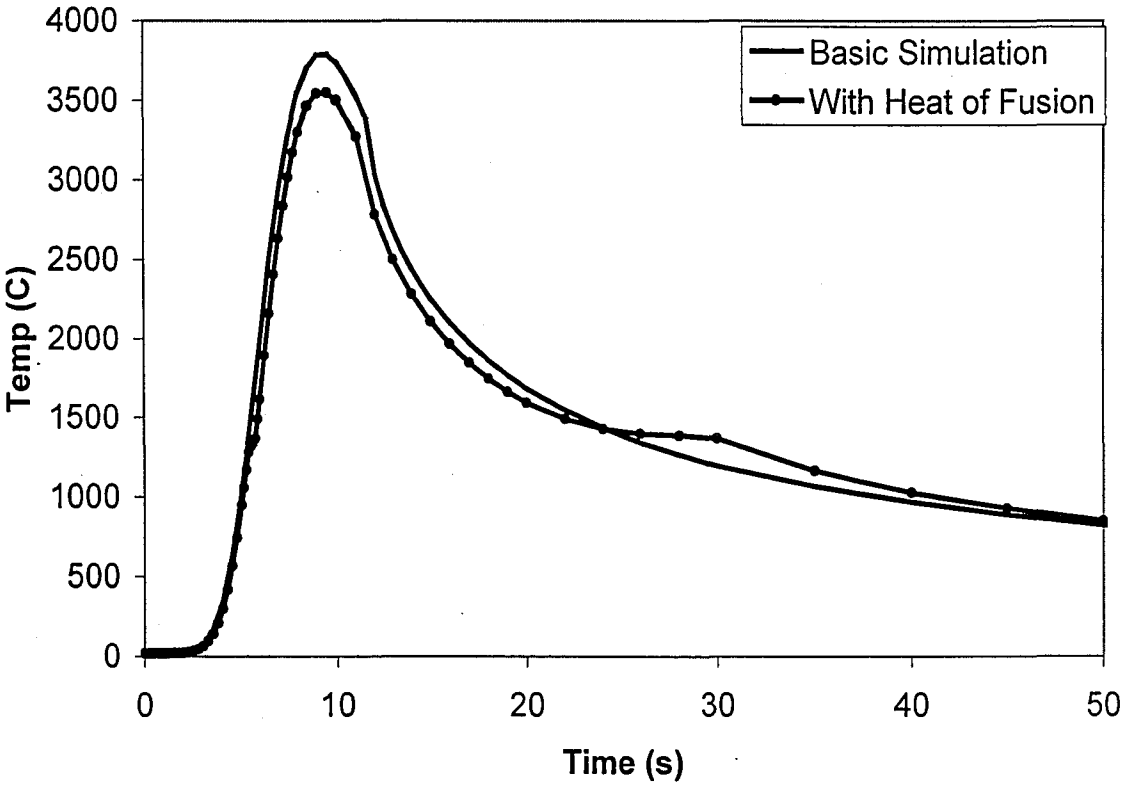

Figure 42 – Temperature Profiles With and Without Heat of Fusion

As neither the adjusted thermal conductivity nor the heat of fusion had a major effect on mechanical results, it is not surprising that the model accounting for both heat of fusion and adjusted thermal conductivity produces similarly negligible changes. Here, the

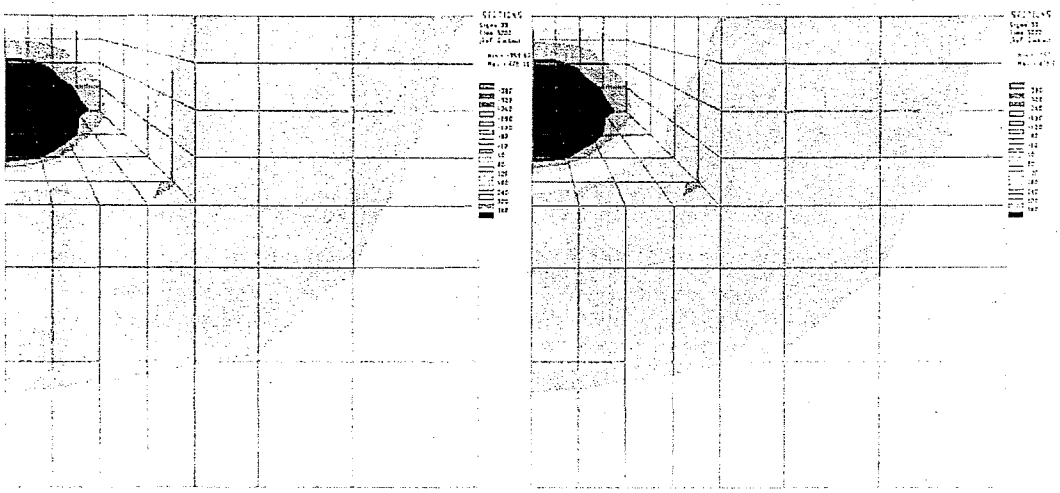

Figure 41 – Final Longitudinal Stress Without (Left) and With (Right) Heat of Fusion

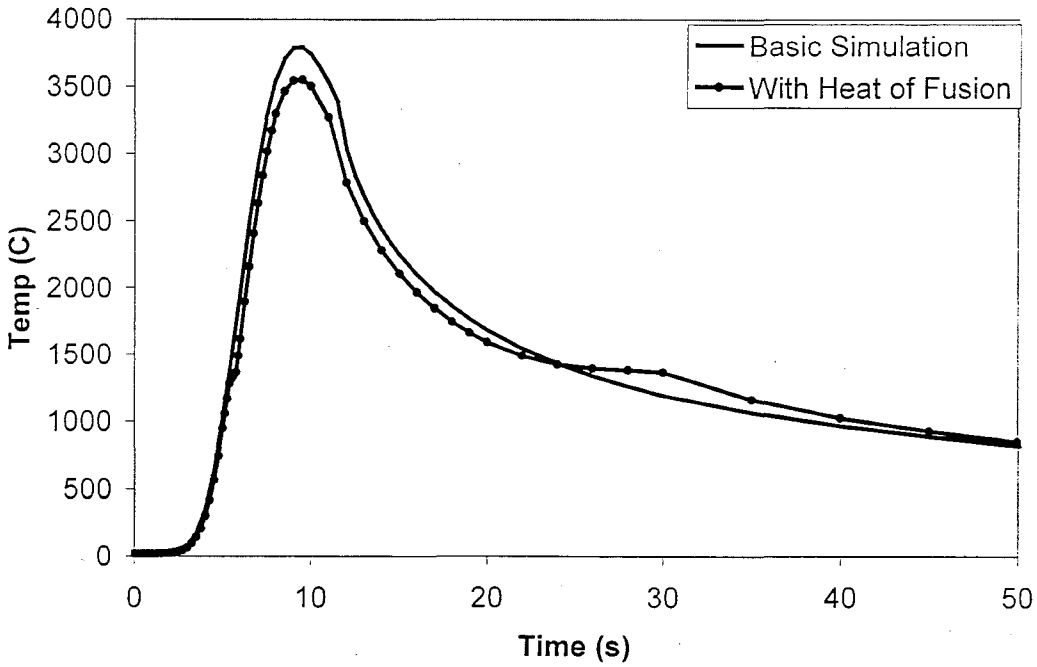

Figure 42 – Temperature Profiles With and Without Heat of Fusion

As neither the adjusted thermal conductivity nor the heat of fusion had a major effect on mechanical results, it is not surprising that the model accounting for both heat of fusion and adjusted thermal conductivity produces similarly negligible changes. Here, the

stress profile is given in Figure 43 while the final cross sections are shown in Figure 44. Again, final longitudinal stresses for the basic simulation are about 350 MPa, while final stresses in the complete model are about 345 MPa.

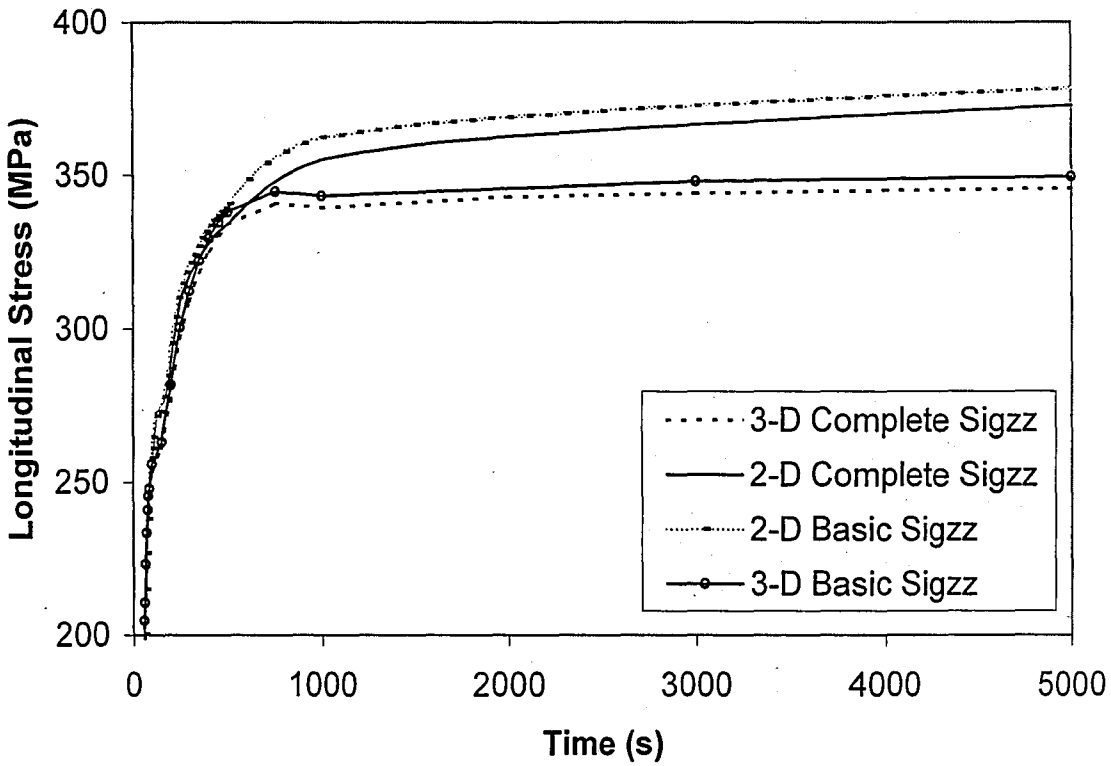

Figure 43 – Longitudinal Stress Results for Basic and Complete Models

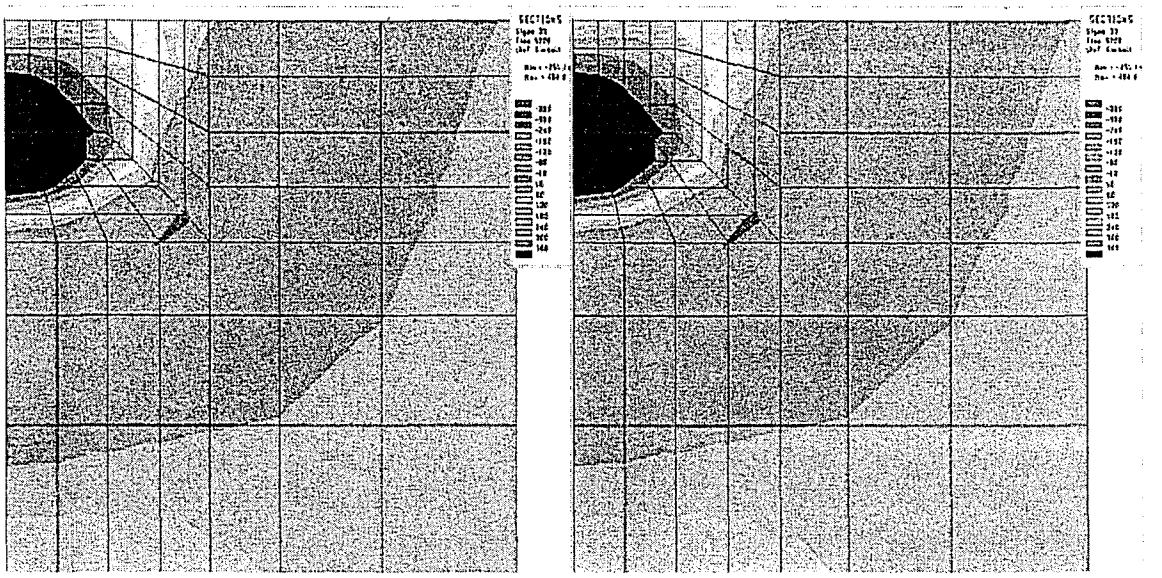

Figure 44 – Final Longitudinal Stress States for Basic (Left) and Complete (Right) Models

While models accounting for metallurgical phase transformations are not considered here, it is reasonable to assume that the latent heats of solid phase transformations would have a negligible effect on both thermal and mechanical models, as these latent heats are generally very small compared to the latent heat of fusion.

If modeling is conducted with interest only in mechanical results, many of the details of the thermal modeling, such as latent heats and adjusted thermal conductivity, may not be necessary. A simple thermal model with a properly calibrated heat source delivers nearly identical results.

3.3 Thermo-Mechanical Models

In addition to mechanical properties such as yield stress, elastic modulus, coefficient of thermal expansion, and Poisson's ratio, one can also specify strain-hardening behavior. As actual plastic strain behavior is difficult to describe numerically, there are several idealized models that are convenient for use in simulations.

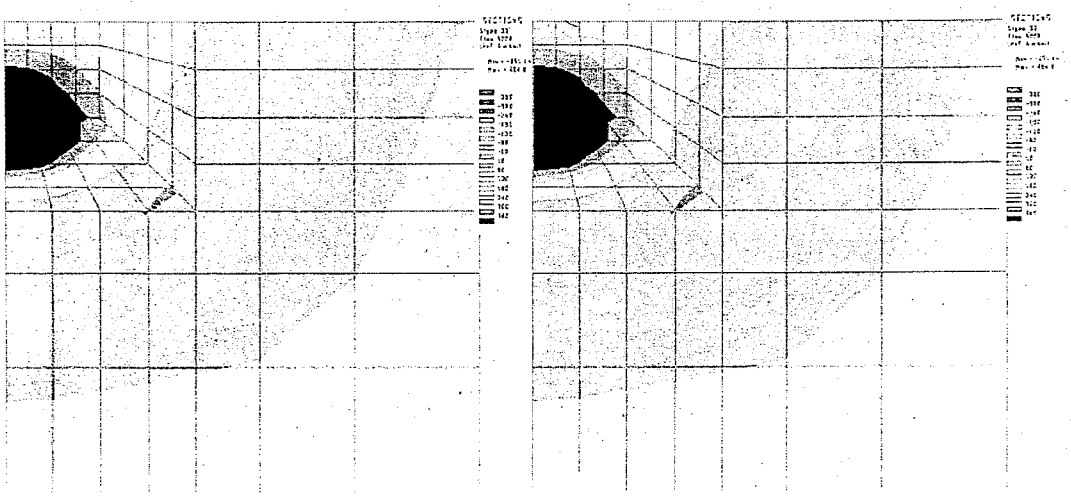

Figure 44 – Final Longitudinal Stress States for Basic (Left) and Complete (Right) Models

While models accounting for metallurgical phase transformations are not considered here, it is reasonable to assume that the latent heats of solid phase transformations would have a negligible effect on both thermal and mechanical models, as these latent heats are generally very small compared to the latent heat of fusion.

If modeling is conducted with interest only in mechanical results, many of the details of the thermal modeling, such as latent heats and adjusted thermal conductivity, may not be necessary. A simple thermal model with a properly calibrated heat source delivers nearly identical results.

3.3 Thermo-Mechanical Models

In addition to mechanical properties such as yield stress, elastic modulus, coefficient of thermal expansion, and Poisson's ratio, one can also specify strain-hardening behavior. As actual plastic strain behavior is difficult to describe numerically, there are several idealized models that are convenient for use in simulations.

The simplest representation of elastic plastic behavior is the elastic perfectly plastic model. This model assumes that once the yield stress has been reached, strain will increase while stress remains the same. Unloading is then elastic, as is loading in the opposite direction. (Ref 27) The stress strain curve for elastic perfectly plastic behavior is shown in Figure 45.

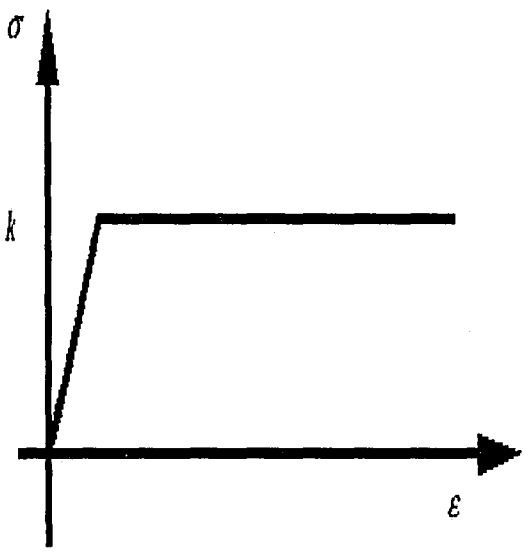

Figure 45 – Elastic Perfectly Plastic Stress Strain Behavior (Ref 29)

In most materials, stress continues to increase during plastic deformation. The mechanical behavior of these materials is not well represented by the elastic perfectly plastic model and requires the use of a strain-hardening model. The stress strain curves for a general strain-hardening model are shown in Figure 46. Since yield stress and elastic modulus are usually both functions of temperature, strain-hardening variables must also change with temperature. (See Figure 47)

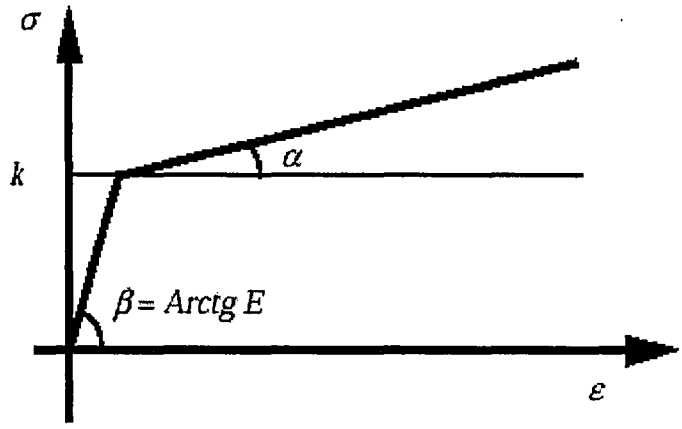

Figure 46 – Stress Strain Behavior with Strain Hardening (Ref 29)

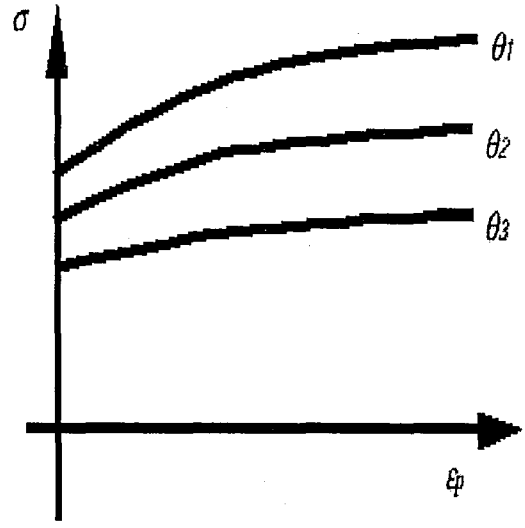

Figure 47 – Temperature Dependent Strain Hardening (Ref 29)

When a material is deformed repeatedly, its mechanical properties may continue to change. This behavior can be accounted for by using adapted strain hardening models. Two models that are commonly used to simulate strain hardening in SYSWELD are the isotropic and kinematic strain hardening models. Isotropic strain hardening corresponds to expansion of the elasticity domain, (See Figure 48) while kinematic strain hardening corresponds to displacement of the elasticity domain. (See Figure 49) Kinematic strain hardening is particularly useful for cyclic applications. (Ref 29) Kinematic strain

hardening is therefore more appropriate for welding applications, while isotropic strain hardening is more appropriate for heat-treating (Ref. 29) Furthermore, it is important to note that both kinematic and isotropic strain hardening models produce identical results if material is not loaded cyclically. For many applications, a combined isotropic and kinematic model gives the most realistic results. (See Figure 50)

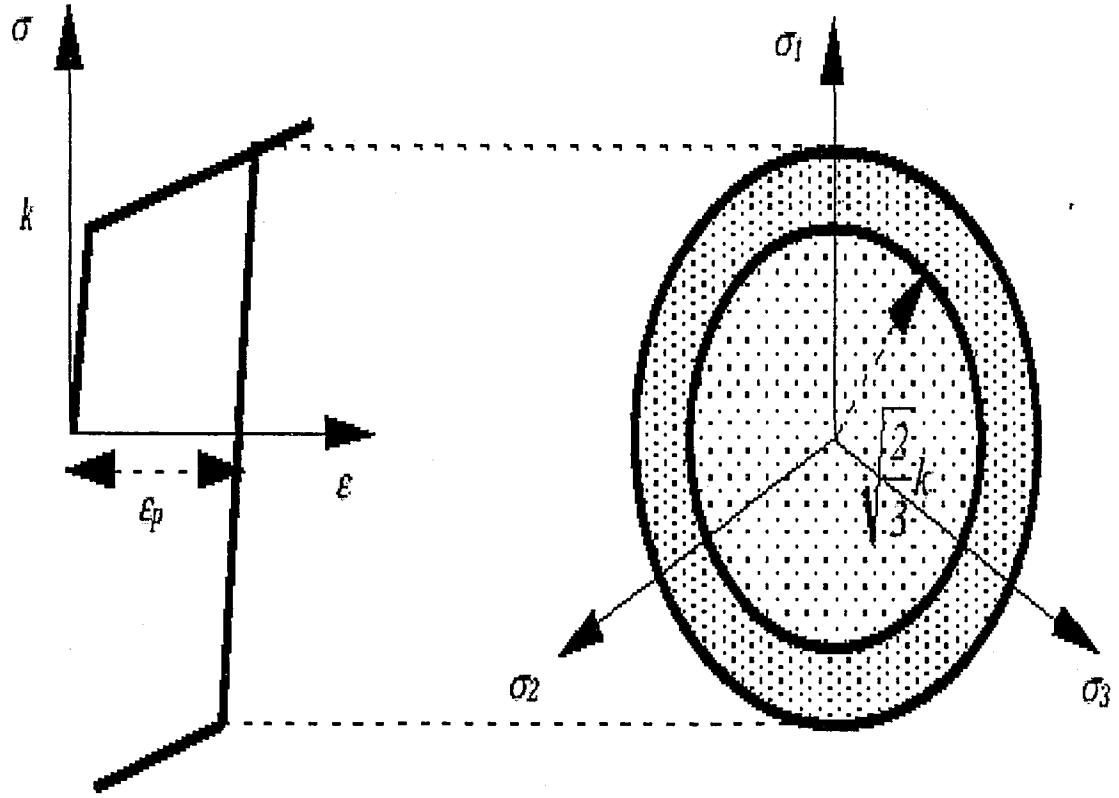

Figure 48 – Stress Strain and Von Mises Yield Surface for Isotropic Strain Hardening Model (Ref 29)

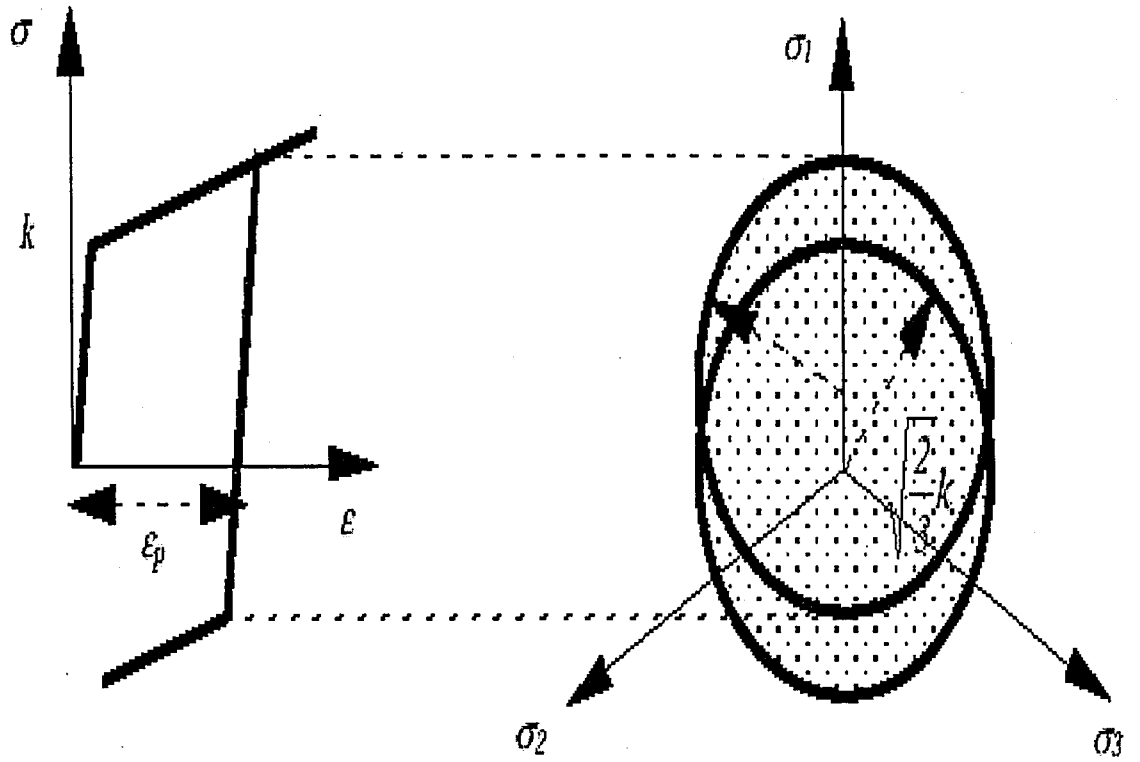

Figure 49 – Stress Strain and Von Mises Yield Surface for Kinematic Strain Hardening Model (Ref 29)

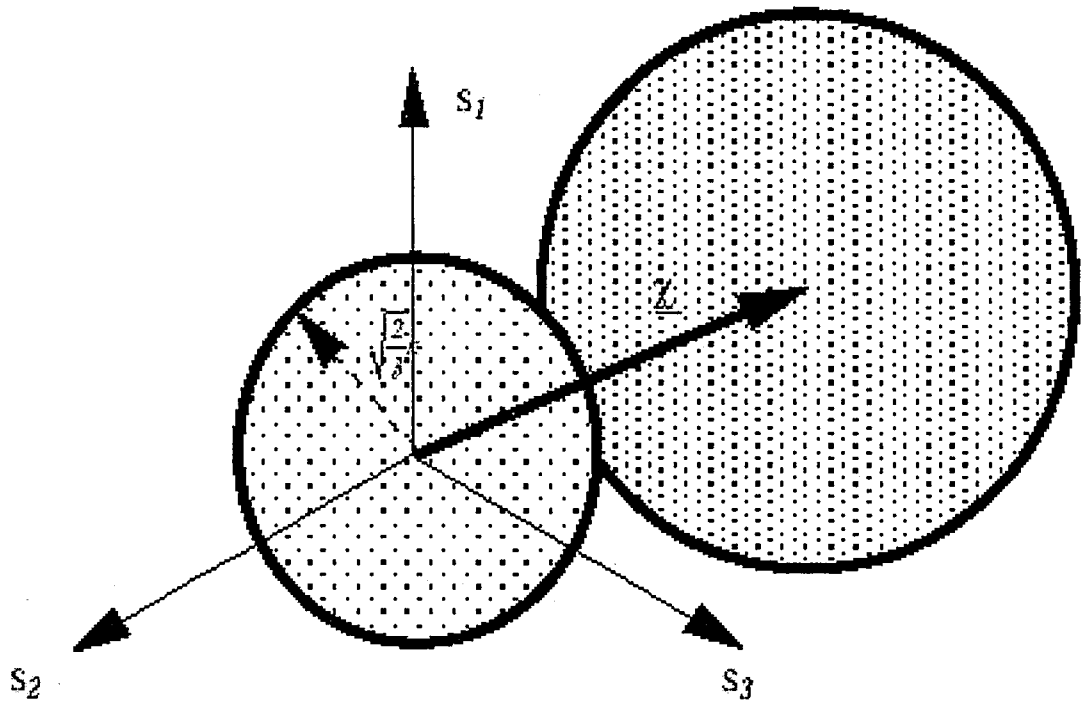

Figure 50 – Von Mises Yield Surface for Combined Strain Hardening Model (Ref 29)

Finally, while mechanical effects of thermal behavior associated with solid phase transformations may be insignificant, mechanical effects due to material property changes associated with solid phase transformations are far from negligible. Materials such as steels exhibit tremendous changes in material properties with solid phase changes, and it is certain that these changes have a dramatic effect on residual stress and distortion in parts.

Chapter 4 –Modeling of LENS

4.1 Model Generation

The goal of this research is to make progress toward the development a computer model that accurately predicts thermo-mechanical behavior of LENS fabricated parts. The preceding chapters have discussed the steps required to generate an accurate model of welding. These steps must now be applied to laser deposited parts. There are several important differences between the previous models and the LENS model. First, all previously considered models were autogenous. As LENS fabricated parts are nothing more than filler metal, the addition of filler metal is clearly not negligible here. Furthermore, the LENS heat source is a laser, while all previously considered models used arc-welding sources. The higher intensity and smaller size of a laser requires significantly finer meshing and time stepping.

All of these factors force the model to be small in physical size to minimize storage and computation requirements. The model generated here to simulate laser deposition consists of 16564 nodes and 18692 linear elements. (Figure 52) Material properties of AL6XN stainless steel were used along with a conical heat source. Material properties are given in Figure 10, while parameters of the source are given in Figure 51.

Max Intensity	Vy	Re	Ri	Ze	Zi
W/mm^3	mm/s	mm	mm	mm	mm
1350	5	0.35	0.15	0.2	-0.3

Figure 51 – Input Parameters for Conical Source

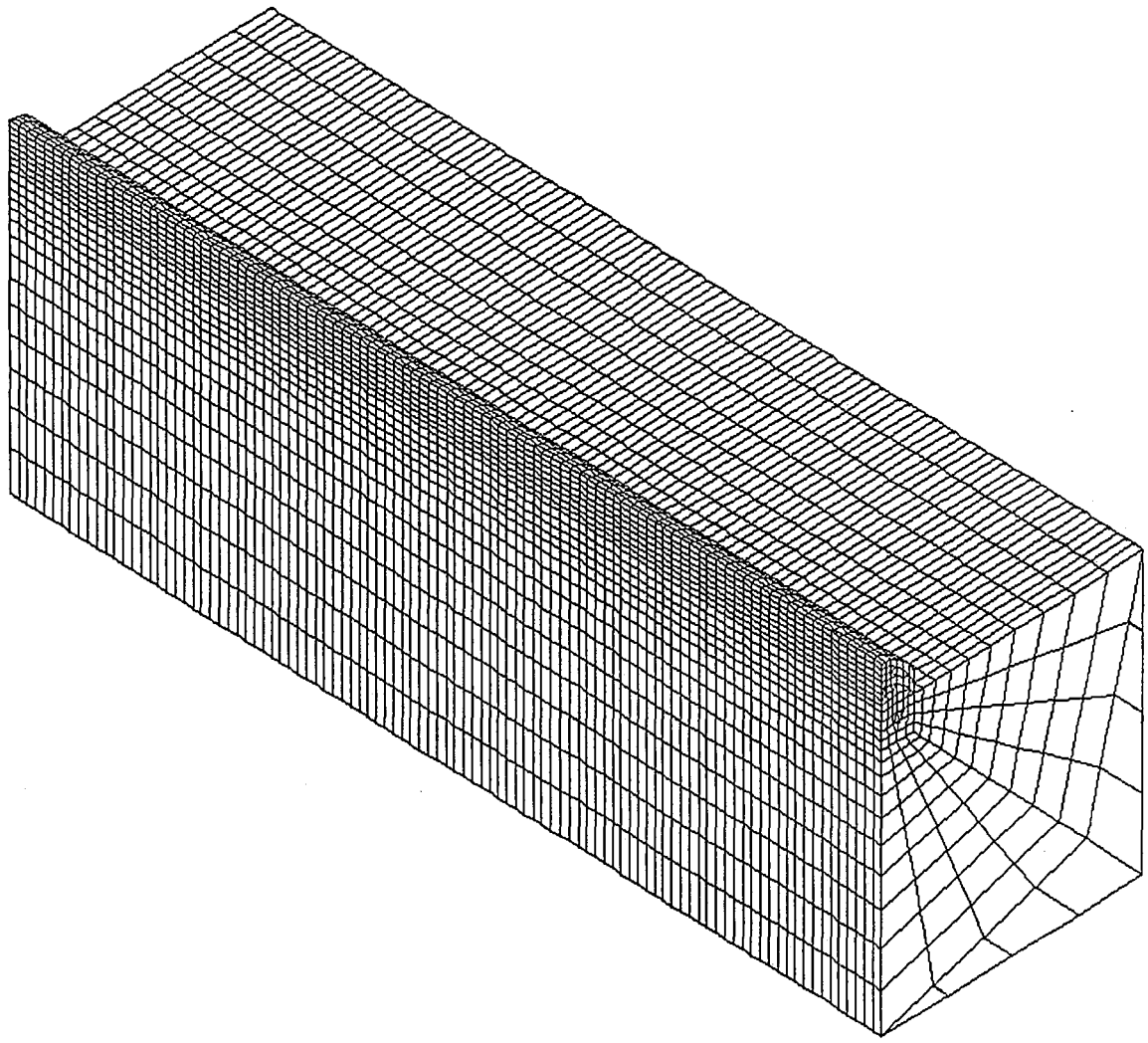

Figure 52 – LENS Mesh

Before the model in Figure 52 was generated, a smaller model was generated that represented a rough first attempt toward lens modeling. This model considered a single pass of a laser source with element activation. Many issues were resolved in this model, but the eventual goal is to model the many passes required to form a LENS part. Therefore, the model represented by the mesh in Figure 52 was generated and considers the additional complexity of a second pass of the laser. It is assumed in this study that if two consecutive passes can be modeled successfully, the addition of further layers should require only increased storage space and computation time.

4.2 Element Activation, Deactivation

To accommodate material addition, it would first appear that one must update the mesh for each time step. As time steps are plentiful and mesh modification is not trivial, this is very awkward in nearly any finite element modeling scheme. Fortunately, SYSWELD and several other packages offer element activation or birthing techniques that avoid the difficulties of mesh modification. With element activation, the entire mesh is created with all filler metal or deposits in place. The deposit material is initially assigned an inactive state, which effectively reduces material properties by a user-specified amount, usually several orders of magnitude. In thermal simulations, thermal conductivity and heat flux are reduced, while in mechanical simulations, the elastic modulus and Poisson's ratio are reduced. Also, inactive elements in thermal simulations are assumed to have no thermal mass ($\rho Cp=0$), while in inactive mechanical elements, density and all forces are set to zero. Once elements are activated, they assume normal properties specified by the user.

Elements can be activated by functions of time and space. In thermal models with element activation, it is recommended that elements be activated just in front of the heat source to avoid numerical instabilities. (Ref 30) To model laser deposition, however, elements were activated just behind the source to better simulate the sprinkling of powder into the molten pool. (See Figure 53, Figure 54) For mechanical models, it is recommended that elements be activated in the center of the molten pool. (Ref 30) Once again, in the LENS modeling, elements are activated just behind the source. It is important to note that elements in mechanical simulations should not be activated in front of elements in the thermal simulations, as incorrect temperature values in uninitialized

elements will surely lead to irregularities in stress predictions. Preliminary results indicate that the location of the activation front has relatively little effect on results, as yield strength is close to zero at the melting temperature. In other words, as long as elements are activated where temperature is above melting, results appear to be quite similar. Models with elements activated just behind the source predict slightly more heating of the part, while models with elements activated in front of the source predict higher temperatures in the bead.

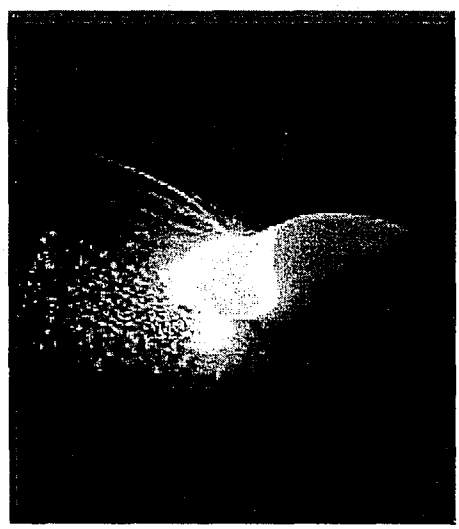

Figure 53 - Close-Up Photograph of LENS Deposit

elements will surely lead to irregularities in stress predictions. Preliminary results indicate that the location of the activation front has relatively little effect on results, as yield strength is close to zero at the melting temperature. In other words, as long as elements are activated where temperature is above melting, results appear to be quite similar. Models with elements activated just behind the source predict slightly more heating of the part, while models with elements activated in front of the source predict higher temperatures in the bead.

Figure 53 - Close-Up Photograph of LENS Deposit

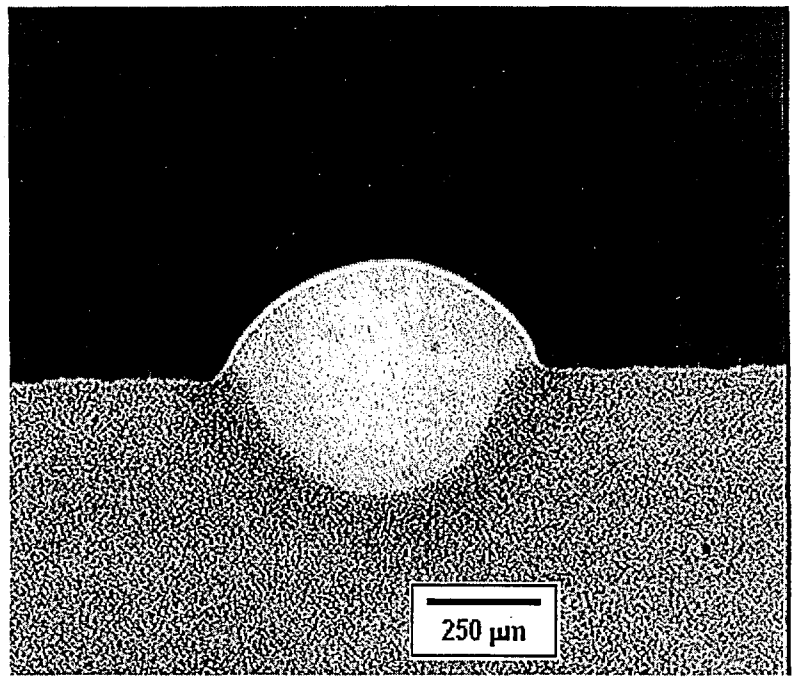

Figure 54 – Cross Section of LENS Deposited Bead

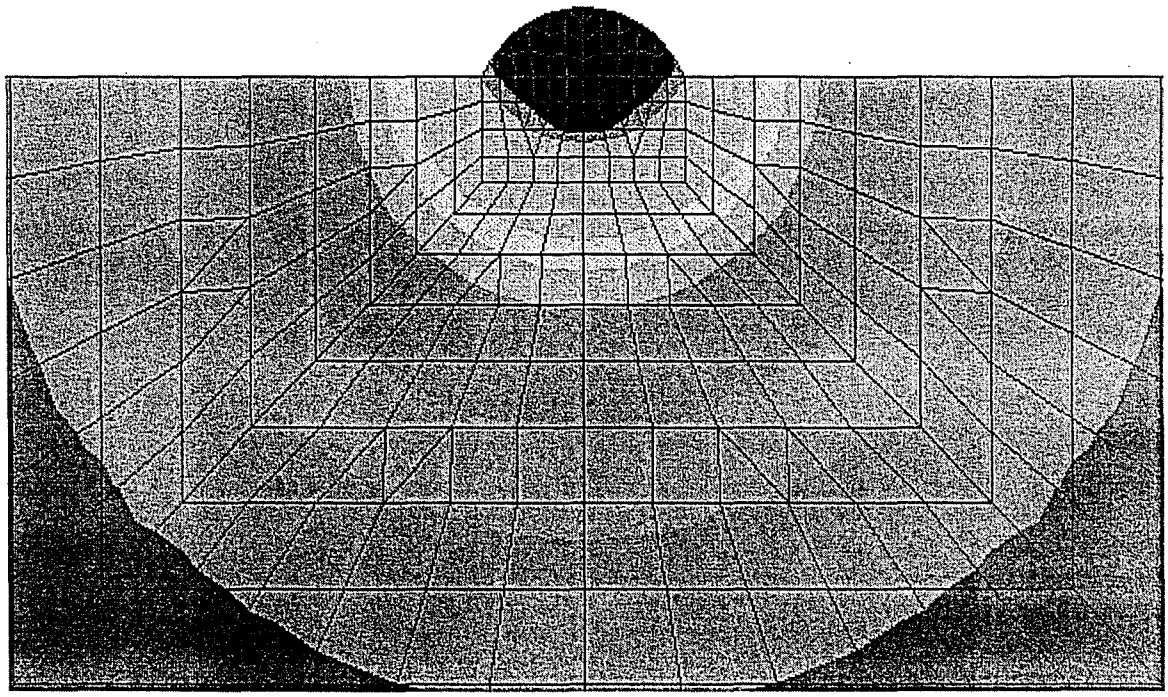

Figure 55 – Finite Element Prediction of Fusion Zone

It is further recommended to use first order (linear) elements in thermal models with element activation for best results. (Ref 31) Quadratic elements have mid-side nodes that can lead to partial activation of elements, which causes instabilities.

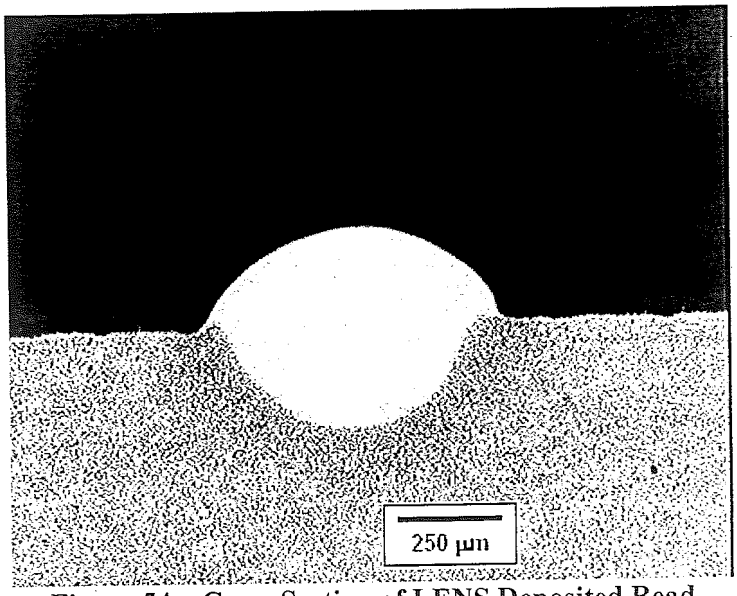

Figure 54 – Cross Section of LENS Deposited Bead

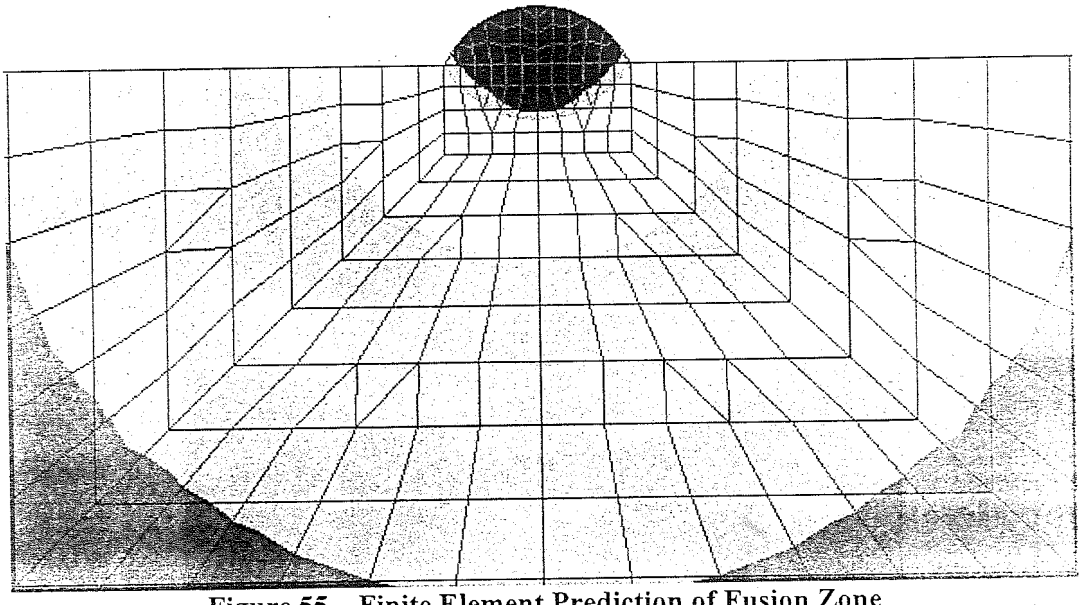

Figure 55 – Finite Element Prediction of Fusion Zone

It is further recommended to use first order (linear) elements in thermal models with element activation for best results. (Ref 31) Quadratic elements have mid-side nodes that can lead to partial activation of elements, which causes instabilities..

Within SYSWELD, element activation is available in thermal enthalpy and thermal metallurgy options. If any material in a simulation exhibits solid phase transformations, the thermal metallurgy option is the obvious choice. If a material can be modeled without solid phase transformations, the thermal metallurgy can still be used. The "METALLURGY.DAT" file must be given with two dummy phases and no reactions. This file is listed in Figure 56.

```
MATERIAL 1 PHASE 2
REACTION
END
```

Figure 56 – Contents of METALLURGY.DAT File

When metallurgy is not of interest, the thermal enthalpy option may be preferable. Comparisons indicate that results are identical, while solution times are far shorter without the added non-linearity of the metallurgy option. It is important to note that within the enthalpy option, specifying the optional "ENTHALPY" property with element activation can be troublesome. As inactive elements have unrealistic physical properties, predicted temperatures are often very large positive or negative values. While this is usually not at all difficult, SYSWELD requires that enthalpy values, if specified, be entered for the full range of temperatures in a part and refuses to extrapolate to meet unreasonable temperatures. As the ENTHALPY label is optional, however, it may be neglected and the specific heat given for a reasonable temperature range. SYSWELD will then extend that data and integrate to determine enthalpy and accommodate temperatures of inactive elements. Mechanical modeling that follows the thermal enthalpy option is also considerably faster than the mechanical metallurgical solution.

Finally, it is essential that loads or constraints that anchor the part or are required for stability are not applied to elements that are inactive at any time. An exception to this

rule involves the symmetry boundary condition, which can be applied to elements as they are activated. (Ref 31)

4.3 Transfer Efficiency

Once a source has been selected but before any meaningful modeling can occur, the numerical heat source must be configured to agree with a real source. The first step to achieve this agreement requires the user to determine how much power is absorbed into the weldment. In many cases, generic transfer efficiency values are tabulated for various materials and types of welding. For laser welding, however, these empirical predictions may not be acceptable. Research at Lehigh University indicates that transfer efficiency depends on surface finish of the weldment and welding parameters. (Ref. 32) Transfer efficiencies were measured by depositing a bead on a quarter inch plate of H13 tool steel, then very quickly moving the test specimen into a Thermonetics Seebeck envelope calorimeter. With this technique, it is possible to measure the total energy transferred by the laser into the specimen. A laser power meter from Kentek was used to determine the total laser power. The transfer efficiency is simply the ratio of the absorbed power to the total power. This ratio is typically about 40% for H13 tool steel and some stainless steels with a 1064 nm ND-YAG laser. Much of the remaining 60% of power is reflected from the surface of the part. (Ref 32) Once the transfer efficiency and the power absorbed by the part are known, the source may be defined and the model run. The results of this preliminary model must be compared with an actual test piece to ensure that the predicted fusion and heat-affected zones agree with the actual ones. In this way, the source can be tuned to give the proper results.

4.4 Thermal Results

To test the effects of different deposition patterns, the following two models were considered. In the first model, the second bead is deposited in the same direction as the first bead, while in the second model, the second bead is deposited in the opposite direction as the first bead.

Thermal results for the first bead for both models are identical, and are shown in Figure 57, Figure 58, and Figure 59.

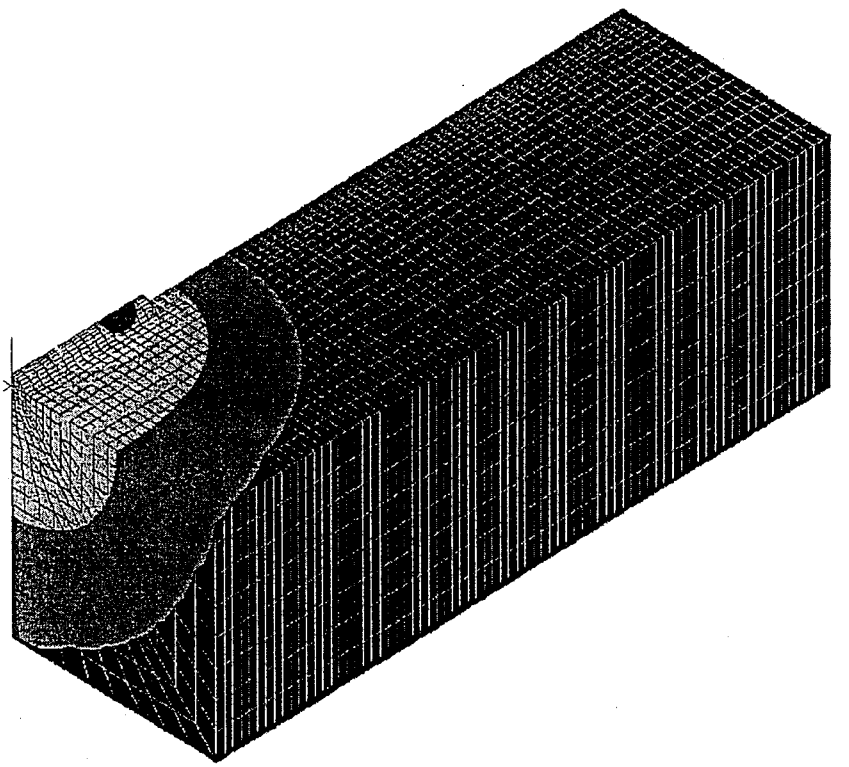

Figure 57 – First LENS Deposit at 0.5s

4.4 Thermal Results

To test the effects of different deposition patterns, the following two models were considered. In the first model, the second bead is deposited in the same direction as the first bead, while in the second model, the second bead is deposited in the opposite direction as the first bead.

Thermal results for the first bead for both models are identical, and are shown in Figure 57, Figure 58, and Figure 59.

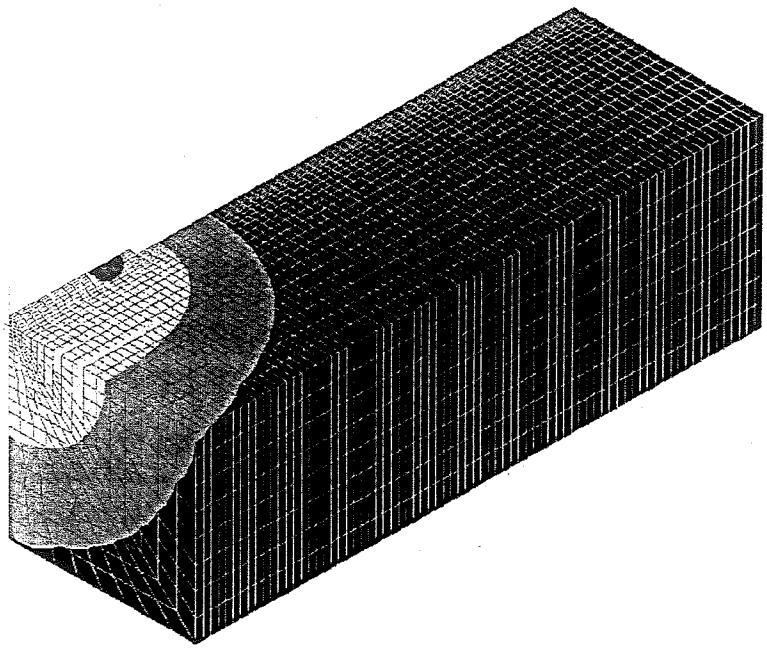

Figure 57 – First LENS Deposit at 0.5s

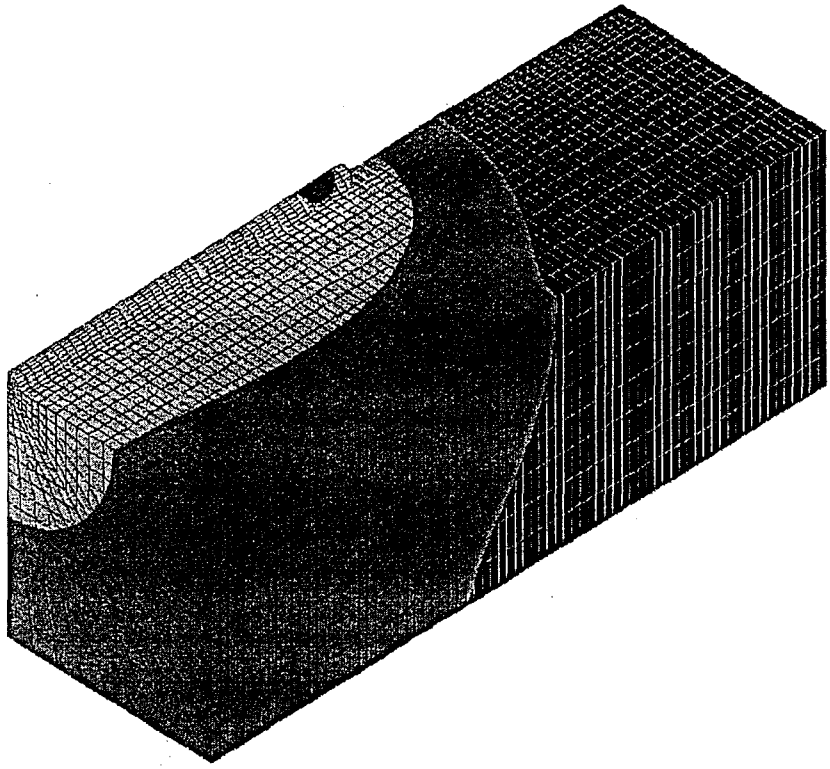

Figure 58 – First LENS Deposit at 1.5s

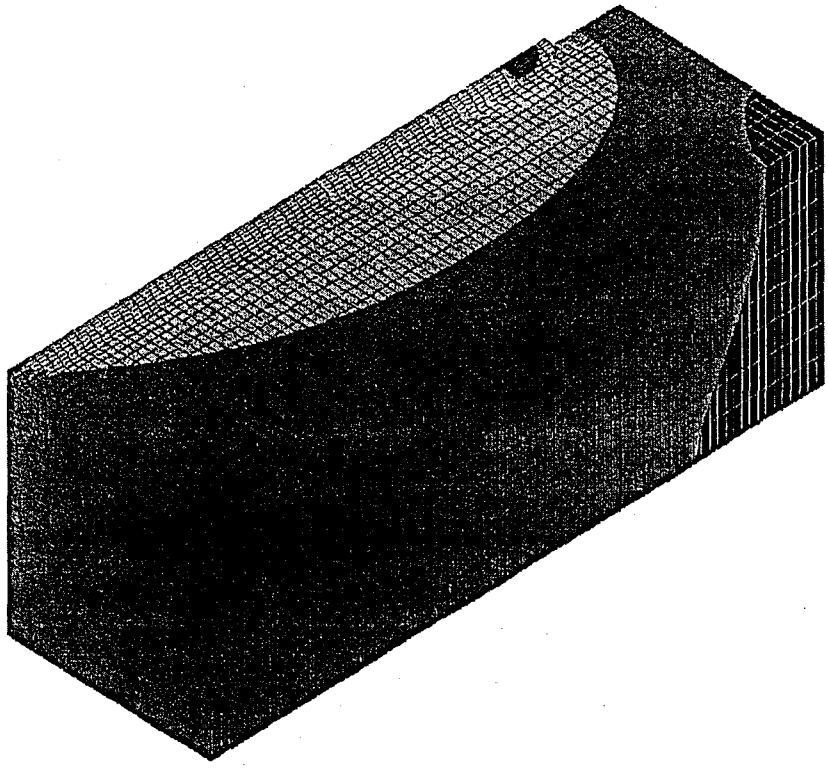

Figure 59 – First LENS Deposit at 2.5s

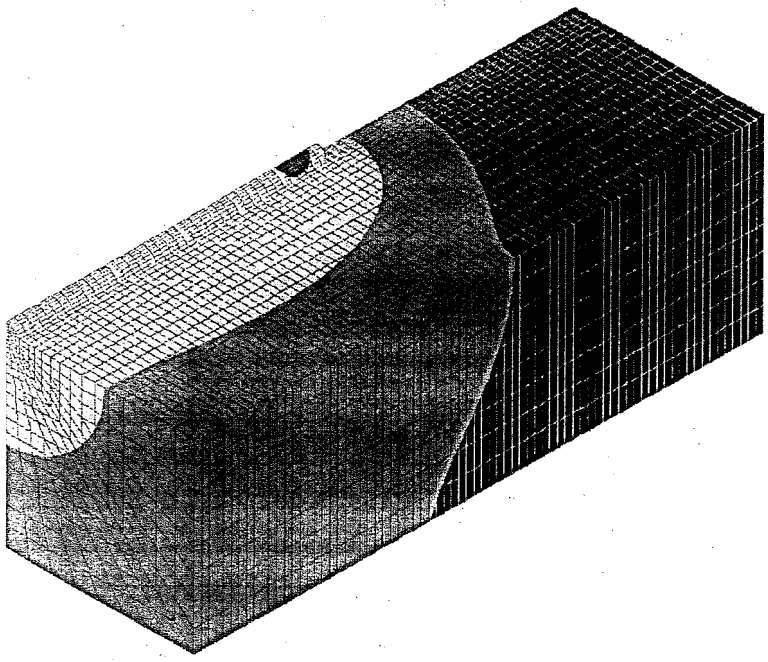

Figure 58 – First LENS Deposit at 1.5s

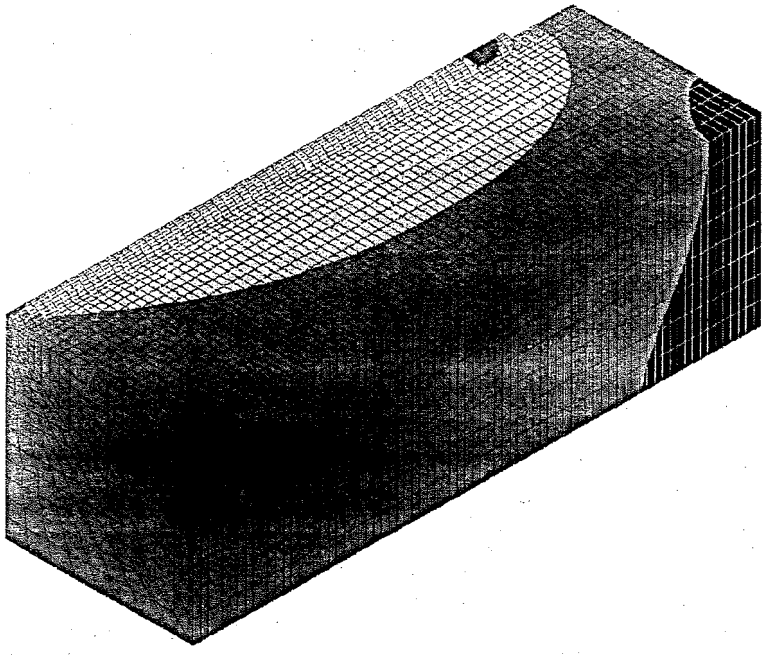

Figure 59 – First LENS Deposit at 2.5s

Graphical representation of thermal results from the second deposit in the first model (with both laser passes in the same direction), are shown in Figure 60, Figure 61, and Figure 62. Thermal profiles for points in the substrate and in both beads are shown in Figure 63.

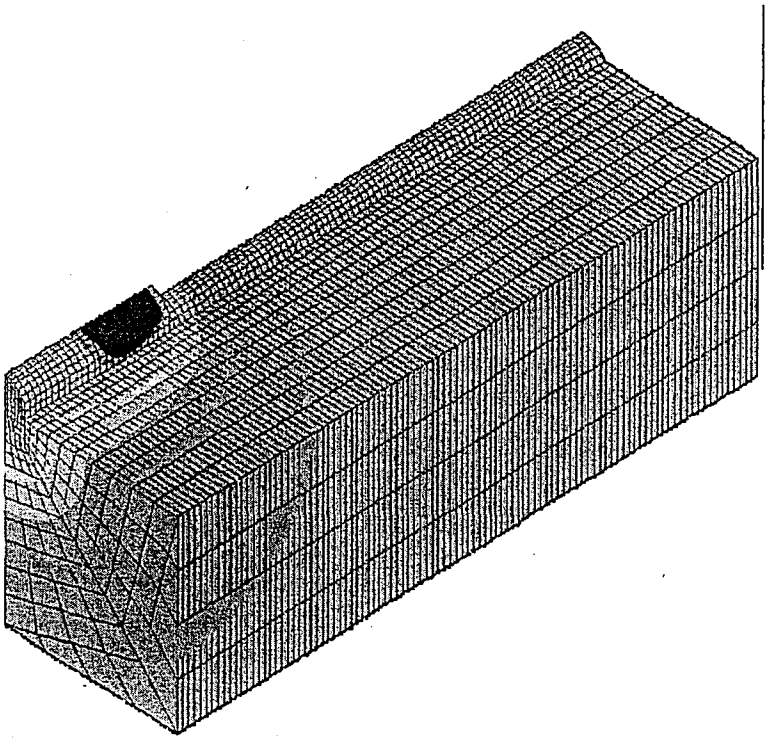

Figure 60 – Thermal Results From Second Pass, Same Direction as First Pass, t=4.75 seconds

Graphical representation of thermal results from the second deposit in the first model (with both laser passes in the same direction), are shown in Figure 60, Figure 61, and Figure 62. Thermal profiles for points in the substrate and in both beads are shown in Figure 63.

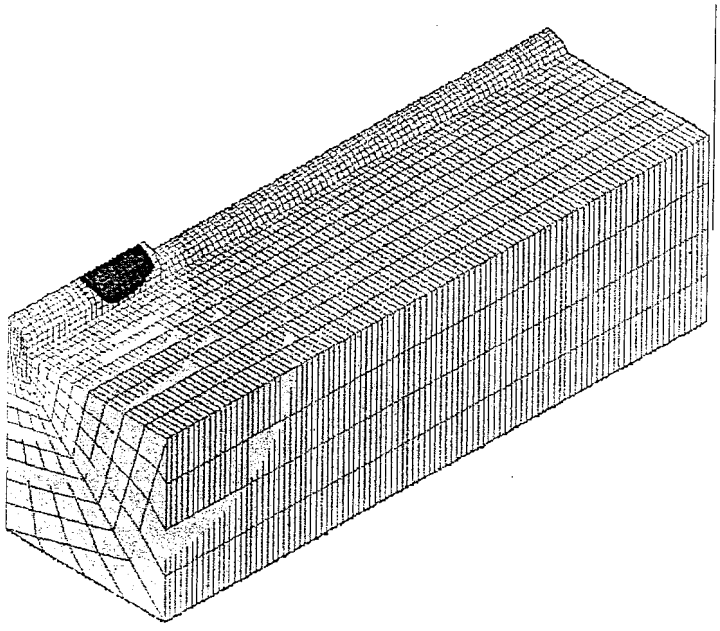

Figure 60 – Thermal Results From Second Pass, Same Direction as First Pass, t=4.75 seconds

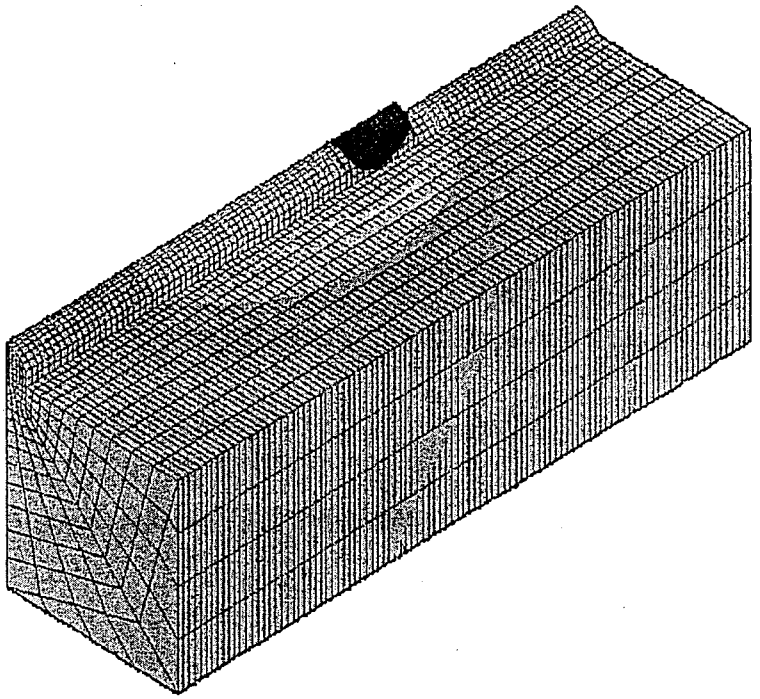

Figure 61 – Thermal Results, Second Pass, Same Direction as First, t=6 seconds

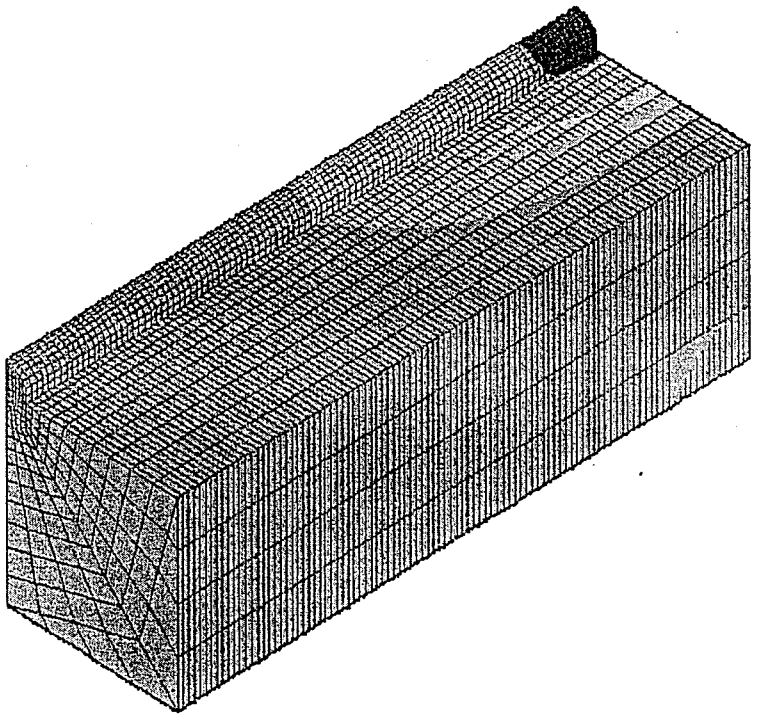

Figure 62 – Thermal Results, Second Pass, Same Direction as First, t=6.5 seconds

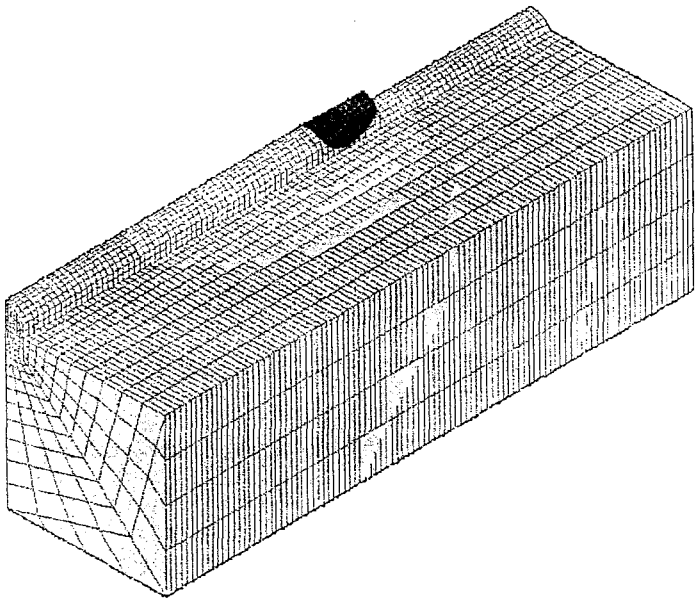

Figure 61 – Thermal Results, Second Pass, Same Direction as First, t=6 seconds

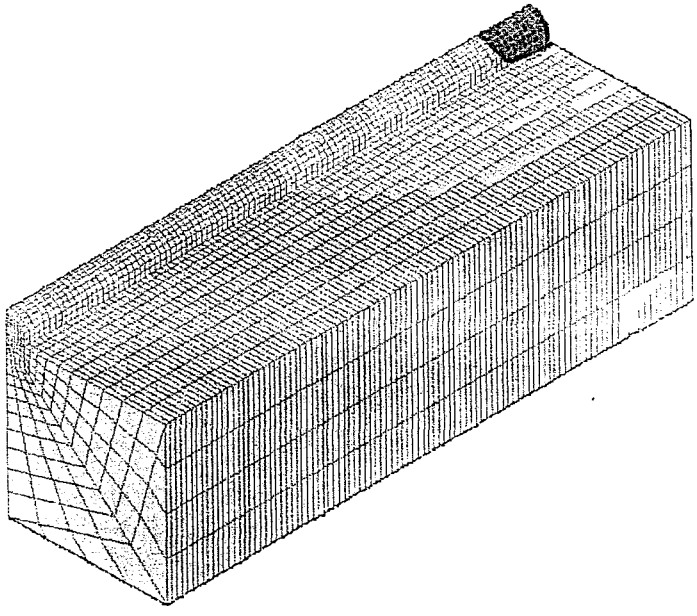

Figure 62 – Thermal Results, Second Pass, Same Direction as First, t=6.5 seconds

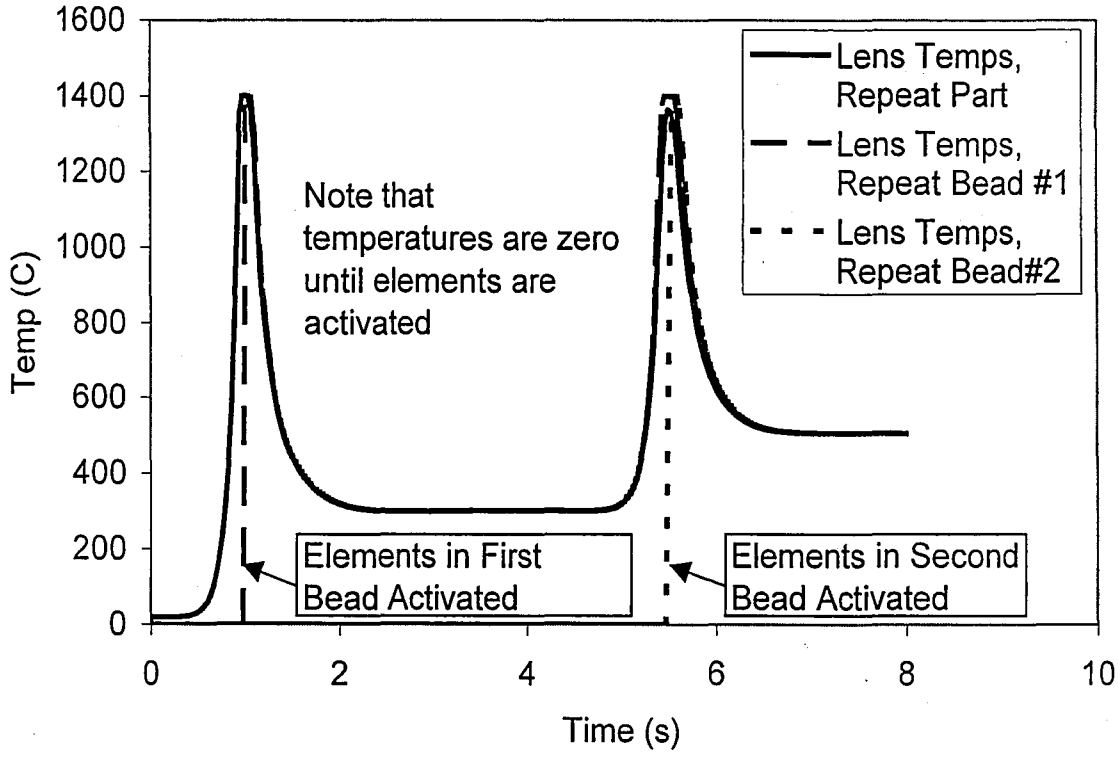

Figure 63 – Thermal Profiles of LENS Model with Second Pass in Same Direction as First Pass

Thermal results for the second deposit in the second model (with the second deposit in the opposite direction from the first) are given in Figure 64, Figure 65, and Figure 66. Thermal profiles in the substrate and both beads are given in Figure 67. As these results were evaluated in the center of the part (longitudinally), the differences between thermal results are subtle. These differences are better observed in Figure 68. Here, it is clear that the two models produce identical results before the second pass, as expected. During the second pass, the model with the same direction for first and second passes produces a slightly higher peak temperature. This trend is continued after the source has passed, when the m model with no change of direction continues to have a slightly higher temperature.

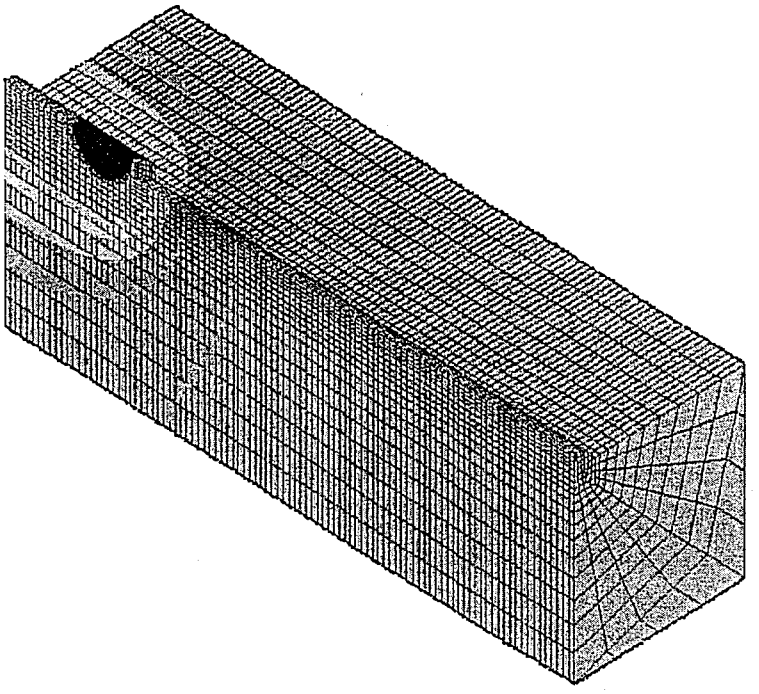

Figure 64 – Thermal Results, Second Pass, Direction Reversed From First Pass, t=4.75 seconds

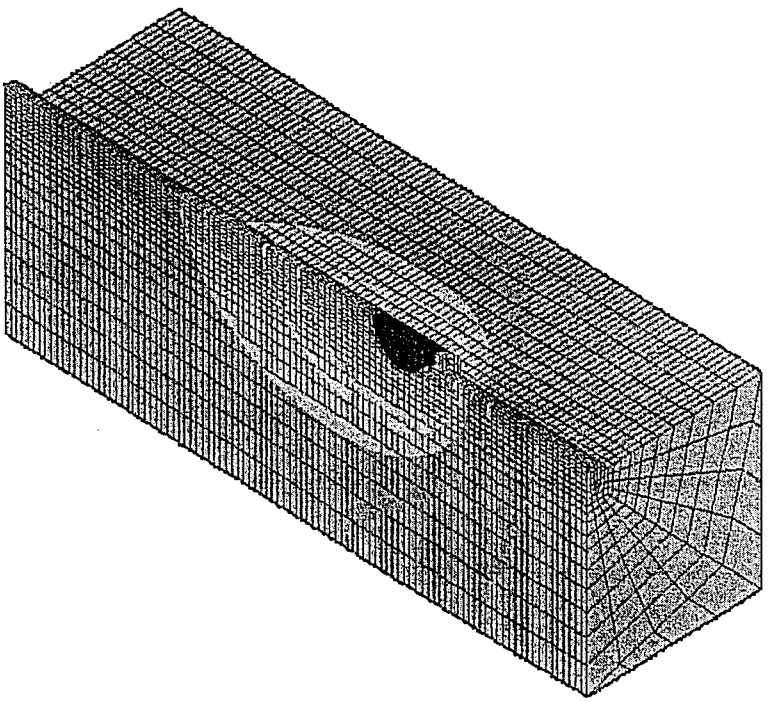

Figure 65 – Thermal Results, Second Pass, Direction Reversed From First Pass, t=6 seconds

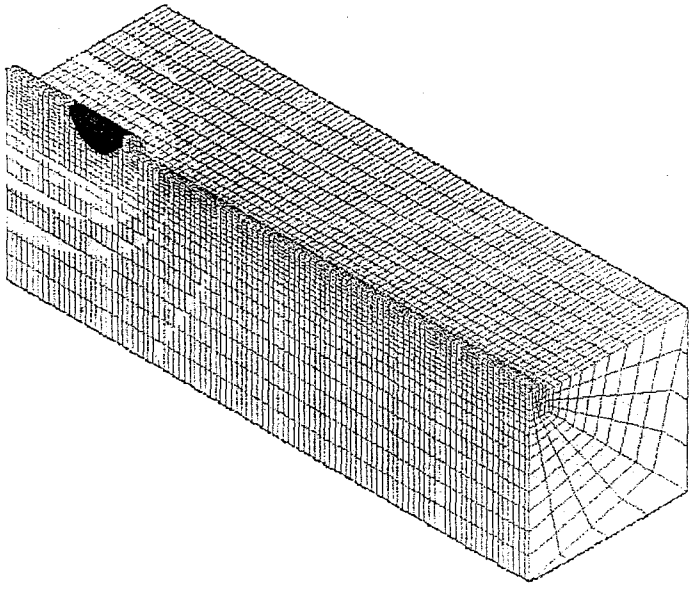

Figure 64 – Thermal Results, Second Pass, Direction Reversed From First Pass, t=4.75 seconds

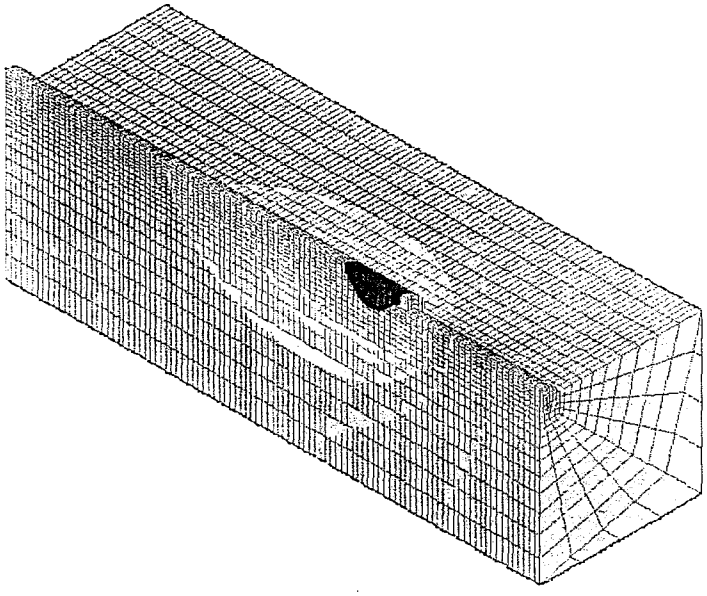

Figure 65 – Thermal Results, Second Pass, Direction Reversed From First Pass, t=6 seconds

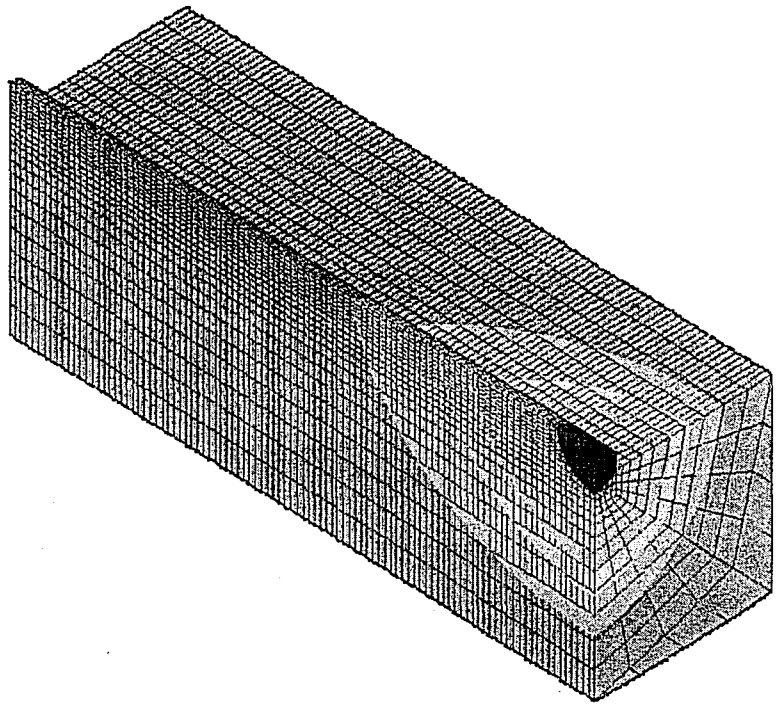

Figure 66 – Thermal Results, Second Pass, Direction Reversed From First Pass, *t*=6.5 seconds

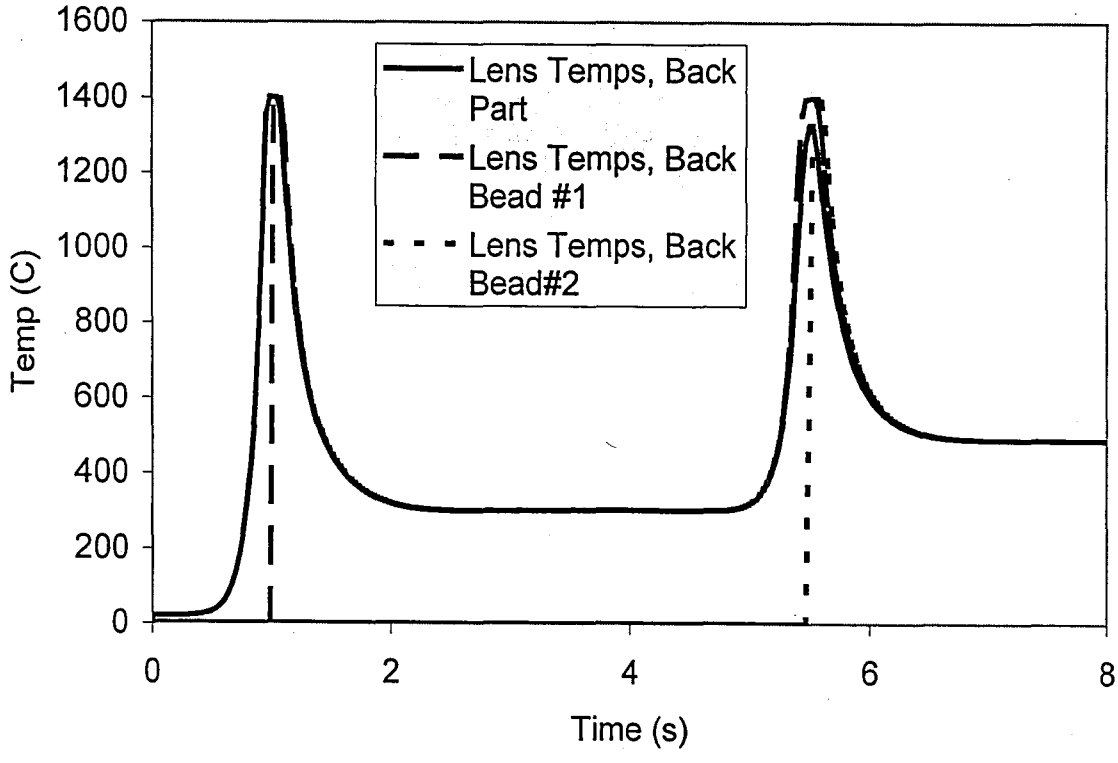

Figure 67 – Thermal Profile for LENS Model with Second Pass in Opposite Direction from First Pass

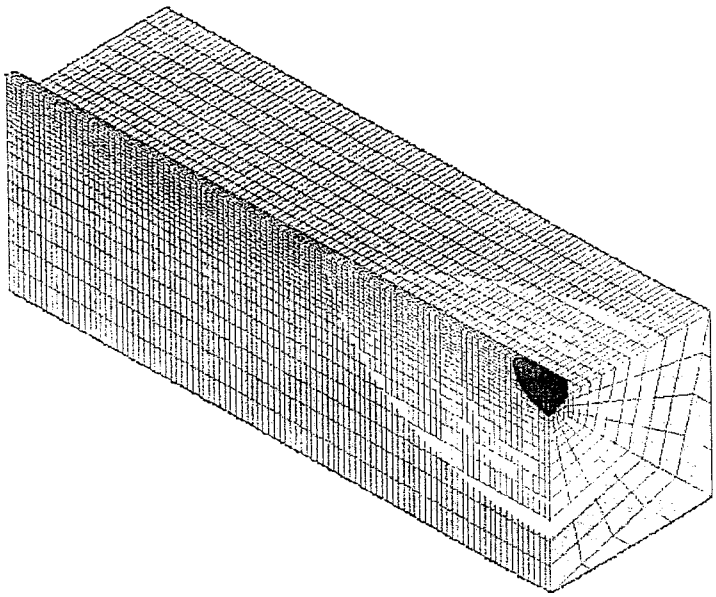

Figure 66 – Thermal Results, Second Pass, Direction Reversed From First Pass, t=6.5 seconds

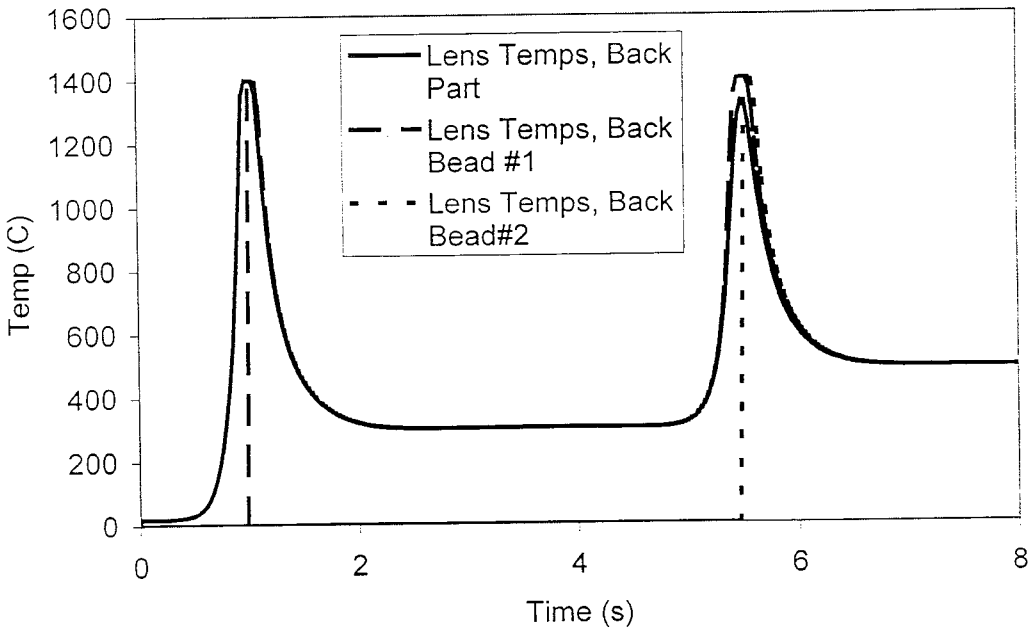

Figure 67 – Thermal Profile for LENS Model with Second Pass in Opposite Direction from First Pass

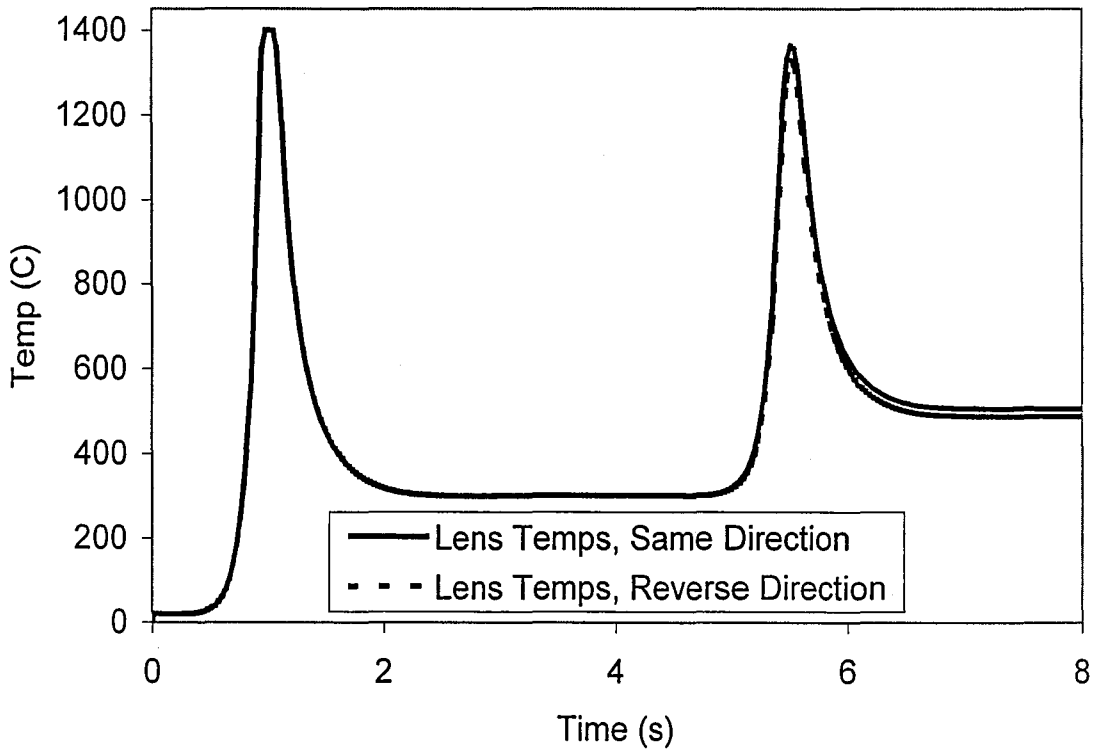

Figure 68 – Temperature Comparison for Different Second Pass Direction

4.5 Mechanical Results

The thermal results in the previous section were used to create mechanical models of the LENS process. In the mechanical models here, both ends of the model are constrained such that there is no displacement in the longitudinal direction. This boundary condition causes excessively high compressive longitudinal stresses while heating. Since the physical size of the model considered here is very small, this boundary condition pretends that this model is a small part of a much longer section. A more complicated elastic constraint would offer more realistic results.

These models are the first step toward the prediction of residual stresses and distortion in LENS parts. Once again, models were generated with both second pass

directions. Longitudinal stresses from the first pass, which are identical in both cases, are shown in Figure 69, Figure 70, and Figure 71

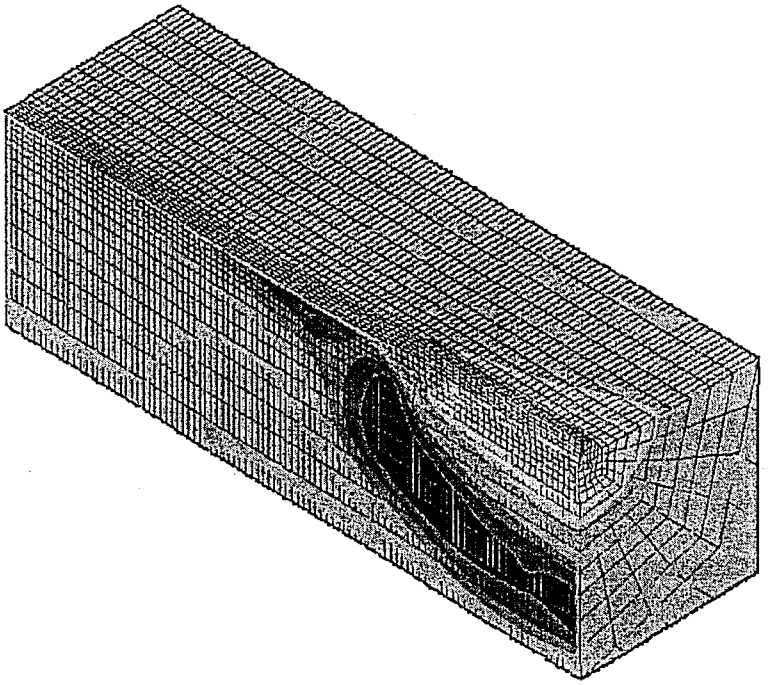

Figure 69 – Longitudinal Stress in First Pass of LENS Model, t=0.5 seconds

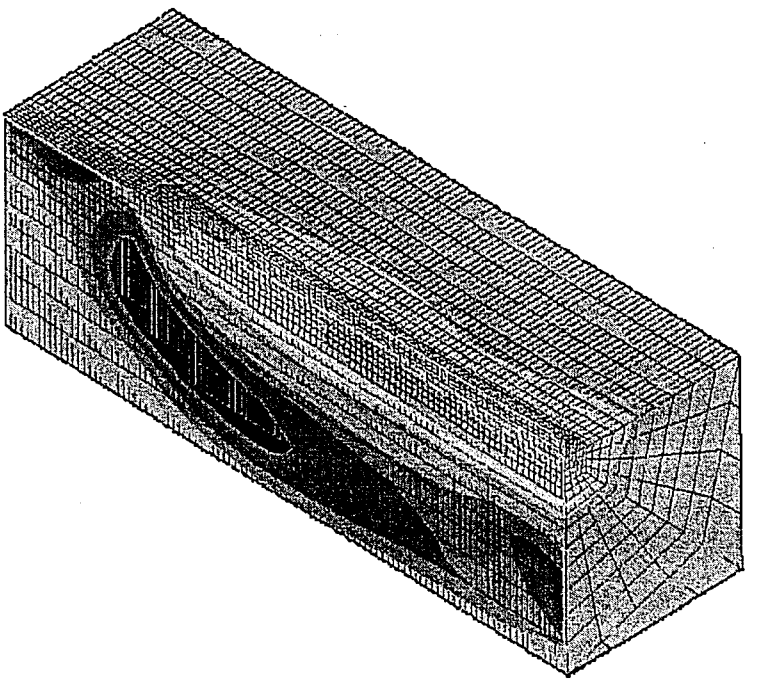

Figure 70 – Longitudinal Stress in First Pass of LENS Model, t=1.5 seconds

directions. Longitudinal stresses from the first pass, which are identical in both cases, are shown in Figure 69, Figure 70, and Figure 71

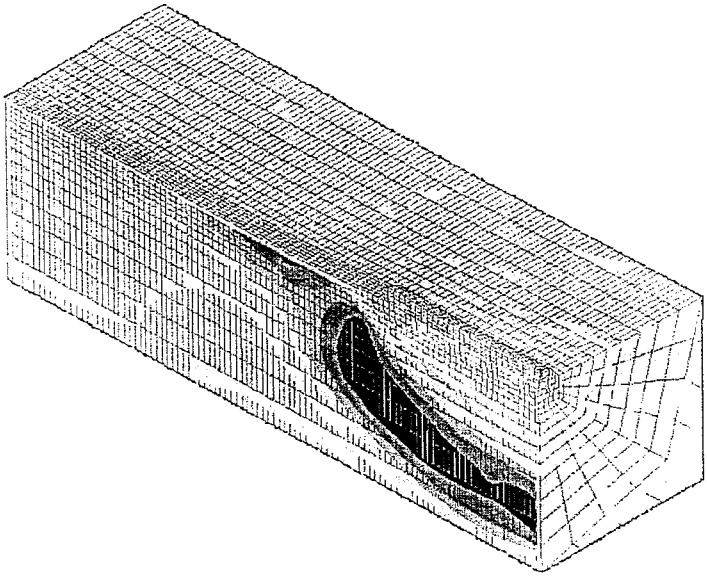

Figure 69 – Longitudinal Stress in First Pass of LENS Model, t=0.5 seconds

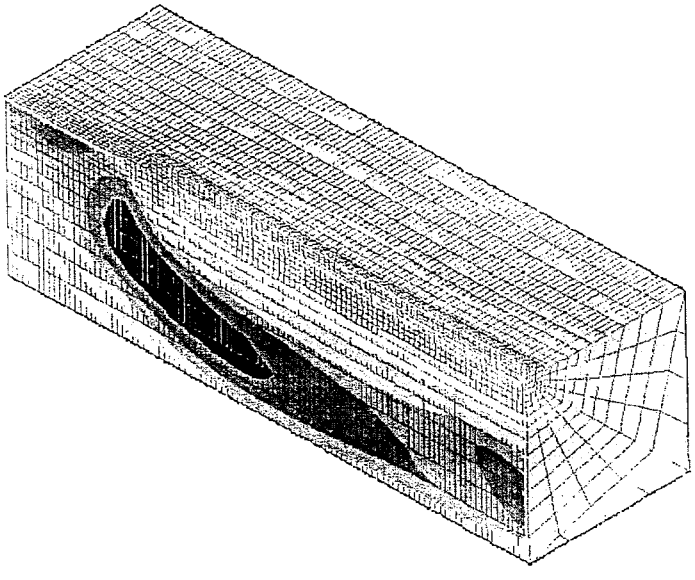

Figure 70 – Longitudinal Stress in First Pass of LENS Model, t=1.5 seconds

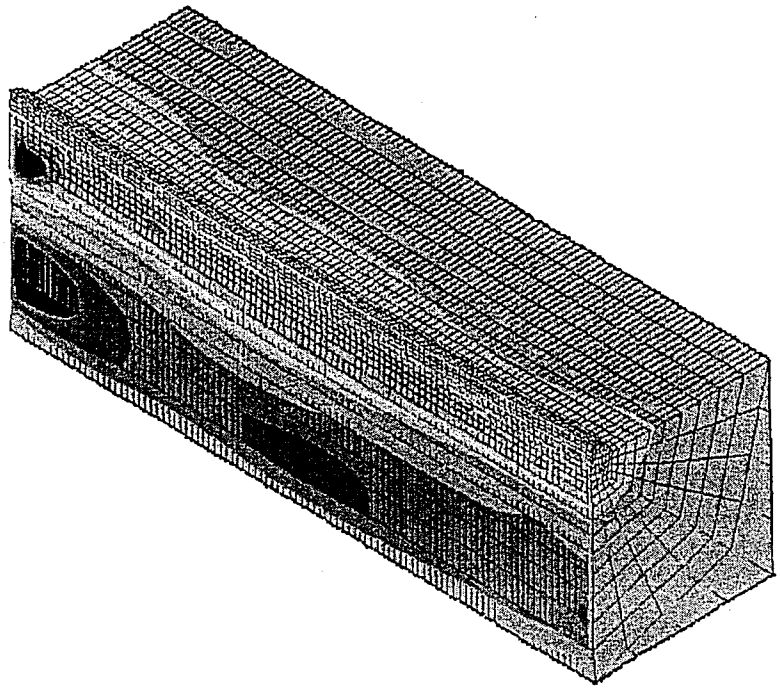

Figure 71 – Longitudinal Stress in First Pass of LENS Model, t=2 seconds

Graphical representation of mechanical results from the second deposit in the first model (with both laser passes in the same direction), are shown in Figure 72, Figure 73, and Figure 74. Longitudinal stress profiles for points in the substrate and in both beads are shown in Figure 75.

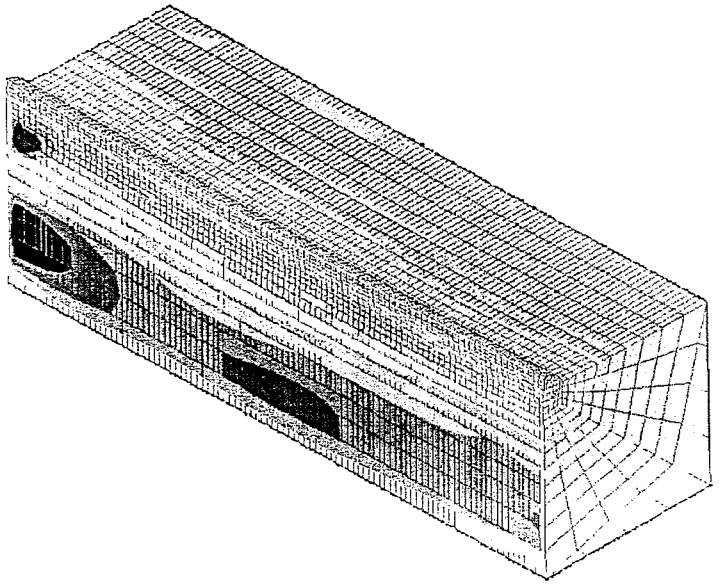

Figure 71 – Longitudinal Stress in First Pass of LENS Model, t=2 seconds

Graphical representation of mechanical results from the second deposit in the first model (with both laser passes in the same direction), are shown in Figure 72, Figure 73, and Figure 74. Longitudinal stress profiles for points in the substrate and in both beads are shown in Figure 75.

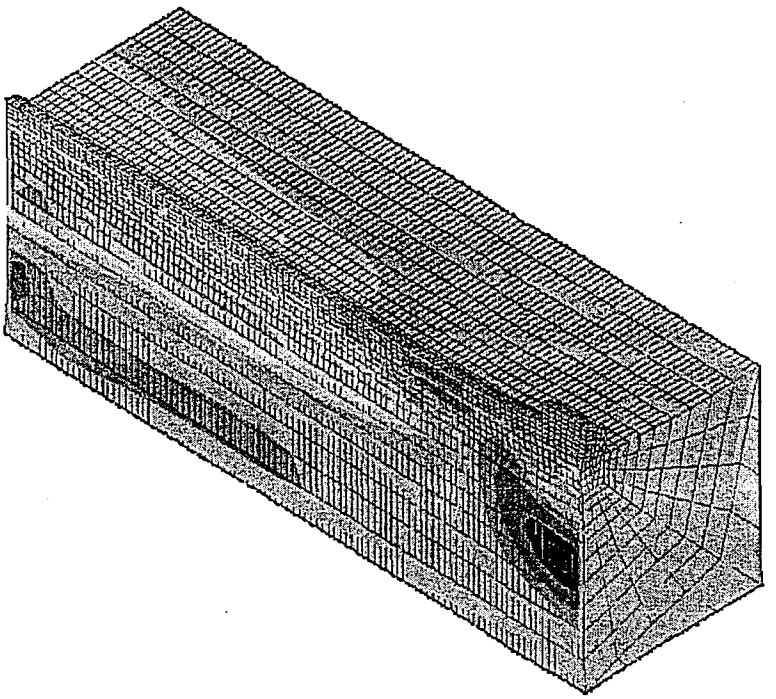

Figure 72 – Longitudinal Stress, Second Pass, Same Direction as First, t=4.625 seconds

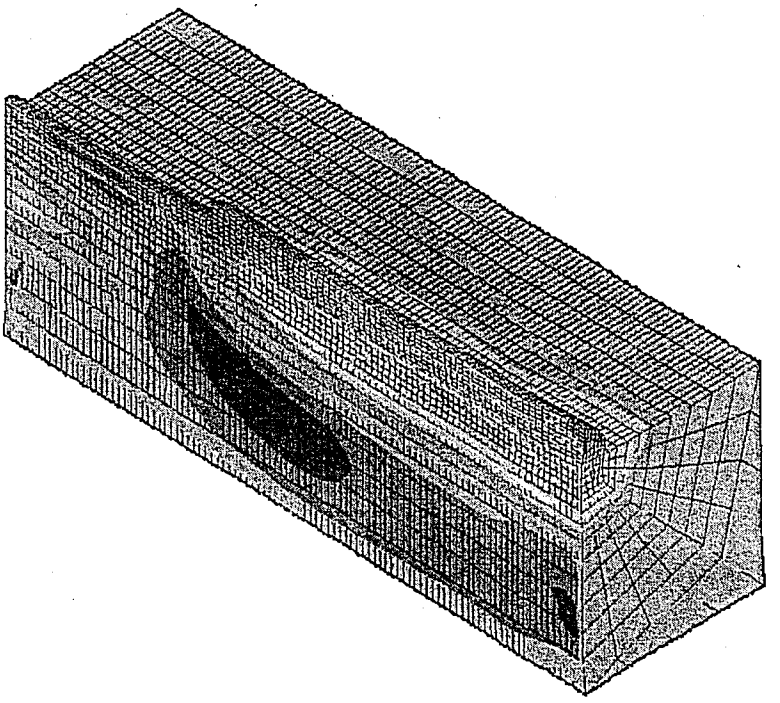

Figure 73 – Longitudinal Stress, Second Pass, Same Direction as First, t=5.625 seconds

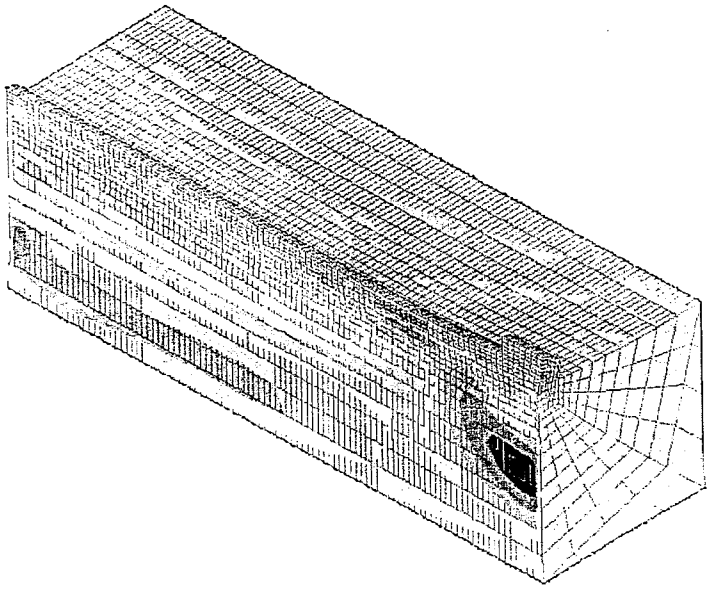

Figure 72 – Longitudinal Stress, Second Pass, Same Direction as First, t=4.625 seconds

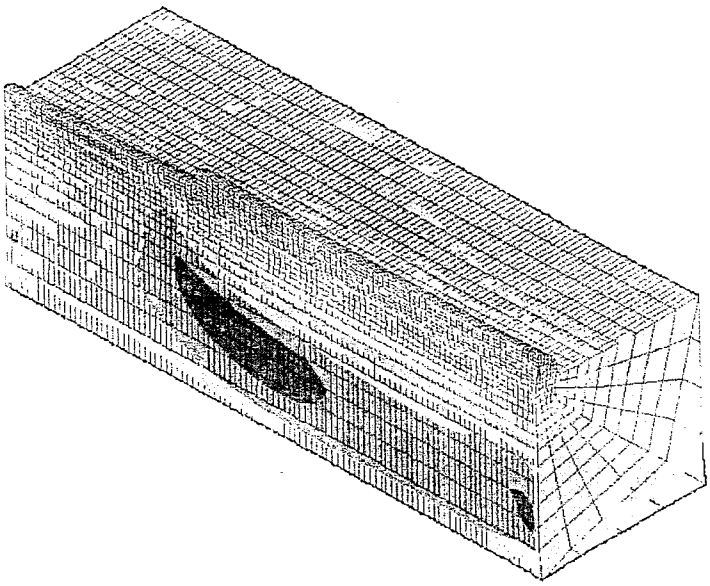

Figure 73 – Longitudinal Stress, Second Pass, Same Direction as First, t=5.625 seconds

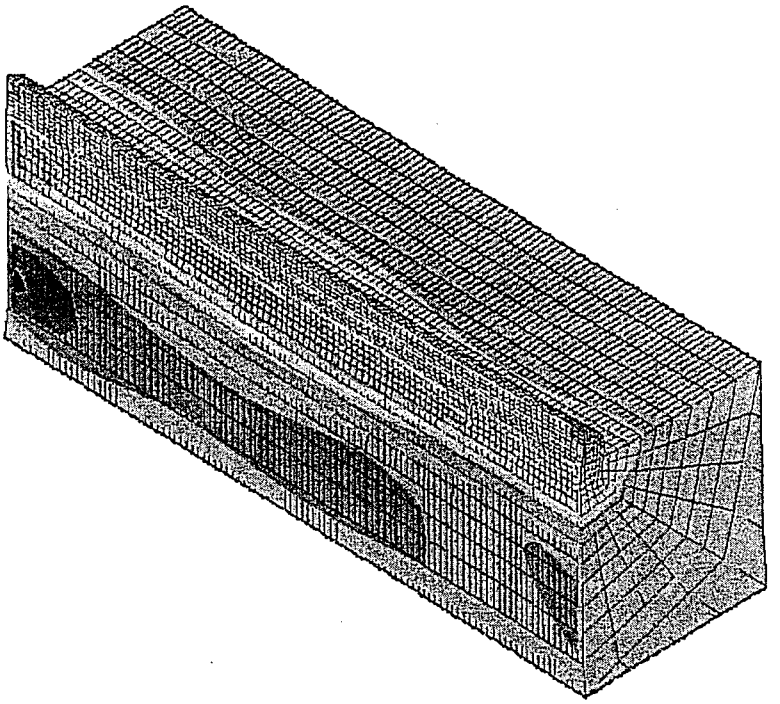

Figure 74 – Longitudinal Stress, Second Pass, Same Direction as First, t=6.5 seconds

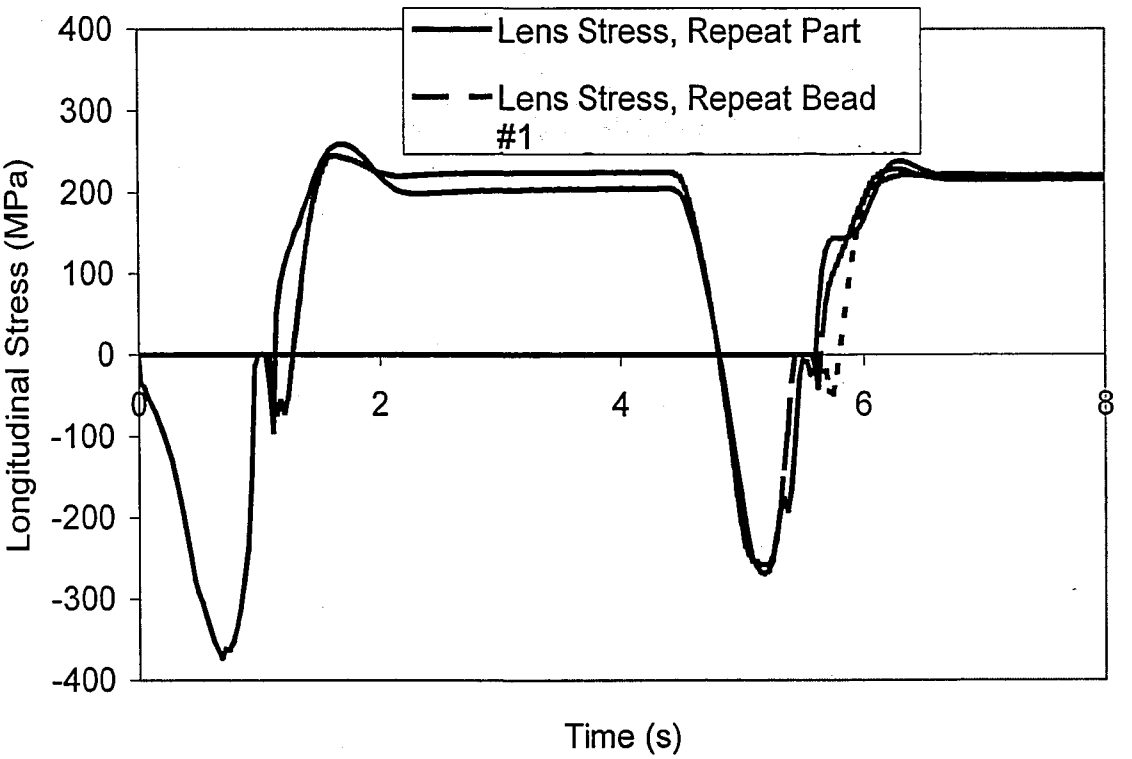

Figure 75 – Longitudinal Stress Profiles, Second Bead Same Direction as First

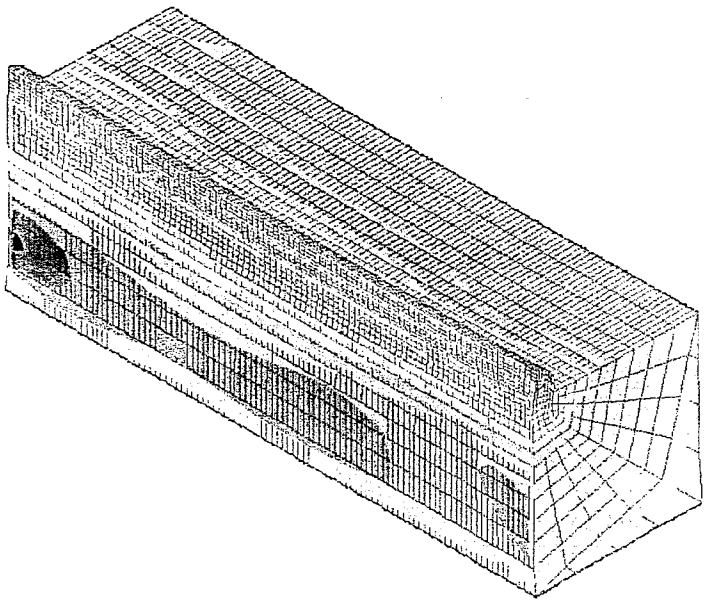

Figure 74 – Longitudinal Stress, Second Pass, Same Direction as First, t=6.5 seconds

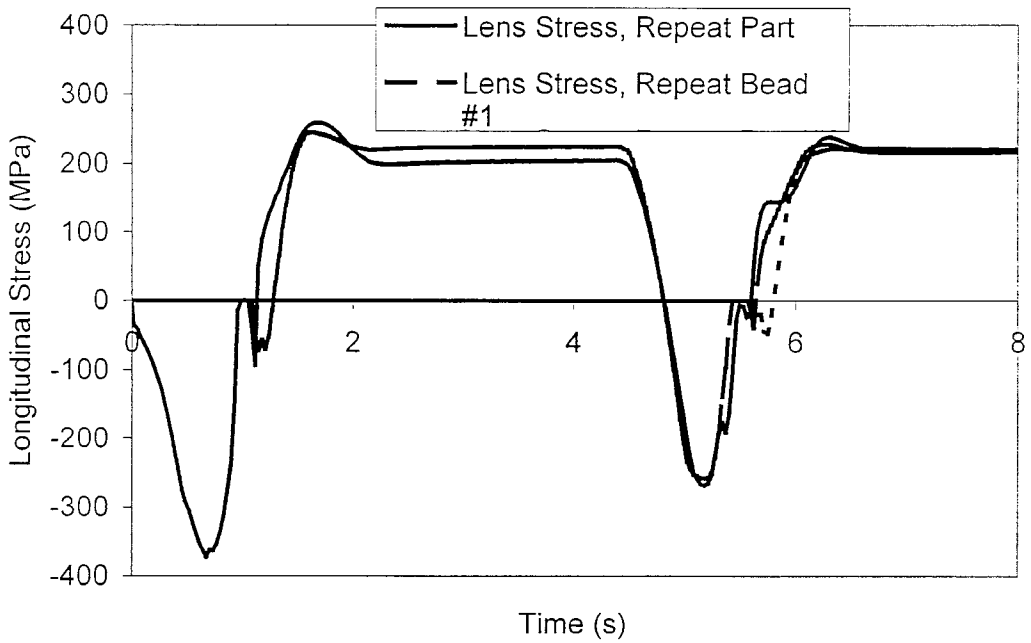

Figure 75 – Longitudinal Stress Profiles, Second Bead Same Direction as First

Mechanical results for the second deposit in the second model (with the second deposit in the opposite direction from the first) are given in Figure 76, Figure 77, and Figure 78. Thermal profiles in the substrate and both beads are given in Figure 79. Once again, these results were evaluated in the longitudinal center of the part, leading to similar looking results. Differences between the two cases are shown in Figure 80. Just before the source arrives at the point of interest for the second pass, the model with the same second pass direction experiences a larger compressive peak than the model with direction change. This greater compressive stress nearly disappears after the laser passes, however, leaving both models in a very similar state during cooling.

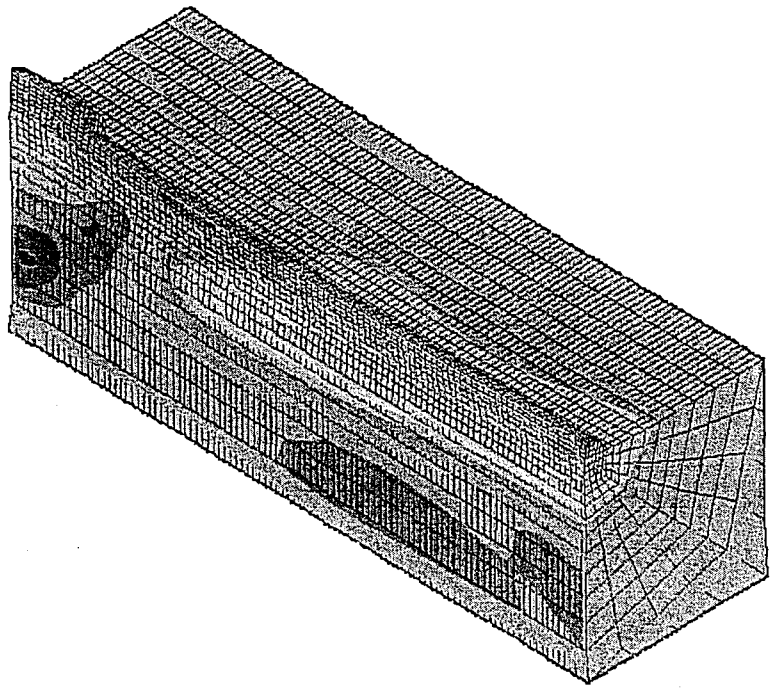

Figure 76 – Longitudinal Stress, Second Pass, Opposite Direction from First, t=4.625 seconds

Mechanical results for the second deposit in the second model (with the second deposit in the opposite direction from the first) are given in Figure 76, Figure 77, and Figure 78. Thermal profiles in the substrate and both beads are given in Figure 79. Once again, these results were evaluated in the longitudinal center of the part, leading to similar looking results. Differences between the two cases are shown in Figure 80. Just before the source arrives at the point of interest for the second pass, the model with the same second pass direction experiences a larger compressive peak than the model with direction change. This greater compressive stress nearly disappears after the laser passes, however, leaving both models in a very similar state during cooling.

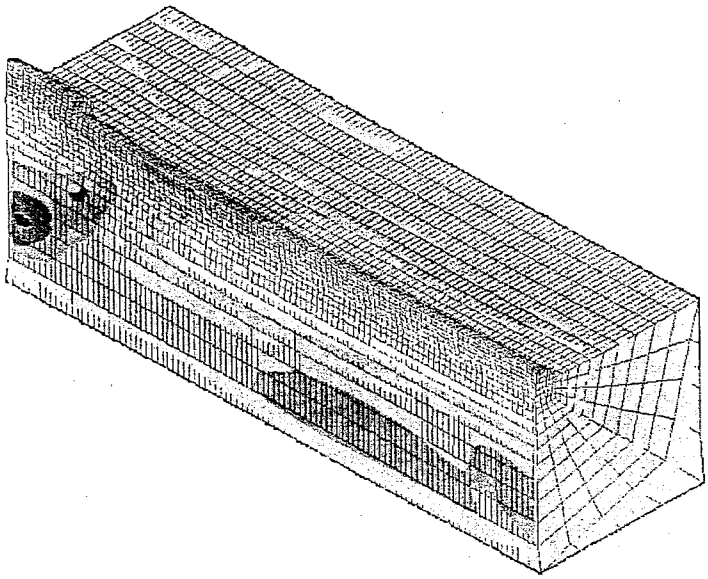

Figure 76 – Longitudinal Stress, Second Pass, Opposite Direction from First, t=4.625 seconds

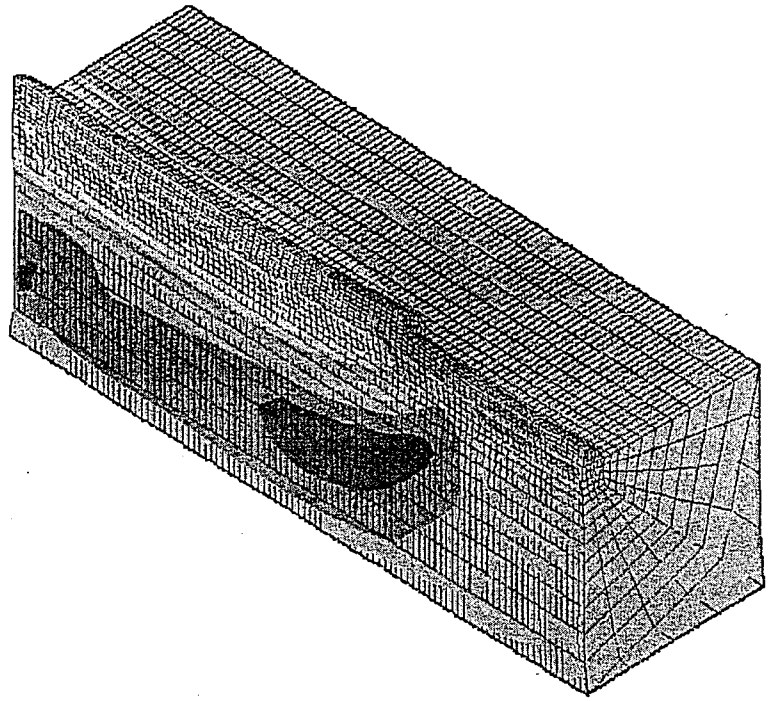

Figure 77 – Longitudinal Stress, Second Pass, Opposite Direction from First, t=5.9 seconds

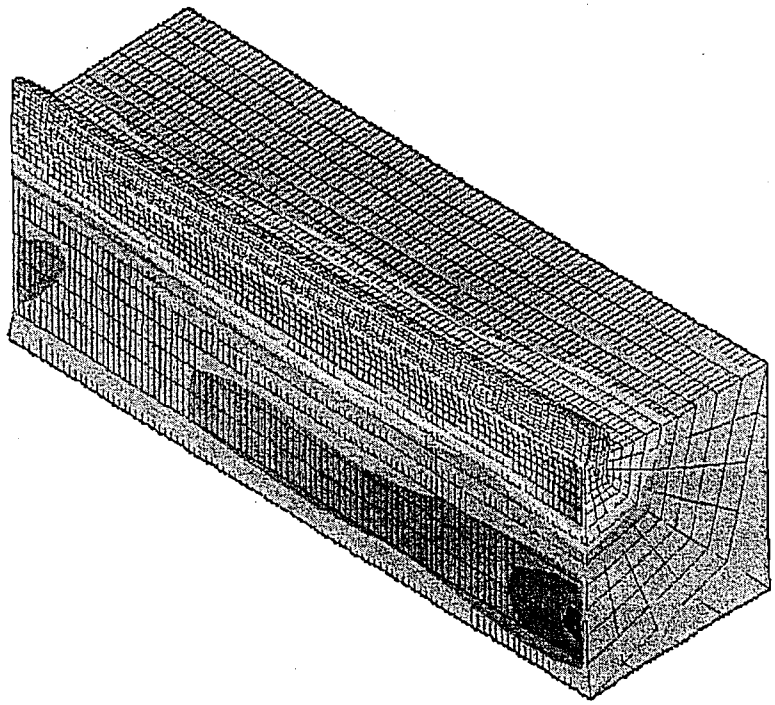

Figure 78 – Longitudinal Stress, Second Pass, Opposite Direction from First, t=6.5 seconds

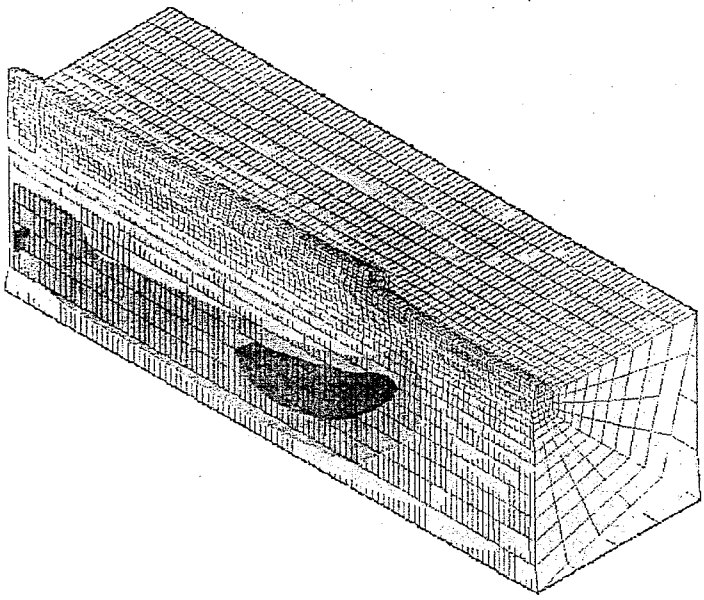

Figure 77 – Longitudinal Stress, Second Pass, Opposite Direction from First, t=5.9 seconds

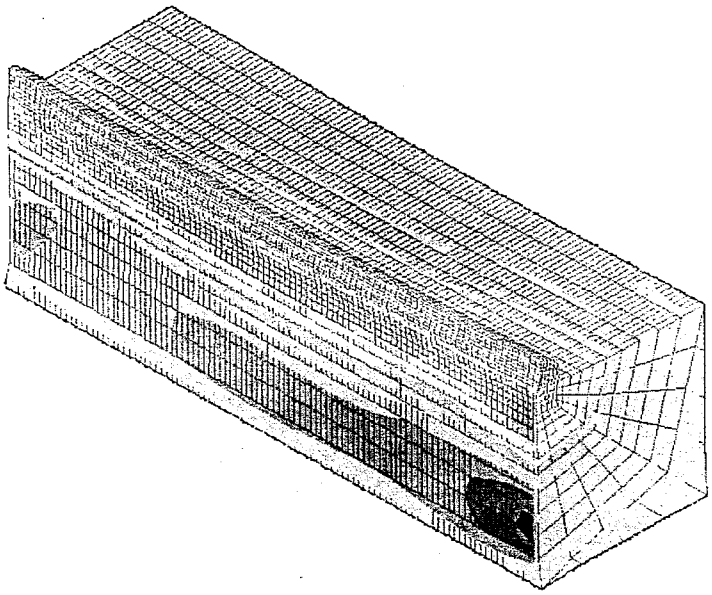

Figure 78 – Longitudinal Stress, Second Pass, Opposite Direction from First, t=6.5 seconds

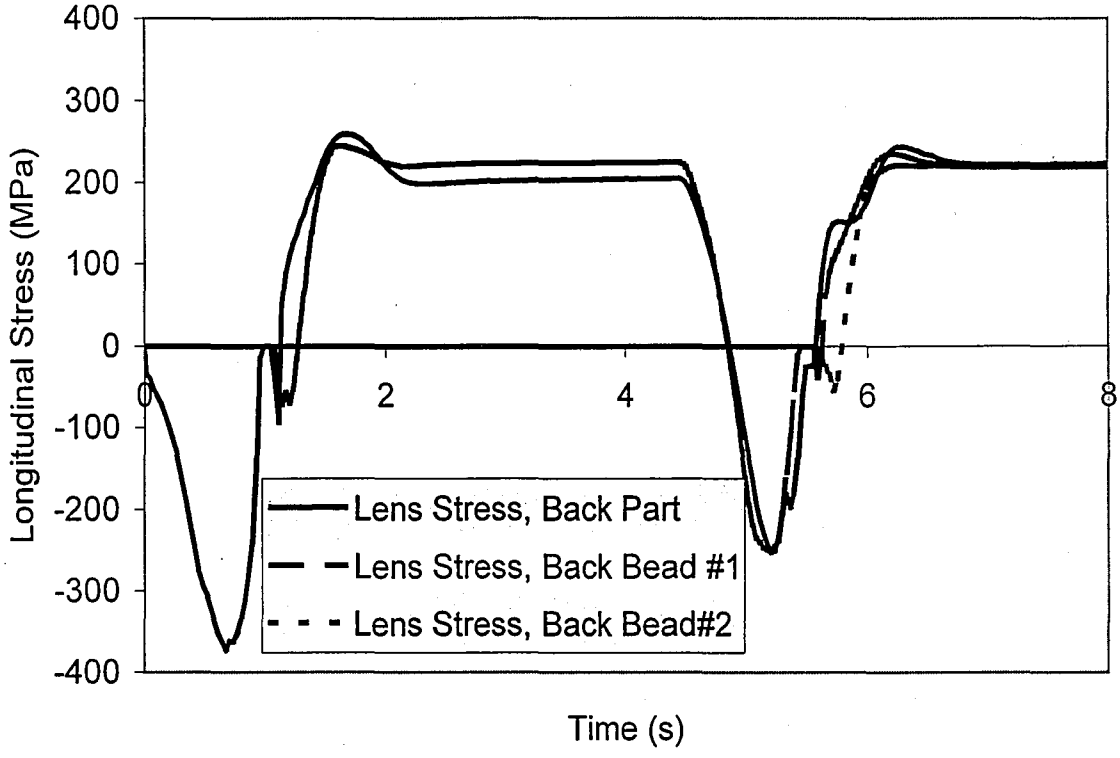

Figure 79 – Longitudinal Stress Profiles, Second Bead Opposite Direction from First

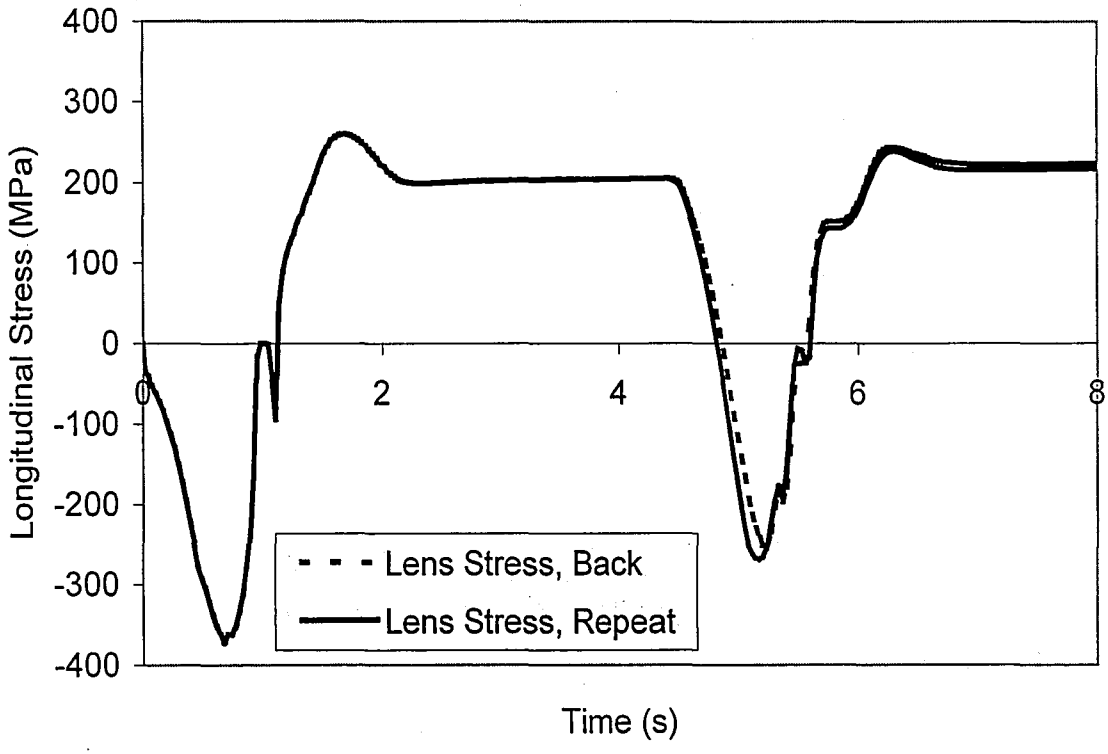

Figure 80 – Mechanical Comparison for Different Second Pass Direction

The results presented here are far from complete. The important point of this research is that models have been generated that successfully simulate two passes of a laser on a LENS line build. With this foundation, the addition of more layers should be relatively trivial, but will require significant computational resources, as the current models required nearly a full day on an SGI Origin 3800 and over twenty-five gigabytes of storage.

Chapter 5 – Conclusions and Future Work

5.1 Future Work

As with any software as powerful and full of features as SYSWELD, it is not reasonable to expect a new user to immediately begin producing useful results. In the case of this research, many months were spent familiarizing and learning about the software capabilities. With that in mind, only preliminary models of the LENS process are presented here. Considerable work must still be done before a model produces truly useful results. Several ideas are listed below for areas in which to concentrate this work to achieve the largest improvements in a short period of time.

The greatest limitations in any modeling procedure are computation time and storage requirements. Both of these factors increase dramatically with larger, three-dimensional meshes. However, if not enough of the physical volume is meshed, the entire model experiences a large temperature increase and temperature profiles and cooling rates are poorly predicted. One method of reducing storage and computation requirements while maintaining accuracy involves the use of plate and shell elements. Plates and shells are essentially two-dimensional elements that mimic three-dimensional behavior. These elements can be joined to three-dimensional elements with transition elements. As one advantage of plate and shell elements is that the elements can be fairly coarse and still deliver reliable results, these elements are not appropriate in areas with high thermal gradients. Therefore, the ability to use solid elements in regions of high thermal gradients and plates and shells elsewhere makes plate and shell elements very attractive, as they offer a significant reduction in solution times and storage requirements without a painful loss of accuracy. While plates and shells are not explored in the current

research, it is very likely that this technique would allow a more realistic model to be created with smaller computational expense. SYSWELD offers a large number of very flexible plate and shell options that are relatively easy to integrate with thermal and mechanical models.

Traditionally, when a three-dimensional mesh is generated to simulate welding, the entire region that will be welded is very refined compared with the rest of the part. Unfortunately, most of the time the simulation is running, the majority of these highly refined elements experience a very small thermal gradient. The only time an element must be refined is during the intense heating and cooling process immediately before and after heat has been applied. Again, dynamically changing the mesh during modeling is normally quite difficult, however SYSWELD includes resources that facilitate this moving mesh refinement. Properly implemented, moving mesh refinement allows the user to generate a fairly coarse mesh and then refine in the area immediately around the heat source. This technique promises a tremendous reduction in computation and storage requirements that would make a larger, more comprehensive LENS model far less demanding that it currently is.

Once the aforementioned mesh reduction techniques are implemented, additional beads may be added to simulate a full line build, and more complicated geometries may be explored, such as thin walled boxes. (See Figure 81 & Figure 82)

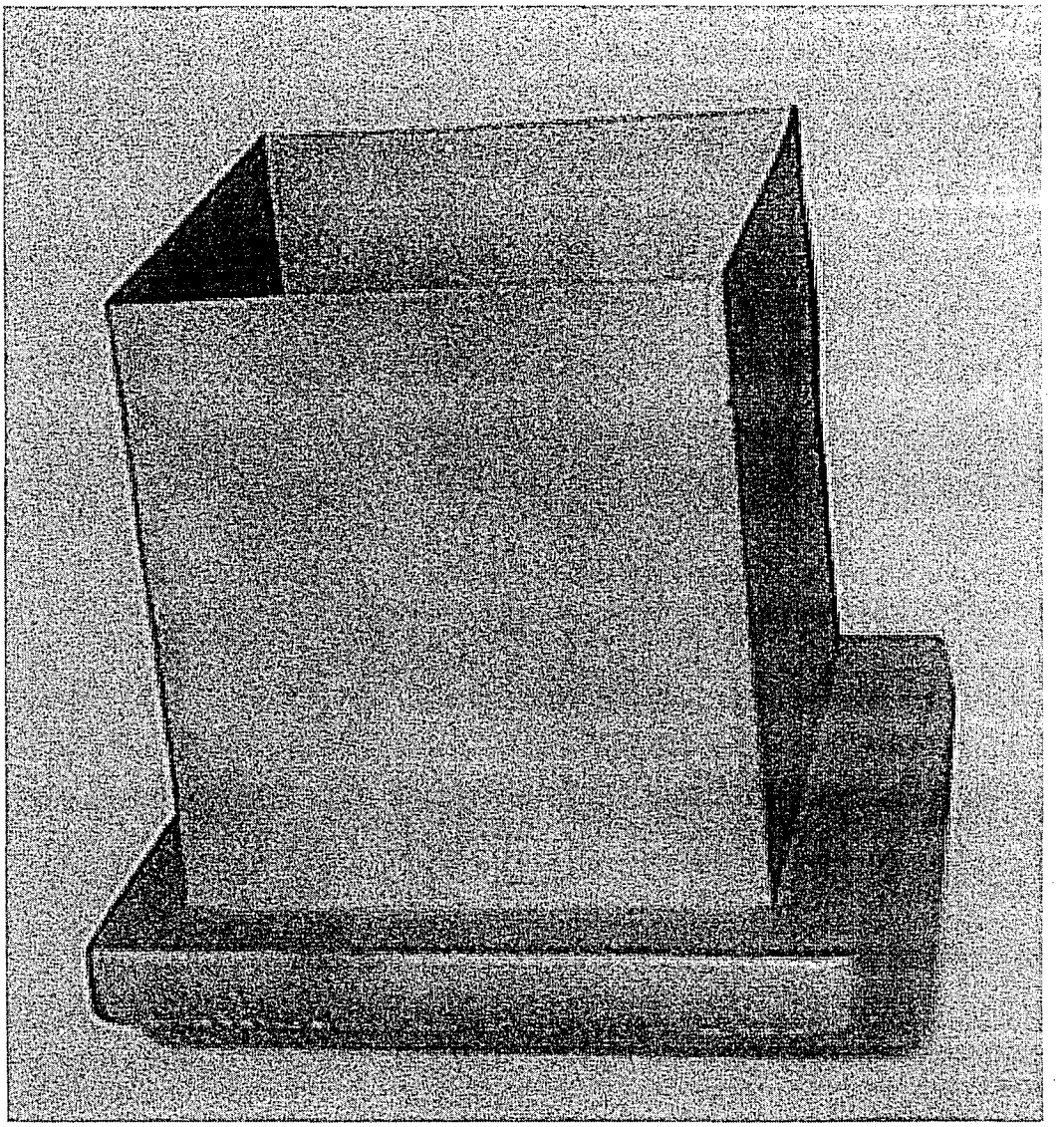

Figure 81- Thin Walled, LENS Deposited Box with Significant Distortion

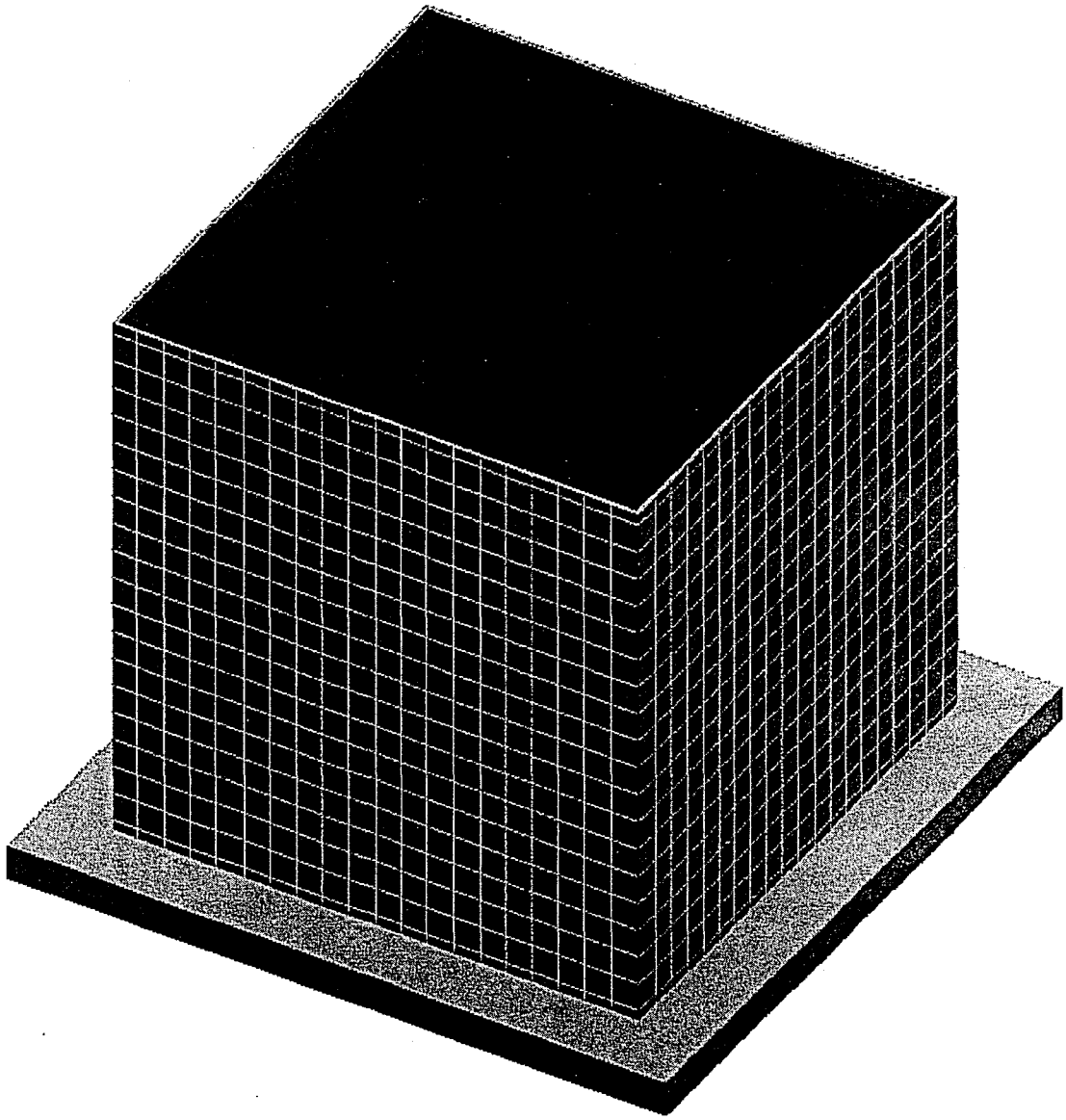

Figure 82 - Computer Model of Thin Walled, LENS Deposited Box

In the simulations considered here, only the simplest strain hardening models were considered. In order to accurately predict material behavior leading to residual stresses and distortion, a more comprehensive strain-hardening model must be implemented. In addition, other materials should also be explored. In this research, AL6XN stainless steel was selected largely because material properties are well understood at high temperatures. In the future, there will certainly be interest in other materials, including many that exhibit solid phase transformations. Therefore, research

must be conducted to develop an understanding of the input of metallurgical information into SYSWELD.

All of the aforementioned improvements will lead to models that deliver improved accuracy and relatively short solution times. However, even the best model is mostly useless if the information that is gained is not applied such that actual part quality improves. After all, the long-term purpose of this project is to study the LENS fabrication process and reduce residual stresses and distortion. Once models are created that can truly depict the thermal and mechanical behavior in the laser deposition process, LENS fabricated parts will be able to reach their full potential.

5.2 Conclusions

Models have been created that offer new insight into the relationships between finite element inputs and results. In addition, preliminary thermal and mechanical models for the lens process have been developed. This work should provide future studies with a firm starting point to further evaluate behavior in laser deposited parts.

References

1) J. Beaman, J. Barlow, D. Bourell, R. Crawford, H. Marcus, K. McAlea, "Solid Freeform Fabrication: A New Direction in Manufacturing," Kluwer Academic Publisher, Norwell, Massachusetts, 1997.
2) J. Halloran, "Adjunct Newsletter No. 6," 24 Feb. 1998, http://www.ehis.navy.mil/bwanew6.htm
3) H. Koukka, "The whole RP family tree," http://ltk.hut.fi/~koukka/RP/rptree.html, 20 April, 2001
4) "Aeromet Corporation," http://www.aeromet.com
5) T. Swain, Optomec Presentation to Lehigh University, July 2000
6) "Precision Optical Manufacturing," http://www.pom.net
7) Bora Yildirim, Nonlinear Thermal Stress/Fracture Analysis of Multilayer Structures using Enriched Finite Elements, Lehigh University, 2000.
8) R. Dykhuizen, D. Dobranich, "Scaling Analysis for LENS process," Sandia National Labs, 1998
9) J. Goldak, A. Chakravarti, M. Bibby, "A New Finite Element Model for Welding Heat Sources," Metallurgical Transactions B, Volume 15B, pp. 299-305, June 1984.
10) Y.V.L.N. Murthy, G. Venkata Rao, P. Krishna Iyer, "Numerical Simulation of Welding and Quenching Processes Using Transient Thermal and Thermo-Elasto-Plastic Formulations" Computers & Structures, Vol. 60, No. 1, pp. 131-154, 1996.
11) K. Masubuchi, "Analysis of Welded Structures-Residual Stresses, Distortion, and Their Consequences," Pergamon Press, 1980.
12) P. Michaleris, A. DeBiccari, Prediction of Welding Distortion, Welding Journal, 76(4): 172-180s, 1997.
13) A. Hoadley, M. Rappaz, "A Thermal Model of Laser Cladding by Powder Injection," Metallurgical Transactions B, Vol. 23B, pp. 631-642, October 1992.
14) A. Nickel, D. Barnett, G. Link, F. Prinz, "Residual Stresses in Layered Manufacturing" Solid Freeform Fabrication Symposium, Austin, Texas, pp. 239-246, 1999.
15) M. Griffith, M. Schlienger, L. Harwell, M. Oliver, M. Baldwin, M. Ensz, M. Essien, J. Brooks, C. Robino, J. Smugeresky, W. Hofmeister, M. Wert, D. Nelson, "Understanding thermal behavior in the LENS process," Materials and Design, Vol 20, Issues 2-3, pp.107-113, June 1999.
16) W. Hofmeister, M. Wert, J. Smugeresky, J. Philliber, M. Griffith, M. Ensz, "Investigating Solidification with the Laser Engineered Net Shaping (LENS) Process," Journal of Materials (JOM), vol. 51, No. 7, July 1999.
17) A. Vasinonta, J. Beuth, M. Griffith, "Process Maps for Laser Deposition of Thin-Walled Structures," Solid Freeform Fabrication Symposium, Austin, Texas, pp. 383-391, 1999.
18) J. Brooks, C. Robino, T. Headley, S. Goods, M. Griffith, "Microstructure and Property Optimization of LENS Deposited H13 Tool Steel," Solid Freeform Fabrication Symposium, Austin, Texas, pp. 375-382, 1999.

19) B. A. B. Anderson, "Thermal Stresses in a Submerged – Arc Welded Joint Considering Phase Transformations", ASME J. Engineering Materials and Technology, vol. 100, pp. 356-362, 1978.
20 W. M. Steen, "Laser Material Processing, Second Addition," Springer, pp. 346, 1998
21) S. Marugan, P.V. Kumar, T.P.S. Gill, B. Raj, and M.S.C. Bose, "Numerical Modeling and Experimental Determination of Temperature Distribution During Manual Metal Arc Welding", Science and Technology of Welding and Joining, vol. 4, number 6, pp. 357-364, 1999.
22) V. Babu, S.A. Korpela, N. Ramanan, "Flow and Temperature Fields in a Weld Pool Formed by a Moving Laser", Journal of Applied Physics, vol. 67, number 9, pp. 3990-3998, 1990.
23) G. Ehlen, A. Schweizer, A. Ludwig, P.R. Sahm, "Macroscopic Modeling of Marangoni Flow and Solute Redistribution During Laser Welding of Steel", 8'th Int. Conf on Modeling of Casting, Welding and Advanced Solidification Process, San Diego, pp. 289
24) C.L. Chan, J. Mazumder, M.M. Chen, "Effect of surface tension gradient driven convection in a laser melt pool: Three-dimensional perturbation model", Journal of Applied Physics, vol. 64, number 11, pp 6166-6174, 1988.
25) C. K. Lueng, R. J. Pick, D. H. B. Mok, Weld. Res. Counc. Bull., vol. 356, pp. 1-10, 1990.
26 SYSWELD 2002, "Computation Rules for Welding and Heat Treatment," SYSWELD Self Training, ESI Group, 2001
27 A.P. Boresi, R.J. Schmidt, O.M. Sidebottom, "Advanced Mechanics of Materials, Fifth Edition", John Wiley & Sons, Inc, pp. 811, 1993
28 L. E. Lindgren, "Finite Element Modeling and Simulation of Welding, Part 1: Increased Complexity", Journal of Thermal Stresses, Vol. 24, pp. 141-192, 2001.
29 SYSTUS 2002, Analysis Reference Manual, ESI Group, 2002
30) SYSWELD 2002, SYSWELD 2002 Example Manual, ESI Group, 2002
31) SYSWELED 2002, SYSWELD 2002 Reference Manual, ESI Group, 2002
32 R. R. Unocic, "A Fundamental Investigation of Process Efficiencies in Laser Engineered Net Shaping (LENS) Solid Freeform Fabrication Process", Thesis, Lehigh University, 2002.

Appendix

Listed here are the input files for the double-deposit LENS simulation discussed above. The only files that is not given here is the geometry file. There is not reasonable to give this information in text format.

THERM1.DAT

```
; In this case, searches file with groups already created
SEARCH DATA 2

; Lowers bandwidth
RENUMBER ITERATION 20
 1 NODE INTER
RETURN

MODIF
NUMBER INIT 1
RETURN


; Enthalpy or Metallurgy Option required to use element
;  activation.  Enthalpy option does not require
;  ENTHALPY label in material properties.
DEFINITION
 WELDING SIMULATION
OPTION THERMAL ENTHALPY SPATIAL
RESTART GEOMETRY

; The STATE label refers to activation programs.  Note that there are
;  three different programs.  The first program, in this case 200, is
;  the  actual activation program.  If you wish to deposit multiple
;  beads, you must also have programs to turn entire beads on and
;  entire beads off.

MATERIAL
 ELEMENTS GROUP $PART$ / C=-10002 KX=-10001 KY=-10001 KZ=-10001--
 RHO=1
 ELEMENTS GROUP $BEAD1$ / C=-10002 KX=-10001 KY=-10001 KZ=-10001--
 RHO=1 STATE=-200
 ELEMENTS GROUP $BEAD2$ / C=-10002 KX=-10001 KY=-10001 KZ=-10001--
 RHO=1 STATE=-300

CONSTRAINTS
 ELEMENTS GROUP $SKINPART$ / KT=1 VARIABLE=10


; A positive number for a table designation (above in constraints
;  (Variable=10)) means that the function is a function of
;  temperature.  A negative number for a table designation (below in
;  loads (Variable=-100)) means that the program is a function of temp
;  and spatial coords.  Here, the first number read is the x coord, the
;  second is y, the third is z, and the fourth is temp.  There are
;  fifth and more arguments, which can be  found in documentation

LOAD
1 welding / LASER HEAT SOURCE
  ELEMENTS GROUP $PART$ / QR=1 VARIABLE=-100
  ELEMENTS GROUP $BEAD1$ / QR=1 VARIABLE=-100
  ELEMENTS GROUP $SKINPART$ / TT 20
TABLE
```

```
; Bead Properties
;  Conductivity
 10001 / 1 20 0.0137 100 .0137 500 0.025 1320 0.04 1400 .160
;  Specific Heat
 10002 / 1 20 0.00403 500 0.004836 1200 0.005239 1325 0.00536--
 1347 .00574 1360 .00625 1366 .0068


; Example of enthalpy inputs.  IMPORTANT: If enthalpy is given,
;  it must be specified for ever value of temperature that
;  the part will experience.  Eg., if the part reaches 1800 degrees,
;  and the top specified enthalpy value is 1600 degrees, the program
;  will stop and complain.

;  Enthalpy
 10003 / 1 0 1.0926 20 1.1726 1320 7.498691--
  1400 10.031403 1700 11.66451 2600 16.563831 3500 21.463152



;Lost of heat by radiation
 10 /  FORTRAN
      FUNCTION F(T)
c  radiative losses : f = sig * e ( t ) * (t + to)(t**2 + to**2)
      E = 0.7
      SIG = 5.67*-8
      T0 = 20.
      T0 = T0 + 273.15
      T1  = T + 273.15
      A = T1 * T1
      B = T0 * T0
      C = A + B
      D = T1 + T0
      D = D * C
      D = D * E
      D = D * SIG
c
c  convective losses = 10 W/m2/K
c
      D = D + 10.
      F = D * 1.*-6
      RETURN
      END


;  Conical heat source, as given by SYSWELD
  100 / FORTRAN
      FUNCTION F(X)
C
C   F    = Q0 * exp( - R^2 / R0^2 ) with
C   R^2 = ( XX-X0 )^2 + ( YY-Y0-VY*T )^2
C   R0   = RE - ( RE-RI )*( ZE-ZZ+Z0 )/( ZE-ZI )
C   IF R0 < RI , R0 = 0. and return
C   IF R0 > RE , R0 = 0. and return
```

```
C
      DIMENSION X(4)
C
C Input
C
      XX = X(1)    ; X Coordinate
      YY = X(2)    ; Y Coordinate
      ZZ = X(3)    ; Z Coordinate
      TT = X(4)    ; Time
C
C Variables
C
      Q0 = 1350     ; Maximal source intensity
      RE = 0.35     ; Gaussian parameter for top radius
      RI = 0.15     ; Gaussian parameter for bottom radius
      ZE = 0.20     ; Upper plane of source
      ZI = -0.3     ; Lower plan of source
      X0 = 0     ; X initial location of source center
      Y0 = 0     ; Y initial location of source center
      Z0 = 0    ; Z initial location of source center
      VY = -5     ; Source displacement velocity
C
C Constant
C
      M1 = -1
C
C R^2 computation
C R2 = A^2 + ( YY - Y0 -VY * TT )^2
C R2 = A + ( YY - Y0 -VY * TT )^2
C R2 = A + B^2
C R2 = A + B
C
      A     = XX X0 -                    ; A     = XX - X0
      A     = A A *                      ; A     = A^2
      B     = YY VY TT * - Y0 -          ; B     = YY -( VY * TT ) - Y0
      B     = B B *                      ; B     = B^2
      R2    = A B +                      ; R2    = A + B
C
C R0^2 computation
C R02 = ( RE - ( RE-RI )*( ZE-ZZ+Z0 )/ A )^2
C R02 = ( RE - ( RE-RI )* A )^2
C R02 = ( RE - A )^2
C R02 = A^2
C
      A     = ZE ZI -                    ; A     = ZE - ZI
      A     = Z0 ZE ZZ - + A /           ; A     = ( ZE - ZZ + Z0 ) / A
      A     = A RE RI - *                ; A     = A * ( RE - RI )
      A     = RE A -                     ; A     = RE - A
      IF( A .LT. RI ) A = 0.             ; if A < RI , A = 0.
      IF( A .GT. RE ) A = 0.             ; if A > RE , A = 0.
      IF( A .EQ. 0. ) RETURN             ; if A = 0. , return
      R02   = A A *                      ; R02   = A^2
C
C F computation
C F = Q0 * exp( - R2 / R02 )
```

```
C F = Q0 * exp( A )
C F = Q0 * A
C
      A    = M1 R2 R02 / *              ; A    = -( R2 / R02 )
      A    = EXP( A )                   ; A    = exp( A )
      F    = Q0 A *                     ; F    = Q0 * A
C
      RETURN
      END

; For thermal models with element activation, it is recommended
;  that elements are activated just in front of the source for
;  the most stability.

;Activation and deactivation function
;
  200 / FORTRAN
       FUNCTION F(X)
       DIMENSION X(4)

     xa   = X[1];
     ya   = X[2];
     za   = X[3];
     time = X[4];
C initial position of heat source in the new frame
      xc = 0;
      yc = 0;
      zc = 0;
CTranslation
      xa = xa - xc
      ya = ya - yc
      za = za - zc
C
C Welding velocity
     wv=-5.0;
C POSITION OF HEAT SOURCE CENTER
    f=0;
    center=wv*time;
    center = center - 0.2;
    if (ya .GT. center) f=1;
    return
    end
;
; Turn off all elements in a bead
;
  300 / FORTRAN
       FUNCTION F(X)
       DIMENSION X(4)
     xa   = X[1];
     ya   = X[2];
     za   = X[3];
     time = X[4];
     f = -1
     return
     end
```

```
;
; Turn on all elements in a bead
;
  400 / FORTRAN
        FUNCTION F(X)
        DIMENSION X(4)
      xa   = X[1];
      ya   = X[2];
      za   = X[3];
      time = X[4];
      f = 1
      return
      end
;
RETURN

SAVE DATA 4

; The BFGS algorithm generally solves very quickly.  See SYSWELD
;  manuals for detailed explanations.
; The iterative solver is much better than the direct solver for
;  meshes greater than 2500 to 3000 elements.
; Use the SYMMETRICAL label whenever it works
; STORE 1 stores every card
; STORE 2 stores every other card, etc
; If a mechanical simulation is to follow the thermal simulation,
;  it is wise to store every card, as the mechanical simulation usually
;  requires finer time steps than a thermal simulation and any
;  additional information is very useful for generating usable
;  results


SEARCH DATA 4
TRANSIENT NON LINEAR
ALGORITHM BFGS IMPLICIT 0.5 ITERATION 150
PRECISION ABSOLUTE NORM 0 FORCE 1*-10 DISPLACEMENT .5
METHOD ITERATIVE SYMMETRICAL
INITIAL CONDITION
 NODES / TT 20
 ELEMENTS GROUP $BEAD1$ / IS -1
 ELEMENTS GROUP $BEAD2$ / IS -1
TIME INITIAL 0.0
 0.03125 STEP 0.015625 / STORE 1
RETURN
SAVE DATA TRAN 10

SEARCH DATA 10
ASSIGN 19 TRAN10.TIT

; It is wise to split the computation into two parts for several
;  reasons:
; First: if your don't and your simulation crashes, you have no results
;  to look at for debugging, as your file has not been explicitly
;  saved.  Again, the ASSIGN command, below, opens the file for
;  reading and writing, so if your simulation crashes in the middle of
```

```
;  a time step, if your file was assigned, you will have all results
;  up to the crash.  If you SEARCH DATA 10, do all of your time steps,
;  and then SAVE DATA TRAN 10, and something happens in the middle of
;  your simulation, everything is lost.
; Second: If you do all of your time steps in the first group of
;  commands (above), and then SAVE DATA TRAN 10, the system create a
;  temporary file into which it dumps results.  This will be called
;  tmp.something, where something is any string of characters.
;  This is no problem as long as your simulation is not large.
;  If your simulation creates a temporary file that is 10 GB and then
;  tries to save it as TRAN10.TIT, you must have 20 GB of free space.
;  If the TRAN10.TIT file is assigned, results are dumped directly into
;  that file and no tmp file is generated.  Therefore, in the above
;  example, only 10 GB of free space is required.  Storage limitations
;  are usually a bigger problem in mechanical simulations


TRANSIENT NON LINEAR
ALGORITHM BFGS IMPLICIT 0.5 ITERATION 150
PRECISION ABSOLUTE NORM 0 FORCE 1*-10 DISPLACEMENT .5
METHOD ITERATIVE SYMMETRICAL
INITIAL CONDITION RESTART CARD LAST
TIME INITIAL RESTART
 2.0 step .015625 / store 1
 3.9375 step .0625 / store 1
RETURN

SAVE DATA 10
DEASSIGN 19
```

THERM2.DAT

```
; Search file from first half of simulation
SEARCH DATA 10

DEFINITION
 WELDING SIMULATION
OPTION THERMAL ENTHALPY SPATIAL
RESTART GEOMETRY

; Here, the only change from the previous file is that the
;  first bead is STATE=-400 (activated) and the the second
;  bead is STATE=-200 (in the process of being activated)

MATERIAL
 ELEMENTS GROUP $PART$ / C=-10002 KX=-10001 KY=-10001 KZ=-10001--
 RHO=1
 ELEMENTS GROUP $BEAD1$ / C=-10002 KX=-10001 KY=-10001 KZ=-10001--
 RHO=1 STATE=-400
 ELEMENTS GROUP $BEAD2$ / C=-10002 KX=-10001 KY=-10001 KZ=-10001--
 RHO=1 STATE=-200

CONSTRAINTS
 ELEMENTS GROUP $SKINPART$ / KT=1 VARIABLE=10

LOAD
1 welding / DISK HEAT SOURCE
  ELEMENTS GROUP $PART$ / QR=1 VARIABLE=-100
  ELEMENTS GROUP $BEAD1$ / QR=1 VARIABLE=-100
  ELEMENTS GROUP $BEAD2$ / QR=1 VARIABLE=-100
  ELEMENTS GROUP $SKINPART$ / TT 20

TABLE

; Bead Properties
;  Conductivity
 10001 / 1 20 0.0137 100 .0137 500 0.025 1320 0.04 1400 .160
;  Specific Heat
 10002 / 1 20 0.00403 500 0.004836 1200 0.005239 1325 0.00536--
 1347 .00574 1360 .00625 1366 .0068
;  Enthalpy
 10003 / 1 0 1.0926 20 1.1726 1320 7.498691--
  1400 10.031403 1700 11.66451 2600 16.563831 3500 21.463152



;Lost of heat by radiation
 10 /  FORTRAN
      FUNCTION F(T)
c  radiative losses : f = sig * e ( t ) * (t + to)(t**2 + to**2)
      E = 0.7
      SIG = 5.67*-8
      T0 = 20.
      T0 = T0 + 273.15
      T1  = T + 273.15
```

```
      A = T1 * T1
      B = T0 * T0
      C = A + B
      D = T1 + T0
      D = D * C
      D = D * E
      D = D * SIG
C
c  convective losses = 10 W/m2/K
c
      D = D + 10.
      F = D * 1.*-6
      RETURN
      END


; The heat source must be adjusted so that it is in the
;  correct position Remember that the initial time for
;  this program is not t=0, but in this case is t=4.5

  100 / FORTRAN
      FUNCTION F(X)
C
C   F   = Q0 * exp( - R^2 / R0^2 ) with
C   R^2 = ( XX-X0 )^2 + ( YY-Y0-VY*T )^2
C   R0  = RE - ( RE-RI )*( ZE-ZZ+Z0 )/( ZE-ZI )
C   IF R0 < RI , R0 = 0. and return
C   IF R0 > RE , R0 = 0. and return
C
      DIMENSION X(4)
C
C Input
C
      XX = X(1)    ; X Coordinate
      YY = X(2)    ; Y Coordinate
      ZZ = X(3)    ; Z Coordinate
      TT = X(4)    ; Time
C
C Variables
C
      Q0 = 1100     ; Maximal source intensity
      RE = 0.35     ; Gaussian parameter
      RI = 0.15     ; Gaussian parameter
      ZE = 0.45     ; Upper plan
      ZI = -0.05     ; Lower plan
      X0 = 0     ; X initial location of source center
      Y0 = 0     ; Y initial location of source center
      Z0 = 0.0    ; Z initial location of source center
      VY = -5     ; Source displacement velocity
C
C Constant
C
      M1 = -1
C
C R^2 computation
```

```
C R2 = A^2 + ( YY - Y0 -VY * TT )^2
C R2 = A + ( YY - Y0 -VY * TT )^2
C R2 = A + B^2
C R2 = A + B
C
      TT   = TT 4.5 -
      A    = XX X0 -                    ; A    = XX - X0
      A    = A A *                      ; A    = A^2
      B    = YY VY TT * - Y0 -          ; B    = YY -( VY * TT ) - Y0
      B    = B B *                      ; B    = B^2
      R2   = A B +                      ; R2   = A + B
C
C R0^2 computation
C R02 = ( RE - ( RE-RI )*( ZE-ZZ+Z0 )/ A )^2
C R02 = ( RE - ( RE-RI )* A )^2
C R02 = ( RE - A )^2
C R02 = A^2
C
      A    = ZE ZI -                    ; A    = ZE - ZI
      A    = Z0 ZE ZZ - + A /           ; A    = ( ZE - ZZ + Z0 ) / A
      A    = A RE RI - *                ; A    = A * ( RE - RI )
      A    = RE A -                     ; A    = RE - A
      IF( A .LT. RI ) A = 0.            ; if A < RI , A = 0.
      IF( A .GT. RE ) A = 0.            ; if A > RE , A = 0.
      IF( A .EQ. 0. ) RETURN            ; if A = 0. , return
      R02  = A A *                      ; R02  = A^2
C
C F computation
C F = Q0 * exp( - R2 / R02 )
C F = Q0 * exp( A )
C F = Q0 * A
C
      A    = M1 R2 R02 / *              ; A    = -( R2 / R02 )
      A    = EXP( A )                   ; A    = exp( A )
      F    = Q0 A *                     ; F    = Q0 * A
C
      RETURN
      END

;Activation and deactivation function
;
; Same caution as above required here.
;  Initial time is 4.5, not zero
;
  200 / FORTRAN
       FUNCTION F(X)
       DIMENSION X(4)

     xa   = X[1];
     ya   = X[2];
     za   = X[3];
     time = X[4];
C initial position of heat source in the new frame
      xc = 0;
      yc = 0;
```

```
      zc = 0;
CTranslation
      xa = xa - xc
      ya = ya - yc
      za = za - zc
C
C Welding velocity
     wv=-5.0;
C POSITION OF HEAT SOURCE CENTER
    f=0;
    time=time-4.5;
    center=wv*time;
    center = center - 0.5;
    if (ya .GT. center) f=1;
    return
    end
;
; Turn off all elements in a bead
;
  300 / FORTRAN
       FUNCTION F(X)
       DIMENSION X(4)
     xa   = X[1];
     ya   = X[2];
     za   = X[3];
     time = X[4];
     f = -1
     return
     end
;
; Turn on all elements in a bead
;
  400 / FORTRAN
       FUNCTION F(X)
       DIMENSION X(4)
     xa   = X[1];
     ya   = X[2];
     za   = X[3];
     time = X[4];
     f = 1
     return
     end
;
RETURN

SAVE DATA 11

; Since the TRAN10.TIT file has already been initialized,
;  it can be assigned right away, with no preliminary
;  calculation required.

SEARCH DATA 11
ASSIGN 19 TRAN10.TIT
TRANSIENT NON LINEAR
ALGORITHM BFGS IMPLICIT 0.5 ITERATION 150
```

```
PRECISION ABSOLUTE NORM 0 FORCE 1*-10 DISPLACEMENT .5
METHOD ITERATIVE SYMMETRICAL
INITIAL CONDITION RESTART CARD LAST
TIME INITIAL RESTART
 4.125 STEP .0625 / STORE 1
 4.4375 STEP .03125 / store 1
 6.5 step .015625/ store 1
 7.0 STEP .03125 / store 1
 8.0 step 0.0625 / store 1
RETURN

SAVE DATA 10
DEASSIGN 19
```

MECH1.DAT

```
; Search results of thermal calculation
SEARCH DATA 10

DEFINITION
    WELDING SIMULATION
OPTION THREE DIMENSIONAL THERMOMECHANICAL
RESTART GEOMETRY
; The TF=1400 label sets the temperature above which the material
;  has no strength.  This is better than trying to set the mechanical
;  properties to zero in the next section, as that leads to zero
;  diagonal terms in the stiffness matrix (a.k.a. singular matrix)
; Also, the STATE label refers to activation programs.  Note that
;  there are three different programs.  The first program, in this
;  case 200, is the actual activation program.  If you wish to deposit
;  multiple beads, you must also have programs to turn entire beads on
;  and entire beads off.
; Finally, the MODEL label refers to strain hardening models.
; MODEL=1 refers to elastic perfectly plastic
; MODEL=2 refers to kinematic strain hardening
; MODEL=3 refers to isotropic strain hardening
; Models 2 and 3 should be accompanied by further parameters.
; All of these models are discussed in detail in the section of the
;  SYSTUS Analysis Reference Manual entitled Material Behavior Laws

MATERIAL PROPERTIES
 ELEMENTS GROUP $PART$ / E=-10001 YIELD=-10005 LX=-10002 LY=-10002 LZ=-
10002--
  MODEL=1 NU=0.3  TF=1400
 ELEMENTS GROUP $BEAD1$ / E=-10001 YIELD=-10005 LX=-10002 LY=-10002
LZ=-10002--
  MODEL=1 NU=0.3 STATE=-200 TF=1400
 ELEMENTS GROUP $BEAD2$ / E=-10001 YIELD=-10005 LX=-10002 LY=-10002
LZ=-10002--
  MODEL=1 NU=0.3 STATE=-300 TF=1400

; Note that only Symmetry constraints may be applied to elements that
will
;  be activated.
CONSTRAINTS
 NODES GROUP $P7$ / UX UY UZ
 NODES GROUP $P93$ / UX UY UZ
 NODES GROUP $D9$ / SYMMETRY
 NODES GROUP $D14$ / SYMMETRY
 NODES GROUP $D20$ / UX
 NODES GROUP $D30$ / UX
 NODES GROUP $D3$ $D4$ $D5$ $D6$ $D7$ / UY
 NODES GROUP $D17$ $D22$ $D27$ $D32$ $D36$ / UY
 NODES GROUP $D38$ / UZ
 NODES GROUP $L100$ / UX UZ

LOADS
1 welding / NOTHING
```

```
TABLE
 10001 / 1 24 195000 93 189000 204 180000 316 171000 427 161000 538
152000--
   982 90000 1093 72000 1200 45000 1216 43000 1237 41400 1250 39500
1256 --
   38000 1289 20000 1308 10000 1330 3000 1340 1240 1350 620 1380 100 --
   1410 100

; If Metallurgy is used, LX, LY, and LZ must be given as thermal
strains,
;  which are simply the coef. of thermal expansion multiplied by the
;  temperature.  Any attempt to use coef. of thermal expansion instead
;  of thermal strains will lead to very wrong results.
;  An example of thermal strains for AL6XN is given in table 10092
 10092 / 1 20 0 100 .001224 200 .00279 300 .004396 400 .00608 500
.007872--
   600 .009686 700 .011628 800 .013728 1200 .023128 1250 .024477 1300--
   1320 .02652
;
; If the metallurgy label is not specified, the coefficient of thermal
;  expansion may be specified as in table 10002
 10002 / 1 20 .0000085 100 .0000153 200 .0000155 300 .0000157--
  400 .000016 500 .0000164 600 .0000167 700 .0000171 800--
  .0000176 1200 .0000196 1250 .0000199 1300 .0000201 1320--
  .0000204

;Yield stress
;
 10005 / 1 21 365 93 325 149 290 204 270 260 255 316 235 371 230 427 --
         230 482 220 538 215 982 70 1093 39 1200 31 1260 28 1300 20
1320 10--
         1350 10

;Activation and deactivation function
; For mechanical simulation, it is recommended (San) that
;  elements are activated in the middle of the weld pool.
  200 / FORTRAN
       FUNCTION F(X)
       DIMENSION X(4)

     xa   = X[1];
     ya   = X[2];
     za   = X[3];
     time = X[4];
C initial position of heat source in the new frame
      xc = 0;
      yc = 0;
      zc = 0;
CTranslation
      xa = xa - xc
      ya = ya - yc
      za = za - zc
C
C Welding velocity
     wv=-5.0;
```

```
C POSITION OF HEAT SOURCE CENTER
    f=0;
    center=wv*time;
    if (ya .GT. center) f=1;
    return
    end

;
; Turn off all elements in a bead
;
  300 / FORTRAN
        FUNCTION F(X)
        DIMENSION X(4)
      xa   = X[1];
      ya   = X[2];
      za   = X[3];
      time = X[4];
      f = -1
      return
      end
;
; Turn on all elements in a bead
;
  400 / FORTRAN
        FUNCTION F(X)
        DIMENSION X(4)
      xa   = X[1];
      ya   = X[2];
      za   = X[3];
      time = X[4];
      f = 1
      return
      end
;
RETURN

SAVE DATA 20

; Load Results from thermal simulation
;  It is also possible to simply search both Data and Tran files
;  with the command SEARCH DATA TRAN 10.  As this command loads
;  both files into memory and transient files can be VERY large,
;  the ASSIGN command, which simply opens the file for reading,
;  is more appropriate for large files
SEARCH DATA 10
ASSI 19 TRAN10.TIT
TEMPERATURE TRANSIENT CARD
DEAS 19

; If an elastic calculation is desired, remove the BEHAVIOR PLASTIC
;  command
; The BFGS algorithm generally solves very quickly.  See SYSWELD
;  manuals for detailed explanations
; The iterative solver is much better than the direct solver for
;  meshes greater than 2500 to 3000 elements
```

```
; Use the SYMMETRICAL label whenever it works
; Even if there is no element activation and therefore no initial
;  condition, include the INITIAL CONDITION command or the simulation
;  can not be restarted after it stops.
; The COMPACT label makes sure that no card numbers are skipped if
;  the STORE 2 command is used
; STORE 1 stores every card
; STORE 2 stores every other card, etc

SEARCH DATA 20
TRANSIENT NON LINEAR STATIC
BEHAVIOUR PLASTIC
ALGORITHM BFGS IMPLICIT 0.5 ITERATION 100
PRECISION ABSOLUTE NORME 0  FORCE 5 DISPLACEMENT 1*-5
METHOD ITERATIVE SYMMETRICAL
INITIAL CONDITION
 ELEMENTS GROUP $BEAD1$ / IS -1
 ELEMENTS GROUP $BEAD2$ / IS -1
TIME INITIAL 0 COMPACT
  0.015625 STEP 0.015625 / STORE 1
RETURN
SAVE DATA TRAN 20

; It is wise to split the computation into two parts for
;  several reasons:
; First: if your don't and your simulation crashes, you
;  have no results to look at for debugging, as your file
;  has not been explicitly saved. Again, the ASSIGN command,
;  below, opens the file for reading and writing, so if your
;  simulation crashes in the middle of a time step, if your
;  file was assigned, you will have all results up to the
;  crash.  If you SEARCH DATA 20, do all of your time steps,
;  and then SAVE DATA TRAN 20, and something happens in the
;  middle of your simulation, everything is lost.
; Second: If you do all of your time steps in the first
;  group of commands (above), and then SAVE DATA TRAN 20,
;  the system create a temporary file into which it dumps
;  results.  This will be called tmp.something, where
;  something is any string of characters.  This is no problem
;  as long as your simulation is not large. If your simulation
;  creates a temporary file that is 10 GB and then
;  tries to save it as TRAN20.TIT, you must have 20 GB of free
;  space. If the TRAN20.TIT file is assigned, results are
;  dumped directly into that file and no tmp file is generated.
;  Therefore, in the above example, only 10 GB of free space
;  is required.
; Another note: Using STORE 2 halves storage requirements
;  compared with STORE 1

SEARCH DATA 20
ASSIGN 19 TRAN20.TIT
TRANSIENT NON LINEAR STATIC
BEHAVIOUR PLASTIC
ALGORITHM BFGS IMPLICITE 1 ITERATION 100
PRECISION ABSOLUTE NORME 0  FORCE 5 DISPLACEMENT 1*-5
```

```
METHOD ITERATIVE SYMMETRICAL
INITIAL CONDITION RESTART CARD LAST
TIME INITIAL RESTART COMPACT
  4.5 STEP 0.015625  / STORE 2
RETURN
SAVE DATA 20
DEAS 19
```

MECH2.DAT

```
; This is the secon step of the mechanical simulation, corresponding
;  with the second bead deposit
; This time, the file containing the first half of the
;  simulation is searched

SEARCH DATA 20

DEFINITION
    WELDING SIMULATION
OPTION THREE DIMENSIONAL THERMOMECHANICAL
RESTART GEOMETRY

; Here, the only change from the previous file is that the first bead
is
;  STATE=-400 (activated) and the the second bead is STATE=-200 (in the
;  process of being activated)

MATERIAL PROPERTIES
 ELEMENTS GROUP $PART$ / E=-10001 YIELD=-10005 LX=-10002 LY=-10002 LZ=-
10002--
  MODEL=1 NU=0.3  TF=1400
 ELEMENTS GROUP $BEAD1$ / E=-10001 YIELD=-10005 LX=-10002 LY=-10002
LZ=-10002--
  MODEL=1 NU=0.3 STATE=-400 TF=1400
 ELEMENTS GROUP $BEAD2$ / E=-10001 YIELD=-10005 LX=-10002 LY=-10002
LZ=-10002--
  MODEL=1 NU=0.3 STATE=-200 TF=1400

CONSTRAINTS
 NODES GROUP $P7$ / UX UY UZ
 NODES GROUP $P93$ / UX UY UZ
 NODES GROUP $D9$ / SYMMETRY
 NODES GROUP $D14$ / SYMMETRY
 NODES GROUP $D20$ / UX
 NODES GROUP $D30$ / UX
 NODES GROUP $D3$ $D4$ $D5$ $D6$ $D7$ / UY
 NODES GROUP $D17$ $D22$ $D27$ $D32$ $D36$ / UY
 NODES GROUP $D38$ / UZ
 NODES GROUP $L100$ / UX UZ

LOADS
1 welding / NOTHING

TABLE
 10001 / 1 24 195000 93 189000 204 180000 316 171000 427 161000 538
152000--
   982 90000 1093 72000 1200 45000 1216 43000 1237 41400 1250 39500
1256 --
   38000 1289 20000 1308 10000 1330 3000 1340 1240 1350 620 1380 100 --
   1410 100

 10092 / 1 20 0 100 .001224 200 .00279 300 .004396 400 .00608 500
.007872--
```

```
   600 .009686 700 .011628 800 .013728 1200 .023128 1250 .024477 1300--
   1320 .02652
;
 10002 / 1 20 .0000085 100 .0000153 200 .0000155 300 .0000157--
  400 .000016 500 .0000164 600 .0000167 700 .0000171 800--
  .0000176 1200 .0000196 1250 .0000199 1300 .0000201 1320--
  .0000204

;Yield stress
;
 10005 / 1 21 365 93 325 149 290 204 270 260 255 316 235 371 230 427 --
         230 482 220 538 215 982 70 1093 39 1200 31 1260 28 1300 20
1320 10--
         1350 10

;Activation and deactivation function
;
; In the activation program, time must be shifted back to position the
;  activation front in the right spot.
  200 / FORTRAN
        FUNCTION F(X)
        DIMENSION X(4)

      xa   = X[1];
      ya   = X[2];
      za   = X[3];
      time = X[4];
C initial position of heat source in the new frame
       time=time-4.5;
       xc = 0;
       yc = 0;
       zc = 0;
CTranslation
       xa = xa - xc
       ya = ya - yc
       za = za - zc
C
C Welding velocity
      wv=-5.0;
C POSITION OF HEAT SOURCE CENTER
     f=0;
     center=wv*time;
     if (ya .GT. center) f=1;
     return
     end

;
; Turn off all elements in a bead
;
  300 / FORTRAN
        FUNCTION F(X)
        DIMENSION X(4)
      xa   = X[1];
      ya   = X[2];
      za   = X[3];
```

```
      time = X[4];
      f = -1
      return
      end
;
; Turn on all elements in a bead
;
  400 / FORTRAN
        FUNCTION F(X)
        DIMENSION X(4)
      xa   = X[1];
      ya   = X[2];
      za   = X[3];
      time = X[4];
      f = 1
      return
      end
;
RETURN

SAVE DATA 20


SEARCH DATA 10
ASSI 19 TRAN10.TIT
TEMPERATURE TRANSIENT CARD
DEAS 19

; Since the TRAN20.TIT file has already been initialized,
;  it can be assigned right away, with no preliminary
;  calculation required.


SEARCH DATA 20
ASSIGN 19 TRAN20.TIT
TRANSIENT NON LINEAR STATIC
BEHAVIOUR PLASTIC
ALGORITHM BFGS IMPLICITE 1 ITERATION 100
PRECISION ABSOLUTE NORME 0  FORCE 5 DISPLACEMENT 1*-5 .
METHOD ITERATIVE SYMMETRICAL
INITIAL CONDITION RESTART CARD LAST
TIME INITIAL RESTART COMPACT
  8.0 STEP 0.015625  / STORE 2
RETURN
SAVE DATA 20
DEAS 19
```

ACTIVE.DAT

```
;This file is used to create groups associated with elements
; activated during a simulation.  This is required if you
; wish to display the deposition of a bead

group create name card1
element criterion active card 1
return

group create name card2
element criterion active card 2
return

group create name card3
element criterion active card 3
return

group create name card4
element criterion active card 4
return

group create name card5
element criterion active card 5
return
```

POST.DAT

```
; Use the assign command for faster reading
;  and smaller storage requirements
; It's ok to say CARD 0 to 400 step 1 even if you don't have
;  400 cards

SEARCH DATA 10
ASSIGN 19  TRAN10.TIT
CONVERSION TRANSIENT
NAME POST11.fdb
ELEMENTS
FILE DISPLACEMENTS
CARD  0 to 400 step 1
RETURN
SAVE DATA 11
DEAS 19
```

POST2.DAT

```
; This file is split into three parts because
;  Sysweld generates errors if POST files are greater
;  than 2 GB

SEARCH DATA 20
ASSIGN 19 TRAN20.TIT
CONVERSION TRANSIENT
NAME POST21.fdb
ELEMENTS
FILE DISPLACEMENTS FORCES
CARD 0 to 85 step 1
RETURN
SAVE DATA 21
DEAS 19

SEARCH DATA 20
ASSIGN 19 TRAN20.TIT
CONVERSION TRANSIENT
NAME POST22.fdb
ELEMENTS
FILE DISPLACEMENTS FORCES
CARD 86 to 170 step 1
RETURN
SAVE DATA 22
DEAS 19

SEARCH DATA 20
ASSIGN 19 TRAN20.TIT
CONVERSION TRANSIENT
NAME POST23.fdb
ELEMENTS
FILE DISPLACEMENTS FORCES
CARD 171 to 260 step 1
RETURN
SAVE DATA 23
DEAS 19
```

RUN.DAT

```
; This file will run the entire thremal part of
;  a simulation.

read therm1.dat
read therm2.dat

; This part creates groups associated with elements
;  activated by each card
search data 10
assign 19 TRAN10.TIT
read active.dat
save data 10
deas 19

; Reads the thermal post-processing file
read post.dat
```

RUNMECH.DAT

```
; Runs entire mechanical simulation
read mech1.dat
read mech2.dat
; Post-Processes mechanical simulation
read post2.dat
```

Vita

Aaron Mengel was born in Mohnton, Pennsylvania on March 30, 1978. He graduated from Governor Mifflin High School in 1996, where he received the Broadbent foundation scholarship. Aaron went on to study Mechanical Engineering at Lehigh University. He graduated with high honors in 2000 and received a Presidential Scholarship. He then went on to conduct research in finite element modeling of welding with specific interest in the LENS process. After graduating in January of 2003, he went on to pursue a career with Knolls Atomic Power Laboratory in Schenectady, New York.

END OF TITLE